SPACE-TIME ADAPTIVE PROCESSING TECHNIQUES FOR MULTICHANNEL MOBILE PASSIVE RADAR

by

Giovanni Paolo BLASONE

Thesis Supervisor

Prof. Pierfrancesco Lombardo
Department of Information Engineering,
Electronics and Telecommunications

This thesis was evaluated by the following external referees:

The time and effort of the external referees in evaluating this thesis,
as well as their valuable and constructive suggestions,
are very much appreciated and greatly acknowledged.

———————————————————————

Abstract

Passive radar technology has reached a level of maturity for stationary sensor operations, widely proving the ability to detect, localize and track targets, by exploiting different kinds of illuminators of opportunity. In recent years, a renewed interest from both the scientific community and the industry has opened new perspectives and research areas. One of the most interesting and challenging ones is the use of passive radar sensors onboard moving platforms. This may offer a number of strategic advantages and extend the functionalities of passive radar to applications like synthetic aperture radar (SAR) imaging and ground moving target indication (GMTI). However, these benefits are paid in terms of motion-induced Doppler distortions of the received signals, which can adversely affect the system performance.

In the case of surveillance applications, the detection of slowly moving targets is hindered by the Doppler-spread clutter returns, due to platform motion, and requires the use of space-time processing techniques, applied on signals collected by multiple receiving channels. Although in recent technical literature the feasibility of this concept has been preliminarily demonstrated, mobile passive radar is still far from being a mature technology and several issues still need to be addressed, mostly connected to the peculiar characteristics of the passive bistatic scenario. Specifically, significant limitations may come from the continuous and time-varying nature of the typical waveforms of opportunity, not suitable for conventional space-time processing techniques. Moreover, the low directivity of the practical receiving antennas, paired with a bistatic omni-directional illumination, further increases the clutter Doppler bandwidth and results in the simultaneous reception of non-negligible clutter contributions from a very wide angular sector. Such contributions are likely to undergo an angle-dependent imbalance across the receiving channels, exacerbated by the use of low-cost hardware.

This thesis takes research on mobile passive radar for surveillance applications one step further, finding solutions to tackle the main limitations deriving from the passive bistatic framework, while preserving the paradigm of a simple system architecture. Attention is devoted to the development of signal processing algorithms and operational strategies for multichannel mobile passive radar, focusing on space-time processing techniques aimed at clutter cancellation and slowly moving target detection and localization.

First, a processing scheme based on the displaced phase centre antenna (DPCA) approach is considered, for dual-channel systems. The scheme offers a simple and effective solution for passive radar GMTI, but its cancellation performance can be severely compromised by the presence of angle-dependent imbalances affecting the receiving channels. Therefore, it is paired with adaptive clutter-based calibration techniques, specifically devised for mobile passive radar. By exploiting the fine Doppler resolution offered by the typical long integration times and the one-to-one relationship between angle of arrival and Doppler frequency of the

stationary scatterers, the devised techniques compensate for the angle-dependent imbalances and prove largely necessary to guarantee an effective clutter cancellation.

Then, the attention is focused on space-time adaptive processing (STAP) techniques for multichannel mobile passive radar. In this case, the clutter cancellation capability relies on the adaptivity of the space-time filter, by resorting to an adjacent-bin post-Doppler (ABPD) approach. This allows to significantly reduce the size of the adaptive problem and intrinsically compensate for potential angle-dependent channel errors, by operating on a clutter subspace accounting for a limited angular sector. Therefore, *ad hoc* strategies are devised to counteract the effects of channel imbalance on the moving target detection and localization performance. By exploiting the clutter echoes to correct the spatial steering vector mismatch, the proposed STAP scheme is shown to enable an accurate estimation of target direction of arrival (DOA), which represents a critical task in system featuring few wide beam antennas.

Finally, a dual cancelled channel STAP scheme is proposed, aimed at further reducing the system computational complexity and the number of required training data, compared to a conventional full-array solution. The proposed scheme simplifies the DOA estimation process and proves to be robust against the adaptivity losses commonly arising in a real bistatic clutter scenario, allowing effective operation even in the case of a limited sample support.

The effectiveness of the techniques proposed in this work is validated by means of extensive simulated analyses and applications to real data, collected by an experimental multichannel passive radar installed on a moving platform and based on DVB-T transmission.

Acknowledgment

First and foremost, I would like to express my sincere gratitude to Prof. Pierfrancesco Lombardo and Prof. Fabiola Colone, for their constant support and inspiration. They encouraged and guided me through the entire work, sharing their knowledge with me and showing a great deal of trust. I am proud to have worked with them during these years.

I am deeply grateful to Dr. Diego Cristallini, Dr. Philipp Wojaczek and the Fraunhofer Institute for High Frequency Physics and Radar Techniques (FHR). Their help and prompt advices have been invaluable for this work. Moreover, they gave me the opportunity for an experimental validation, sharing with us the outcomes of their acquisition campaigns.

I would like to extend my sincere thanks to the entire RRSN group at Sapienza University, for the incredible working environment and the wonderful people who make it up. I realized in these challenging months how much I miss the time we spent together. Thanks for the fun, the help, the moral support, the stimulating conversations and all the light-hearted but never banal moments we shared in our lab.

A huge thank also goes to my friends, for always being there for me when I needed it most.

Thank you, Valentina for your encouragement and your love. You made everything special.

Finally, I say a special thank you to my family, for their support, their infinite patience, and the trust they have always shown in me. There are simply not enough words to express how thankful I am to you.

The following papers were published as a result of this PhD research

Journal Papers

J1. G. P. Blasone, F. Colone, P. Lombardo, P. Wojaczek and D. Cristallini, "Passive Radar DPCA schemes with adaptive channel calibration," in *IEEE Transactions on Aerospace and Electronic Systems*, vol. 56, no. 5, pp. 4014-4034, Oct. 2020.

J2. G. P. Blasone, F. Colone, P. Lombardo, P. Wojaczek and D. Cristallini, "Passive Radar STAP detection and DOA estimation under antenna calibration errors," in *IEEE Transactions on Aerospace and Electronic Systems*, doi: 10.1109/TAES.2021.3061803.

J3. G. P. Blasone, F. Colone, P. Lombardo, P. Wojaczek and D. Cristallini, "Dual cancelled channel STAP for target detection and DOA estimation in Passive Radar," submitted for publication in *Sensors*.

J4. P. Wojaczek, D. Cristallini, D. W. O'Hagan, F. Colone, G. P. Blasone and P. Lombardo, "A three-stage inter-channel calibration approach for Passive Radar on moving platforms exploiting the minimum variance power spectrum," in *Sensors* 2021, 21(1), 69.

Conference Papers

C1. G. P. Blasone, F. Colone, P. Lombardo, P. Wojaczek and D. Cristallini, "A two-stage approach for direct signal and clutter cancellation in passive radar on moving platforms," *2019 IEEE Radar Conference (RadarConf)*, Boston, MA, USA, 2019, pp. 1-6.

C2. G. P. Blasone, F. Colone and P. Lombardo, "Facing channel calibration issues affecting passive radar DPCA and STAP for GMTI," *2020 IEEE International Radar Conference (RADAR)*, Washington, DC, USA, 2020, pp. 31-36.

Honours and Awards

Some results of this PhD research have been awarded of the following recognitions:

H1. Finalist in Student Paper Competition at 2020 IEEE International Radar Conference (RADAR), Washington, DC, USA, for paper C2.

H2. Finalist in Three Minute Thesis (3MT) contest at 2020 IEEE Radar Conference (RadarConf), Florence, Italy.

Contents

List of Figures

List of Tables

Nomenclature

$\boldsymbol{x}$	Boldface and lower-case letter denotes vector
$\boldsymbol{X}$	Boldface and upper-case letter denotes matrix
x	Letter in normal font denotes a scalar
$\boldsymbol{I}_N$	N×N identity matrix
j	The imaginary unit
$\widehat{(.)}$	Estimate of (.)
$(.)^T$	Transpose of (.)
$(.)^*$	Conjugate of (.)
$(.)^H$	Hermitian (or conjugate transpose) of (.)
$\lvert . \rvert$	Modulus of (.) for scalars; Determinant for matrices
$\lfloor . \rfloor$	Floor of (.)
$(.)!$	Factorial of (.)
$\exp(.)$	Exponential function
$\log_{10}(.)$	Logarithm of (.) relative to base 10
$E\{.\}$	Statistical expectation of (.)
$\arg(.)$	Argument of (.)
$\mathrm{median}(.)$	Median of values in (.)
$Re(.), Im(.)$	Real and Imaginary part of (.)
$\otimes$	Kronecker product
c	Speed of light
λ	Wavelength
f_D	Doppler frequency
d	Array element spacing
v_p	Platform velocity
v_b	Bistatic radial velocity
R_b	Bistatic range
φ	Azimuth angle of receiver to scatterer line of sight

ϑ	Depression angle of receiver to scatterer line of sight
ψ	Angle between platform velocity and array end-fire
ϕ	Angle between array end-fire and receiver to scatterer line of sight
B	Signal bandwidth
M	Number of pulses
L	Number of Doppler bins
N	Number of spatial channels
K	Number of training data

List of Acronyms

ABPD	Adjacent Bin Post – Doppler
AMF	Adaptive Matched Filter
CA	Clutter Attenuation
Cal-GLRT	Calibrated Generalized Likelihood Ratio Test
CR	Cancellation Ratio
CFAR	Constant False Alarm Rate
CNR	Clutter to Noise power Ratio
COTS	Commercial Off the Shelf
CPI	Coherent Processing Interval
CRB	Cramér – Rao lower Bound
CUT	Cell Under Test
DDC	Doppler Dependent Calibration
DDC-RB	Doppler Dependent Calibration in Range Bands
DFT	Discrete Fourier Transform
DOA	Direction of Arrival
DPCA	Displaced Phase Centre Antenna
DSI	Direct Signal Interference
DVB-T	Digital Video Broadcasting – Terrestrial
ECA	Extensive Cancellation Algorithm
ECA-CD	Extensive Cancellation Algorithm by Carrier and Doppler
FFT	Fast Fourier Transform
FM	Frequency Modulation
GLRT	Generalized Likelihood Ratio Test
GMTI	Ground Moving Target Indication
ICM	Internal Clutter Motion
IF	Improvement Factor
IID	Independent and Identically Distributed

IO	**I**lluminator of **O**pportunity
LA	**L**eading **A**ntenna
LOS	**L**ine **of S**ight
MC	**M**onte **C**arlo
MDV	**M**inimum **D**etectable **V**elocity
ML	**M**aximum **L**ikelihood
MLE	**M**aximum **L**ikelihood **E**stimator
MTI	**M**oving **T**arget **I**ndication
NC-GLRT	**N**on − **C**oherent **G**eneralized **L**ikelihood **R**atio **T**est
OFDM	**O**rthogonal **F**requency **D**ivision **M**ultiplexing
PCL	**P**assive **C**oherent **L**ocation
PD	**P**robability of **D**etection
PFA	**P**robability of **F**alse **A**larm
PRF	**P**ulse **R**epetition **F**requency
QAM	**Q**uadrature **A**mplitude **M**odulation
QPSK	**Q**uadrature **P**hase-**S**hift **K**eying
RAM	**R**adiation **A**bsorbing **M**aterial
RCS	**R**adar **C**ross **S**ection
RMS	**R**oot **M**ean **S**quare
RX	**R**eceiver
SAR	**S**ynthetic **A**perture **R**adar
SCC	**S**ingle **C**alibration **C**oefficient
SCR	**S**ignal to **C**lutter power **R**atio
SINR	**S**ignal to **I**nterference-plus-**N**oise power **R**atio
SNR	**S**ignal to **N**oise power **R**atio
STAP	**S**pace − **T**ime **A**daptive **P**rocessing
TA	**T**railing **A**ntenna
TX	**T**ransmitter
UHF	**U**ltra − **H**igh **F**requency
ULA	**U**niform **L**inear **A**rray
VHF	**V**ery **H**igh **F**requency

Chapter 1
Introduction

This Chapter introduces the main topics addressed in the thesis and gives an overview of the motivations behind this work. After a brief contextual background, the goals of this dissertation and its main innovative contributions are illustrated. Finally, the outline of the thesis is reported.

1.1 Overview and motivations

Passive radar is a particular type of bistatic radar, which does not transmit a dedicated electromagnetic signal, instead it exploits already existing signals emitted by non-cooperative sources to perform target detection, localization and/or imaging, [1][2]. Such sources are usually referred to as illuminators of opportunity and they can be broadcast transmitters for public utility, communication systems, other radar systems, etc.

Passive radar technology is very appealing for both civilian and defence applications, as it generally offers low cost of construction, operation, and maintenance, due to the lack of a dedicated transmitter, as well as the capability of undercover operation, being the possibility of locating and jamming the radar virtually ruled out. In addition, it is efficient in the spectrum usage, as no dedicated spectrum needs to be allocated, and it can be easily deployed in sensitive areas, e.g. coastal or urban areas, thanks to its limited environmental impact and lack of electromagnetic pollution. On the other hand, the main drawbacks are related to the dependence on an external transmission, which is not under the control of the radar operator and whose waveform is not specifically designed for radar purposes. This may decrease the reliability of the system and generally complicate the signal processing stage.

In recent years, passive radar systems have reached a stage of relative maturity, for what concerns stationary sensor operations, widely proving their ability to detect, localize and track moving targets, by exploiting the signals emitted by different kinds of illuminators of opportunity. Nowadays, several system prototypes, as well as commercial products, are available and successfully employed in the context of air traffic monitoring, coastal surveillance, security and military applications.

In the last few years, passive radar technology has been gaining a renewed and increasing attention in the scientific community. The recent developments in this field have opened new

perspectives and innovative areas of research and applications, [3]-[5]. Among them, the application of passive radar systems to airborne or ground moving platforms is one of the most interesting and challenging. Currently, several research groups are investigating the potentialities offered by mobile passive radar, for the purpose of target detection and ground imaging, [6]-[32].

The use of passive radar receivers on mobile platforms may offer a number of strategic advantages compared to stationary ground-based solutions and it extends the functionalities of this kind of sensors, making them attractive for applications like synthetic aperture radar (SAR) imaging [6]-[9] and ground moving target indication (GMTI) [12]-[28]. Moreover, it might yield the typical benefits of passive radar to airborne class systems.

The lack of a dedicated transmitter unit and the common adoption of commercial-off-the-shelf (COTS) hardware components for the receiving system, lead to a reduction of weight, energy consumption and generally cost. For these reasons, mobile passive radar could be easily installed on small vehicles, boats, ultralight aircrafts, or unmanned aerial vehicles (UAVs), representing an appealing solution for covert and/or low-cost monitoring operations over wide areas.

Although the proof of concept of an airborne passive radar for imaging and moving target detection has been given [6]-[10], the potential strategic advantages of passive radar mounted on a moving platform are paid by the presence of Doppler distortions on the received signals, induced by the receiver motion, which can adversely affect the performance of the system.

First, some effort must be put into a proper collection and reconstruction of the reference signal regardless of the platform motion, [31],[32]. Moreover, in surveillance applications, the detection of moving targets with a small radial velocity component is hindered by the spread in Doppler of clutter echoes, due to the relative motion of the receiver with respect to the stationary scene. This latter effect, typical of moving radar, tends to be even more stressed at the VHF/UHF bands of the most widely used illuminators of opportunity, due to the wide antenna beams typically available. As a result, the detection of slow-moving targets requires a proper suppression of clutter returns, which can be achieved by exploiting space-time processing, applied to the signals collected by multiple receiving channels.

The feasibility of this concept has lately been preliminarily demonstrated by researchers, [12]-[15]. However, such technology is still far from being mature and there is still great field for research. Indeed, several challenges must be faced in order to make space-time processing effectively applicable in the mobile passive radar case. Most of them are connected to the characteristics of the exploited waveform of opportunity and more in general to the passive bistatic scenario.

The continuous and time-varying waveforms of the typically exploited illuminators of opportunity are not suitable for the conventional space-time clutter suppression techniques, conceived for standard pulsed radar. Moreover, their typical ill-suited ambiguity functions may compromise the detection capability and reduce the separation between range cells,

generally required by adaptive techniques. In addition, the system must deal with the bistatic geometry and the presence of a strong direct signal interference from the exploited transmitter of opportunity, as well as short-range echoes, which frequently represent the dominant components in the received signal.

Due to the typically exploited wavelengths and the related antenna size, the available receiving antennas are generally limited in number and characterized by a low directivity. This is paired with a bistatic illumination from broadcast transmitters, which do not focus the signal energy only in the direction of interest, resulting in a simultaneous reception of non-negligible clutter contributions arriving from a very a wide angular sector. This further increases the clutter Doppler bandwidth and may easily raise channel calibration issues. Besides, the limited performance of the COTS components commonly used in low-cost passive radar hardware and the long wavelength of typical opportunity signals may pose some limitations to the accuracy (or the feasibility) of preliminary system calibrations. As a result, the received echoes may be easily affected by non-negligible amplitude and/or phase imbalances across the receiving channels, depending on their direction of arrival.

All the above issues contribute to making GMTI from passive radar on moving platforms a challenging application. The need for practical and effective solutions to tackle these issues and thus contribute to the maturity of mobile passive radar technology is at the base of this dissertation. Specifically, the attention is focused on developing signal processing algorithms and operational strategies for space-time clutter filtering and slow-moving target detection and localization, while possibly preserving the paradigm of a simple system architecture.

1.2 Background

The purpose of this Section is to provide the necessary background to better understand the motivation for the advancement developed and explored in this work. First, the main principles of passive bistatic radar are illustrated. Then, a brief overview is given of DVB-T as illuminator of opportunity. Finally, the concept of passive radar on moving platforms is introduced. Note that this Section is certainly not intended to be exhaustive. For a complete and detailed discussion on these topics, the interested reader is referred to the relevant cited literature and the references therein.

1.2.1 Passive bistatic radar

A passive bistatic radar (or passive coherent location – PCL) system is a receive-only system, which does not emit electromagnetic energy to detect targets, instead it uses already existing signals transmitted by other non-cooperative sources [1][2]. These sources are commonly referred to as illuminators of opportunity and they can be broadcast transmitters, communication systems, other radar systems and so on.

A typical passive radar operates in bistatic geometry, characterized by the displacement of the receiver (RX) and the transmitter (TX). Generally, two receiving channels are required, referred to as *reference* and *surveillance* channels, respectively pointed towards the TX and the surveyed area. Since the transmitted signal waveform is unknown at the receiver, the reference channel has the role of collecting a clean replica of the signal. Then, reflections from potential targets must be found, by cross-correlating the reference signal with the signal collected by the surveillance channel.

The bistatic range and the bistatic velocity of the target are measured by analysing the time delay between the direct signal and the reflected echo and its rate of change, namely the Doppler shift. In Figure 1.1, a bidimensional example of bistatic geometry is sketched. Specifically, the relative bistatic range is measured as

$$R_B = R_{TX} + R_{RX} - B_{TX-RX} \tag{1.1}$$

where R_{TX} and R_{RX} denote the target distance from TX and from RX, respectively, while $B_{TX\text{-}RX}$ represents the distance between the TX and RX, referred to as *baseline*. The bistatic range locates the target on an ellipsoid, referred to as bistatic iso-range ellipsoid, having the TX and the RX as its foci. The resolution in bistatic range is given by

$$\Delta R_B = c/B \tag{1.2}$$

where c denotes the speed of light and B the frequency bandwidth of the exploited signal. As a result, the echoes of two point-like targets can be discriminated if their bistatic ranges differ by more than ΔR_B.
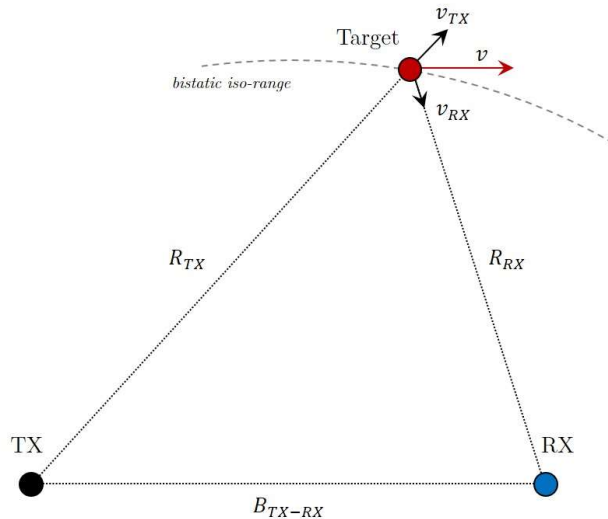
Figure 1.1: Sketch of passive radar bistatic geometry.

The target bistatic velocity is measured from the Doppler frequency shift of its echo, defined as the rate of change of the bistatic range over time. In the case where both the TX and the RX are stationary, the target bistatic Doppler frequency is given by

$$f_D = \frac{v_b}{\lambda} = \frac{v_{TX} + v_{RX}}{\lambda} \qquad (1.3)$$

where λ denotes the carrier frequency wavelength of the exploited signal, while v_b is the target bistatic radial velocity, given by the sum of the target radial velocity components towards the RX and the TX. Notice that the bistatic Doppler frequency is equal to zero for targets moving along the baseline or along the bistatic iso-range. The resolution in bistatic Doppler frequency is determined by the length of the coherent processing interval (CPI), namely the integration time T_{int}, being equal to

$$\Delta f_D = 1/T_{int} \qquad (1.4)$$

Figure 1.2 sketches a block diagram of the basic processing scheme of passive radar, which typically includes the following fundamental steps.

(i) Disturbance Cancellation. The reference signal is first used to remove the undesired contributions that have been received on the surveillance channel. Such disturbances result from the fraction of direct signal from TX, received by the sidelobes or backlobes of the surveillance antenna, as well as the clutter/multipath echoes from the stationary scene. These undesired contributions can severely hinder the detection of target echoes. To solve this problem, several algorithms have been developed in the context of stationary passive radar, [67]. Among them the extensive cancellation algorithm (ECA), proposed in [68]-[70], are able to remove the direct signal interference (DSI) and clutter contributions by projecting the surveillance signal into a subspace orthogonal to the disturbance subspace. Basically, the undesired interference signal is estimated by means of delayed and weighted replicas of the reference signal, and then subtracted from the surveillance signal.

(ii) Range-Doppler map evaluation. After disturbance cancellation, the bistatic range-Doppler map is evaluated by means of the two-dimensional (2D) cross-correlation between the surveillance signal and different Doppler shifted replicas of the reference signal. As a result, the received data are range-compressed and Doppler processed, and the resulting ambiguity function depends on the characteristics of the exploited waveform of opportunity. A number of algorithms have been developed for an efficient implementation of this stage [3], since it usually requires a relatively high computational load and might involve a large volume of data, due to the long integration times (order of magnitude of seconds) typically required to extract the low-power target signal from the disturbance.

(iii) Target detection. Finally, the presence of potential targets in the range-Doppler map is detected, by comparing the level of signal in a given cell under test (CUT) with a properly selected threshold, scaled in order to guarantee a desired false alarm probability (PFA). The most used detection schemes have the property to guarantee a constant false alarm rate (CFAR), by adapting to the local disturbance level. The target detection stage is then typically followed by additional processing steps, aimed at target localization, tracking or feature extraction.
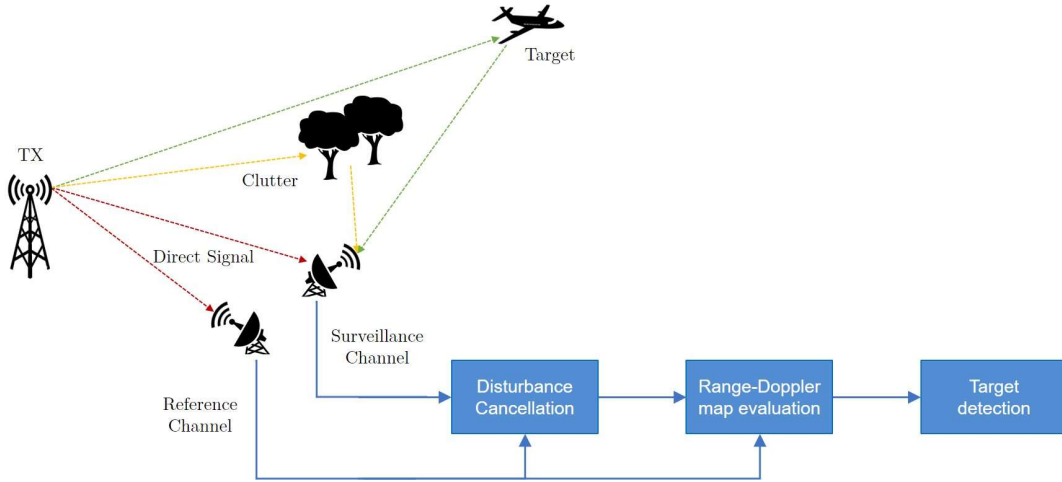
Figure 1.2: Sketch of passive radar basic signal processing scheme.

1.2.2 DVB-T as illuminator of opportunity

Nowadays, a large number of transmitters for telecommunications, radio navigation, and remote sensing applications, are available to be used as illuminators of opportunity for passive radar. They include terrestrial sources, such as FM radio, digital audio broadcasting (DAB), digital video broadcasting – terrestrial (DVB-T), Wi-Fi and mobile communications networks (e.g. GSM, UMTS, LTE), as well as satellite sources, like digital video broadcasting – satellite (DVB-S), global navigation satellite system (GNSS), and so on.

Among the opportunity sources, the digital modulated transmissions are particularly attractive, due to a number of advantages. They are characterized by a constant bandwidth, which provides constant range resolution. Moreover, they allow an ideal recovery of the transmitted signal, by means of a decode/recode strategy. The reference signal can be directly recovered from one (or more) of the surveillance channels, without necessarily requiring an additional dedicated reference channel, thus reducing the system complexity.

Over the past years, DVB-T transmitters have been among the most employed illuminators of opportunity, thanks to their generally high transmit power, relatively broad bandwidth, wide coverage, and large diffusion. DVB-T standard is very popular and is established almost

worldwide (with some adaptations). Its transmissions are in the ultra-high frequency (UHF) band, which has the property to travel beyond the radar horizon and penetrate foliage, thus increasing the radar potentialities. In addition, the DVB-T signal benefits from the typical characteristics of the digital orthogonal frequency-division multiplexing (OFDM) modulation and its known coding scheme [38]-[44].

The main parameters of DVB-T signal are listed in Table 1.1, for a typical 8 MHz channels, distinguishing between the 2k and 8k mode specifications [36]. Each DVB-T channel exploits the OFDM modulation over N_c carriers, spaced by Δf (depending on 2k or 8k mode), within a bandwidth of 7.61 MHz. The transmitted data are mapped over N_d data carriers, according to a quadrature phase-shift keying (QPSK), or a 16- or 64- quadrature amplitude modulation (QAM) and are organized in symbols of duration $T_u = 1/\Delta f$. Each OFDM symbol is cyclically extended with a guard interval of duration T_g in order to avoid inter-symbol interference, making the overall symbol duration equal to $T_s = T_u + T_g$. The signal structure is organized in frames, consisting of 68 OFDM symbols (see Figure 1.3). In addition to the data carriers, the DVB-T signal contains N_p pilot carriers, at fixed (continual pilots) and changing (scattered pilots) frequency positions, and N_{tps} transport parameter signalling (TPS) carriers, which are used for signal synchronisation, channel estimation, and system parameters transmission.

In this work, the attention is focused on systems exploiting DVB-T transmitters as illuminators of opportunity, and more in general on waveform based on OFDM modulation.

Table 1.1
Main parameters of DVB-T signal

Parameters	2k mode	8k mode
Number of carriers, N_c	1705	6817
Number of data carriers, N_d	1512	6048
Number of pilot carriers, N_p	176	701
Number of TPS carriers, N_{tps}	17	68
Carrier modulation	QPSK, 16QAM, 64QAM	
Elementary period, δt	$7/64$ µs	
Useful symbol duration, T_u	224 µs	896 µs
Guard interval, T_g	1/4, 1/8, 1/16, 1/32 of T_U	
Total symbol duration, T_s	$T_u + T_g$	
Carrier spacing, $\Delta f = 1/T_u$	4464 Hz	1116 Hz
Total bandwidth, B	7.61 MHz	
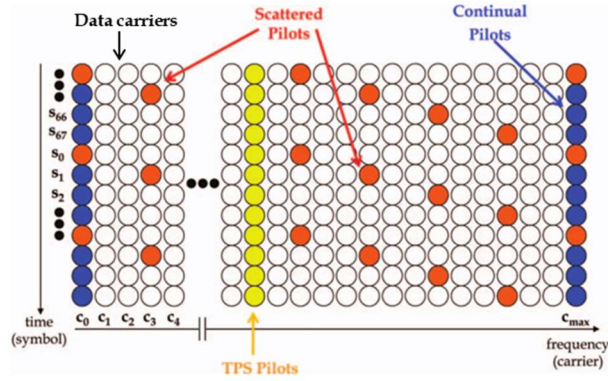
Figure 1.3: Sketch of the DVB-T frame structure.

As mentioned, a key advantage is the possibility to ideally recover the reference signal thanks to the digital modulation. A clean replica of the transmitted signal, free of multipath echoes and other undesired contributions, can be reconstructed from the signal collected at one or more surveillance channels, without having to use the generally few available spatial degrees of freedom (DOF) for a dedicated reference channel.

The reconstruction of the DVB-T reference signal is based on the following steps [38]: (i) synchronization in time and frequency on the transmitted signal and estimation of the channel transfer function by exploiting the pilot carriers; (ii) decoding of the signal down to the sequence of bits; (iii) remodulation of the symbol sequence according to the DVB-T standard.

This thesis will refer to this decode/recode approach for recovering of the reference signal. The possibility of a correct decoding depends on the level of direct signal with respect to noise, the channel transfer function, the forward-error-correction method, as well as on the platform speed [37]. In fact, such process is applicable also to moving receiver, being DVB-T standard reasonably robust against time-varying channels [31].

1.2.3 Passive radar on moving platforms

In recent years, stationary passive radar has become a relatively established technology. The first commercial systems started to appear in the market for various applications and recent advances are mainly aimed at increasing the reliability and capabilities of the system.

On the other hand, the concept of mobile passive radar is still an emerging research area and it has not yet reached a comparable level of operational capability. The idea is to install a passive radar receiver onboard an airborne or ground moving platform and to exploit terrestrial or satellite illuminators of opportunity for the purpose of target detection and/or ground imaging (see Figure 1.4).

Several research groups have been investigating the potentialities of mobile passive radar, especially in the context of SAR imaging, [6]-[9], and GMTI surveillance, [12]-[28]. In this thesis, attention is mainly focused on surveillance applications.

8
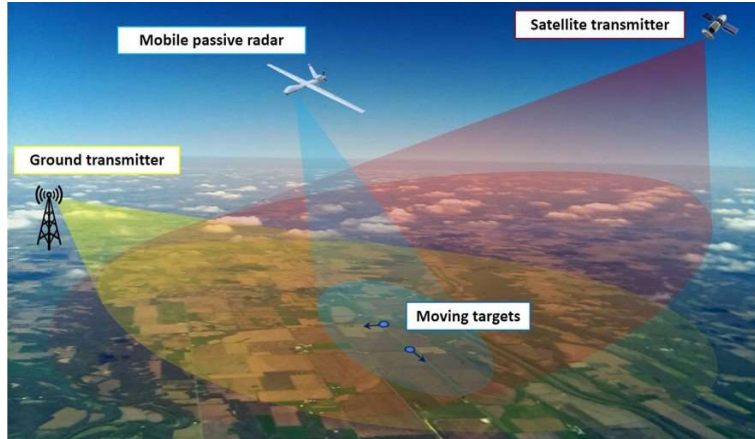
Figure 1.4: Sketch of an airborne passive radar system.

One of the main challenges is the detection of moving targets with a small radial velocity component, namely such that to appear within the clutter Doppler bandwidth. In fact, the relative motion of the receiver with respect to the stationary scene determines a spread in Doppler of the clutter returns. This latter effect, well known from standard airborne radar, tends to be even more stressed due to the broad antenna beams typically available at VHF/UHF bands of most widely used illuminators of opportunity. As a result, the detection of slow-moving targets requires a proper suppression of clutter echoes, which can be achieved by exploiting space-time processing, applied on signals collected by multiple receiving channels, with some along track displacement.

It is worth highlighting that the techniques traditionally employed for direct signal and clutter suppression in passive radar, such as ECA [68]-[70] and other time-domain adaptive filtering techniques [67], are not suited for suppression of the Doppler-spread clutter observed by a moving receiver. Although adaptations of such techniques are possible, [29][30], they reveal limitations for wide range-Doppler extensions of clutter and, most importantly, they would not be able to discriminate the presence of potential moving targets beneath the clutter.

Conversely, space-time adaptive processing (STAP) and similar techniques, borrowed from airborne active radar literature, allow an effective suppression of clutter in the angle-Doppler domain, by operating a two-dimensional filtering of the signal. Such techniques, enabled by the availability of both temporal and spatial degrees of freedom, i.e. multiple receiving channels, have been widely studied for standard active radar in the last decades and many adaptations have been proposed in literature, [46]-[51].

However, providing GMTI capability to mobile passive radar poses several challenges. Some of them are due to the impact of receiver motion on the passive radar operations, other are associated to the non-straightforward application of standard methodologies from active moving radar in the passive bistatic scenario.

Specifically, some of the main issues to be addressed are summarized in the following:

- the reference signal should be properly collected and reconstructed by the system regardless of the platform motion;

- the continuous and time-varying nature of the exploited waveforms of opportunity is not suitable for the conventional space-time processing techniques, rather conceived for pulsed radar with periodic waveforms;

- the ambiguity function of opportunity signals is not suited for radar purposes and must be controlled to preserve the detection capability and the separation between range cells, required by adaptive techniques;

- the bistatic geometry and the strong direct signal interference coming from transmitter, typically dominating the received signal, must be properly handled and suppressed along with the Doppler-spread clutter echoes;

- the low directivity of receiving antennas, due to the typically exploited wavelengths, paired with a bistatic broadcast illumination, further increases the clutter Doppler bandwidth and easily raises channel calibration issues, due to simultaneous reception of clutter echoes from potentially all directions;

- the use of low-cost COTS hardware components and the long wavelength of the opportunity signals compared to the practical antenna sizes pose limitations to the accuracy (or the feasibility) of preliminary system calibrations, resulting in non-negligible angle-dependent imbalances across the receiving channels;

- the limited number and low directivity of receiving antennas make target localization a critical task, therefore the available spatial degrees of freedom must be conveniently exploited both for space-time clutter filtering and for target DOA estimation;

- the bistatic illumination offered by ground-based transmitters tends to generate non-homogeneous clutter scenarios, thus limiting the effectiveness of adaptive techniques.

In the recent literature, only some of the above issues have been addressed.

The use of space-time processing methods for moving target detection in passive radar was considered for the first time in [24][25]. The authors generalized STAP for noise-like signals and proposed it for passive radar exploiting GSM and DVB-T transmissions, showing results against simulated data for a moving receiver and experimental data for a stationary platform.

The first proof of concept of an airborne passive radar exploiting FM transmission was given in [10]. The detection of targets from mobile passive radar was demonstrated and the behaviour of stationary ground clutter was analysed. However, a method for ground clutter suppression was not applied.

The desirable low-cost characteristic of passive radar, the typical size of the antennas at VHF/UHF bands and the high data rate of digital broadcast transmissions suggest the use of only few spatial channels and a simple processing architecture. For this reason, a displaced phase centre antenna (DPCA) approach represents a particularly suitable solution for mobile passive radar and has been primarily considered in [12]-[20].

DPCA performs a non-adaptive subtraction of radar echoes collected by two along-track displaced receiving antennas at the times that their two-way phase centres occupy the same spatial position, [46]. Echoes from stationary background are ideally cancelled out, being the performance only limited by thermal noise and internal clutter motion. Conversely, echoes from moving targets, shifted in phase due to their own radial motion, are preserved and can be ideally detected. Actually, several other factors can affect the cancellation performance, such as non-perfect alignment of the antenna phase centres (DPCA condition), temporal variability of the waveform, as well as possible imbalance between the receiving channels.

In [12][13], the authors considered the use of DPCA to suppress clutter returns against experimental data from an airborne FM-based passive radar and against simulated DVB-T data. The authors state that the continuous-wave characteristic of broadcast transmissions allows to apply any required temporal delay between the signals collected at the two channels, being only limited by the sampling frequency. This mitigates the typical constraints posed by DPCA on the pulse repetition frequency (PRF) of conventional pulsed radar. However, the authors do not consider the impact of the digital waveform ambiguity function and, most importantly, of the temporal variability of the opportunity waveform, which can severely limit the clutter cancellation performance, even assuming a perfect DPCA condition.

To this aim, in [15] a processing scheme was proposed, based on a reciprocal range compression strategy in conjunction with a flexible DPCA approach, which allows an effective application of DPCA in mobile passive radar. The flexible DPCA approach relaxes the constraint on the system equivalent PRF, also when a batch architecture is adopted for signal processing, which is typical of passive radar exploiting digital waveforms. The use of a reciprocal filter in lieu of a conventional matched filter at the range compression stage has a twofold role: it eliminates the undesirable structures and grating lobes arising in the signal ambiguity function, and it removes the performance limitations deriving from the temporal variability of the waveform. The effectiveness of this scheme was demonstrated for a DVB-T based mobile passive radar against both simulated and experimental data.

Other contributions focused on the impact of the receiver motion on the reference signal estimation and passive radar operations. In [11], the effects of signal mismatches on the correlation process in a moving passive radar are analysed. In [31], the authors investigate the impact of the motion induced Doppler shift on the reference signal reconstruction and provide potential solutions. In [32], an improved reference signal estimation capability is achieved by exploiting antenna and polarimetric diversity.

The work described in this thesis starts from the approach proposed in [15] for passive radar DPCA and is aimed at addressing the still open issues and developing *ad hoc* solutions to overcome them. In fact, despite the effectiveness of the techniques devised and the progress that has been made, the performance and the operational capability of mobile passive radar might still be strongly limited. Specifically, the problem of channel imbalance is proved to be particularly critical in the passive radar framework, both because it is very likely to occur

and because it exhibits some peculiar aspects deriving from the passive bistatic operation, which hinder the application of conventional calibration strategies and may severely compromise the system performance, especially in the case of GMTI applications.

1.3 Aims of the thesis and innovative contributions

The goal of this thesis is to contribute to research on multichannel mobile passive radar, developing signal processing techniques and operational strategies aimed at GMTI applications. Specifically, the attention is focused on space-time processing methodologies and *ad hoc* solutions are devised to address the main limitations deriving from the passive bistatic framework and especially associated to the problem of inter-channel imbalance.

As observed in the previous Sections, several aspects brought in by the passive bistatic operation make channel imbalance a critical issue in mobile passive radar, limiting the applicability of conventional calibration strategies and compromising the system performance. These aspects must be properly tackled in order to guarantee an effective clutter cancellation and slow-moving target detection capability, as well as their correct angular localization.

The solutions proposed in this work, takes advantage of some peculiar characteristics of passive radar systems, such are the typical long coherent integration times. Moreover, they are designed to preserve the paradigm of reduced complexity and simple system architecture.

The main innovative contributions made by this thesis are briefly detailed in the following.

The work starts from the analysis of a DPCA approach, for systems featuring two receiving channels. In this case, the presence of an angle-dependent channel imbalance may severely compromise the cancellation capability of clutter contributions simultaneously arriving from very different angular directions. In addition, the strong direct signal interference (DSI) from the transmitter of opportunity, which typically dominates the received signal, must also be rejected, and further complicates the possibility of a simple calibration strategy.

In this context, the following main contributions are made by this work:

- An experimental assessment of the critical effects of channel imbalance in passive radar DPCA and of the limits of a calibration strategy based on the direct signal.

- The investigation of the potential benefits deriving from the integration of time-domain filtering methods, such as ECA, and the DPCA approach, for an effective suppression of DSI and clutter contributions.

- The development of adaptive clutter-based channel calibration strategies, derived from the SAR-GMTI literature and tailored for the passive radar case, which take advantage of the fine Doppler frequency resolution offered by the long CPIs typically used in these applications, to provide an angle-dependent compensation of channel imbalance.

- The demonstration against experimental data of the strict need for a localized digital calibration strategy to enable an effective DPCA clutter suppression in passive radar.

Then, to overcome the intrinsic limitations of a DPCA approach, attention is devoted to adaptive methodologies based on STAP, for systems featuring multiple receiving channels. In this case, the clutter cancellation capability is provided by the adaptivity of the space-time filter. Therefore, the effects of channel calibration errors on target signal can be addressed, mitigating the negative impact on target detection and localization performance.

In this context, the following main contributions are made by this work:

- The definition of a post-Doppler STAP approach for passive radar, which makes use of the long integration time and the resulting fine Doppler resolution to reduce the size of the adaptive problem and intrinsically compensate for the angle-dependent channel errors, by operating on a clutter subspace accounting for a limited angular sector.

- The introduction and performance assessment of novel space-time generalised likelihood ratio test (GLRT) schemes specifically devised for mobile passive radar in the presence of an unknown imbalance affecting the receiving channels.

- The characterization of the target angular localization problem in mobile passive radar featuring few wide beam antennas, which requires convenient exploitation of the spatial DOF both for space-time clutter filtering and for target DOA estimation.

- The definition of a calibration strategy for spatial steering vector in desired direction, which exploits the one-to-one relationship between angle of arrival and Doppler frequency of stationary scatterers and enables an accurate target DOA estimation.

Finally, efforts are aimed at further reducing the computational complexity of passive radar STAP in multichannel systems, as well as at increasing its robustness against adaptivity losses. In fact, the heterogeneity of a real clutter scenario, exacerbated by the bistatic acquisition geometry of passive radar exploiting ground-based illuminators, as well as by the anomalous propagation of long wavelength signals, may impact the effectiveness of STAP by limiting the number of relevant training data, usefully exploitable for adaptivity.

In this context, the following main contribution is made by this work:

- The introduction of a dual cancelled channel STAP approach, which allows to reduce the computational cost and simplify the target DOA estimation process, compared to the equivalent full array STAP solution. The considered scheme allows effective operation even in the case of a limited sample support, by reducing the number of adaptive DOF in the space-time processing steps.

It is finally worth noting, that the processing techniques and operational strategies devised in this work, which define a set of effective methodologies for GMTI in mobile passive radar, are all tested against real data. Specifically, the experimental validation exploits a set of data acquired by a multichannel passive radar receiver developed by Fraunhofer FHR, mounted on a ground moving platform and exploiting DVB-T transmissions.

1.4 Outline of the thesis

The remainder of this thesis is organized as follows.

Chapter 2 addresses the problem of DSI and clutter cancellation in mobile passive radar employing DPCA approach. Signal processing strategies are developed to compensate for the limitations deriving from imbalances affecting the two receiving channels. A two-stage approach is proposed, consisting of a preliminary DSI removal at each channel, followed by an effective DPCA clutter suppression, enabled by an adaptive channel calibration. Different clutter-based calibration strategies are analysed, aimed at maximizing the cancellation performance by compensating for angle dependent channel errors. The effectiveness of the scheme is demonstrated against experimental data from a DVB-T based mobile passive radar.

Chapter 3 considers the use of a post-Doppler STAP approach for clutter cancellation and moving target detection and localization in multichannel mobile passive radar, in the presence of an angle-dependent imbalance affecting the receiving channels. While the clutter suppression capability is guaranteed by the adaptive space-time filtering, different solutions are compared, aimed at mitigating the impact of channel calibration errors on target detection and localization performance. A spatially non-coherent detection scheme is compared with a fully coherent STAP detector, where clutter echoes are exploited for steering vector calibration. Finally, the target localization problem is addressed and the STAP scheme is employed for maximum likelihood (ML) estimation of target DOA, against the impact of channel imbalance. The effectiveness of the proposed strategies is validated against simulated and experimental data from a DVB-T based mobile passive radar.

Chapter 4 proposes a dual cancelled channel STAP scheme aimed at reducing the system computational complexity, as well as the number of required training data, compared to a conventional full-array solution. The proposed scheme is shown to yield comparable performance with respect to the equivalent full array solution, both in terms of target detection capability and DOA estimation accuracy, despite the lower computational cost. Moreover, it offers increased robustness against adaptivity losses, operating effectively even in the presence of a limited set of training data, as often available in highly non-homogeneous clutter scenarios experienced in bistatic passive radar. The effectiveness of the proposed scheme is tested against simulated and experimental data from a DVB-T based multichannel mobile passive radar, proving its suitability for passive radar GMTI applications.

Chapter 5 summarizes the main results of this study and provides an outlook for further work.

Chapter 2

Passive Radar DPCA schemes with adaptive channel calibration

This Chapter addresses the problem of DSI and clutter cancellation in passive radar on moving platforms employing DPCA approach. The attention is focused on the development of signal processing strategies able to compensate for the limitations deriving from the amplitude and phase imbalances possibly affecting the two channels employed on receive. Section 2.1 introduces the main addressed issues and the motivations behind the study. In Section 2.2, the adopted signal model and the processing scheme are described. Section 2.3 illustrates the acquisition campaign and the experimental dataset and gives evidence of the limits of using the direct signal from the illuminator of opportunity as a source for channel calibration, due to angle-dependent channel imbalances. Section 2.4 introduces a two-stage cancellation approach, which consists of a preliminary DSI removal at each channel, followed by DPCA clutter suppression, made effective by a clutter-based channel calibration. In Section 2.5, different strategies for adaptive channel calibration are investigated, aimed at maximizing the cancellation performance by compensating for the angle and range dependent channel errors. In Section 2.6, the effectiveness of the scheme is demonstrated against experimental data from a DVB-T based mobile passive radar in the presence of both real and synthetic moving targets. Finally, conclusions are drawn in Section 2.7.

2.1 Introduction

The detection of slow-moving targets against a Doppler-spread clutter induced by receiver motion represents one of the main challenges of mobile passive radar and required the use of multiple receiving channels and space-time processing techniques. As stated in the previous Chapter, the desirable low-cost characteristic of passive radar, the typical size of antennas at VHF/UHF bands and the high data rate of digital broadcast transmissions suggest the use of only few spatial channels and a simple processing scheme. For this reason, a DPCA approach has been primarily considered.

Conventional DPCA performs a non-adaptive subtraction of properly delayed radar echoes collected by two along-track displaced receiving channels, [46]. Thus, it requires a simple

architecture and limited computational load, which make it attractive for the passive radar application. Notice that DPCA and more in general space-time processing intended for passive radar require the availability of at least two surveillance channels; reference signal can be whether reconstructed from one of them or received by a dedicated reference channel.

As known, DPCA poses strong constraints on the antenna phase centres alignment and it is intrinsically sensitive to imbalances between the receiving channels, which have to be identical to provide an effective suppression of the stationary scene returns. For this reason, the scheme in [15] includes a simple approach for channel calibration, which compensates for the amplitude and phase inequalities by exploiting the direct signal contribution from the transmitter, assumed as a strong and reliable source. In principle, DSI can be seen as a stationary return and DPCA should suppress it together with the other clutter components.

Following the preliminary analysis in [17] and [18], it is shown that channels imbalance can be angle dependent due to non-identical receiving antenna patterns (especially outside the main lobe region). This might be a critical problem in passive radar, typically employing low directivity antennas in VHF/UHF bands, especially when clutter echoes and DSI come from different directions of arrival (DOA). In this case, the simple calibration proposed in [15] proves to be ineffective and alternative solutions should be found.

Channel imbalance is a well-known issue in conventional active radar. Its role has been largely analysed in literature in the context of array beamforming and space-time processing [46],[47]. For specific applications and operational conditions, an accurate factory or in-field calibration might be not feasible or not sufficient. Methods for array self-calibration have been studied [52]-[56], as well as space-time techniques in the presence of steering vector mismatch [57]-[59]. Specific strategies for adaptive digital channel calibration based on the received data have been developed in [60]-[63] for the case of SAR-GMTI, taking advantage of the clutter angle-Doppler dependence.

This study aims at developing ad-hoc solutions for the passive radar case, when using a DPCA approach for clutter cancellation. For this purpose, we need to tackle all the critical aspects brought in by the passive bistatic operation, while preserving the low-cost approach provided by the DPCA technique. Among the critical aspects, the use of COTS components and the wavelength of the typically exploited signals of opportunity may pose some limitations to a preliminary system calibration. Moreover, the low directivity of receiving antennas, the typical sidelobe level, and the bistatic geometry characterized by predominantly omni-directional transmissions determine the need for an accurate channel calibration on a very wide angular sector in order to achieve a good clutter cancellation, especially for an essentially non-adaptive approach like DPCA. This is further exacerbated by the presence of a strong continuous-wave direct signal component coming from the illuminator of opportunity and by its multipath replicas. However, the typical passive radar operates with very long integration times, which potentially provide a fine Doppler frequency resolution and in turn a good angular discrimination capability.

Different strategies for digital channel calibration are proposed, directly operating on the range-Doppler maps and exploiting the clutter returns. Starting from the simple estimation of a single calibration coefficient, the flexibility of the calibration model is progressively increased, in order to compensate for potential angle and range dependent channel errors, thus maximizing the resulting cancellation capability at the output of the DPCA subtraction.

The effectiveness of the considered processing scheme, along with the channel calibration approaches, is investigated against experimental data from a DVB-T based passive radar system mounted on a ground-based moving vehicle. The performance is analysed in terms of disturbance cancellation capability, as well as of signal-to-clutter-plus-noise ratio (SCNR) improvement against a real cooperative aerial target, employed during the experimental campaign. In addition, results are reported also for synthetic targets injected into the real clutter data.

2.2 Signal model and processing scheme

2.2.1 System geometry and signal model

Let us consider a passive radar receiver mounted on a moving platform that exploits a ground-based transmitter as illuminator of opportunity (see Figure 2.1). The platform moves at constant velocity v_p on a straight line. Two parallel receiving channels are available, displaced by d in the along-track direction, in a side-looking configuration. They are referred to as leading antenna (LA) and trailing antenna (TA).
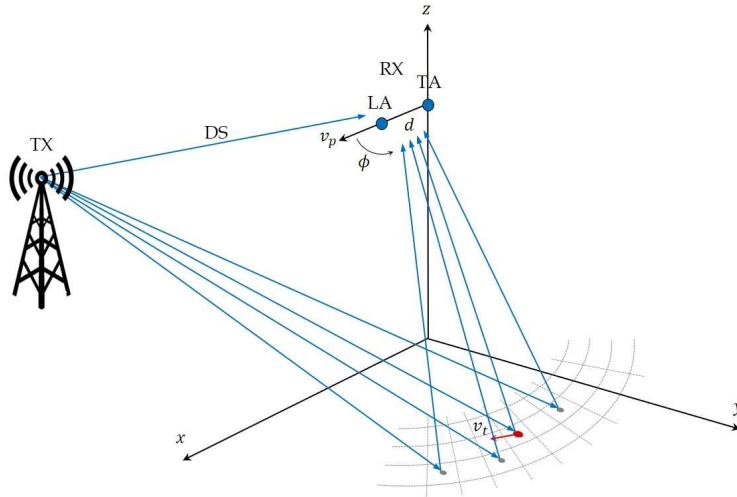
Figure 2.1: System geometry for a dual-channel mobile passive radar exploiting a ground-based stationary transmitter as illuminator of opportunity.

The discrete time baseband signal representing the clutter contribution received at the two antennas can be expressed as the superposition of echoes from stationary scatterers at different bistatic ranges R_q $(q = 1, \dots, N_R)$ and different angles ϕ:

$$r_C^{(LA)}[l] = \sum_{q=1}^{N_R} \int_\phi G_q^{(LA)}(\phi) \, A_q(\phi) \sum_n s_n\big[l - nL - l_{\tau_q}\big] e^{j2\pi \frac{v_p}{\lambda} \cos \phi nT} \, d\phi$$

$$(2.1)$$

$$r_C^{(TA)}[l] = \sum_{q=1}^{N_R} \int_\phi G_q^{(TA)}(\phi) \, A_q(\phi) \sum_n s_n\big[l - nL - l_{\tau_q}\big] e^{j2\pi \frac{v_p}{\lambda} \cos \phi \, nT} e^{-j2\pi \frac{d}{\lambda} \cos \phi} d\phi$$

where

- ϕ denotes the angle between the platform velocity vector and the receiver to scatterer line of sight (LOS), while l is the time index, representing the l-th sample of the signal sampled at frequency f_s;

- the transmitted signal has been partitioned in batches of duration T and $s_n[l]$ denotes the n-th batch, including $L = Tf_s$ samples; notice that the Doppler induced phase term within each batch has been neglected;

- $A_q(\phi)$ is the complex amplitude and $l_{\tau_q} = f_s R_q/c$ the bistatic propagation delay of echo from clutter patch at angle ϕ and range R_q;

- $G_q^{(LA)}(\phi)$ and $G_q^{(TA)}(\phi)$ are the complex gains of the LA and TA channels respectively; they represent the overall receiver chains, there including the antenna patterns, and encode possible amplitude and phase imbalance between the two channels;

- $f_D(\phi) = \frac{v_p}{\lambda} \cos \phi$ is the bistatic Doppler frequency of the generic clutter patch at angle ϕ, λ being the signal carrier wavelength;

Notice that the expressions above might also include the direct signal contribution from the exploited illuminator of opportunity.

2.2.2 DPCA processing scheme

The considered processing scheme, originally presented in [15] for a DVB-T based passive radar, is sketched in Figure 2.2. After a pre-processing stage, including synchronization to the transmitter and demodulation/remodulation of the reference DVB-T signal, the bistatic range-Doppler map is evaluated by means of a batch processing strategy:

i. the received signal is subdivided into short consecutive batches of duration T, deliberately selected to be equal to single OFDM symbols;

ii. range compression is performed on a batch-by-batch basis, using the reconstructed version of the reference signal and implementing a reciprocal filtering strategy;

iii. consecutive batches are coherently combined by means of a discrete Fourier transform (DFT) to synthesize the Doppler dimension.

The batches processing architecture significantly reduces the computational load in passive radar exploiting wideband digital waveform. Moreover, it recreates the conventional fast-
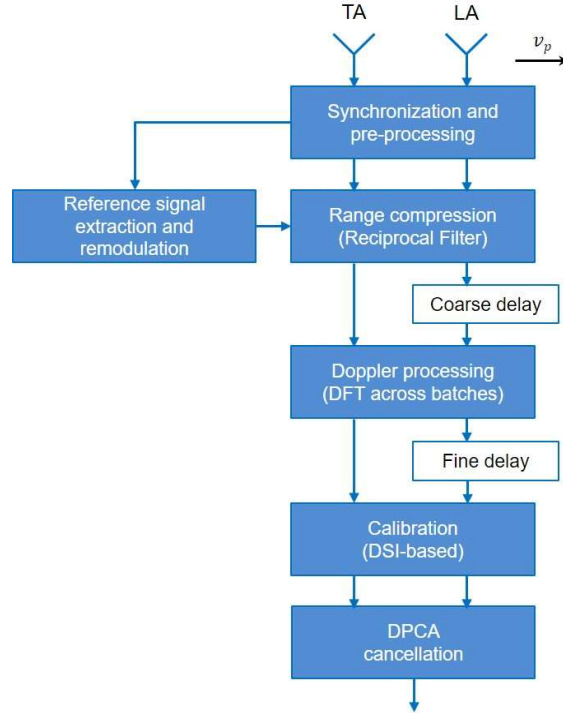
Figure 2.2: Sketch of the flexible DPCA processing scheme as proposed in [15].

time/slow-time framework of a pulsed radar operating at an equivalent PRF given by the inverse of the batch length ($\text{PRF} = 1/T$).

The use of a reciprocal filter at the range compression stage has a twofold objective.

On the one hand, it allows to control the sidelobes level and mitigate the undesired structure and grating lobes arising in the signal ambiguity function, which may hinder the detection of target echoes, especially when OFDM transmissions are exploited [39]-[44]. In Figure 2.3, the impulse responses of one DVB-T symbol after range compression by means of a matched filter and a reciprocal filter are compared.

On the other hand, the use of the reciprocal filter yields significant advantages to the subsequent DPCA stage [15]. In fact, at the expense of a limited and predictable loss compared to the matched filter, the reciprocal filter allows to remove the temporal variability

(a)   (b)
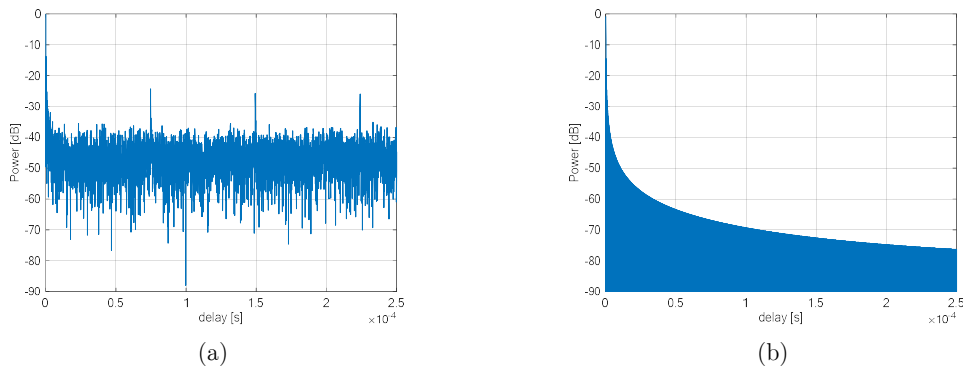
Figure 2.3: Impulse response of one DVB-T symbol after (a) mathed fitler and (b) reciprocal filter.

of the batch impulse response, due to the time-varying characteristics of the employed waveform of opportunity, so that an ideal clutter cancellation can be in principle obtained based on subsequent observations of a stationary scene. Notice that, in order to benefit from the two advantages above, a perfect reconstruction of the reference signal should be made available via the mentioned decode/recode approach. This intrinsically removes the effect of the multipath contributions to the reference signal.

A DPCA stage is then applied by resorting to a flexible technique, which allows to relax the constraint posed on the equivalent PRF. For bistatic radar employing a stationary transmitter, DPCA condition is given by:

$$T_{DPCA} = K * PRI = K * T = d/v_p \tag{2.2}$$

where K is the integer number of symbols after which the two-way phase centres occupy the same position. Since this condition is hardly verified in real environment, in flexible-DPCA technique, the required time shift is performed in two steps: a coarse delay T_q quantized to the equivalent PRI is applied in time domain; a residual fine delay T_f is compensated in frequency domain by a linear phase term. In detail:

$$T_q = \left\lfloor \frac{d}{v_p T} \right\rfloor T$$
$$\tag{2.3}$$
$$T_f = T_{DPCA} - T_q$$

The platform velocity must be measured by means of an inertial measurement unit (IMU) or estimated from the data. Based on this strategy, DPCA condition can be effectively established also when a batches architecture is adopted.

The described processing scheme should in principle provide an ideal cancellation of stationary background, by means of a simple subtraction of the delayed observations from the two channels, provided that the following conditions are met:

- perfect DPCA condition established by compensation of time delay according to (2.3);
- negligible internal clutter motion (ICM), i.e. constant amplitude $A_q(\phi)$ within the CPI;
- compensation of the potential amplitude and/or phase imbalance between the receiving channels.

Therefore, even assuming the first two conditions, DPCA performance strongly relies on the adoption of a proper calibration strategy before channel subtraction (see calibration block in Figure 2.2).

Starting from the signal model in (2.1) and following the same formalism adopted in [15], after range compression by reciprocal filtering, delay compensation and Doppler processing,

the clutter contribution at the generic range-Doppler bin $[l, m]$ of LA and TA channels can be expressed as follows:

$$z_C^{(LA)}[l, m] = \sum_{q=1}^{N_R} \int_{\phi} G_q^{(LA)}(\phi) \, A_q(\phi) \, g_r\left[l - l_{\tau_q}\right] g_d\left[\frac{m}{NT} - \frac{v_p}{\lambda}\cos\phi\right] \, d\phi$$

$$z_C^{(TA)}[l, m] = \sum_{q=1}^{N_R} \int_{\phi} G_q^{(TA)}(\phi) \, A_q(\phi) \, g_r\left[l - l_{\tau_q}\right] g_d\left[\frac{m}{NT} - \frac{v_p}{\lambda}\cos\phi\right] \, d\phi$$

(2.4)

where $g_r[l]$ denotes the output of reciprocal range compression filter, equal for each signal batch, and $g_d[m]$ denotes the output of Doppler processing over N consecutive batches (equal to a digital sinc function in case of uniform windowing [15]). Notice that generic cell $[l, m]$ is characterized by the superposition of clutter echoes from different range cells and different angular positions. As apparent, the clutter cancellation achievable by subtraction of the two range-Doppler maps in (2.4) would be hindered by the imbalance between receiving channels $\Gamma_q(\phi) = G_q^{(TA)}(\phi)/G_q^{(LA)}(\phi)$.

The simplest model for channel calibration is based on the assumption of an angle-invariant amplitude and phase channel imbalance, namely $\Gamma_q(\phi) = \Gamma_0$, that can be easily compensated for by applying a single complex multiplicative coefficient at one of the two channels output. This was basically the model adopted in [15], where the sought coefficient was estimated based on the DSI contribution. However, in the following, it is shown that such a simplifying hypothesis, in some cases, does not guarantee an effective calibration of the receiving channels, hence more realistic models will be adopted for the channels imbalance by properly taking into account the angle dependency.

2.3 Experimental data and limitations of a DSI-based channel calibration

2.3.1 Overview of the acquisition campaign

The proposed processing schemes and channel calibration strategies are tested against a set of experimental data acquired by a DVB-T based multichannel passive radar system mounted on a ground moving platform.

The acquisition campaign was conducted by Fraunhofer FHR in a rural area of the Eifel region, in western Germany. The selected DVB-T illuminator of opportunity was the Eifel/Scharteberg transmitter, shown in Figure 2.4(a). The passive radar system consisted of four receiving channels, serving as surveillance channels, connected to discone antennas (omni-directional in azimuth), and displaced in the along-track direction. As receivers two PARASOL units, designed by Fraunhofer FHR, were employed, each providing two receiving

channels [64]. Radiation absorbing material (RAM) was placed on one side, in order to attenuate the back lobes contributions and thus forming a single side-looking configuration. A close-up of the array is shown in Figure 2.4(c). Notice that only four central elements were connected to the receiving units, while the external ones were dummy elements resistively loaded. The system was mounted on a trailer behind a van (see Figure 2.4(b)). The parameters of the exploited DVB-T transmission are reported in Table 2.1, as well as the main system and processing parameters.

For the purpose of our study, the signals collected by only two out of the four receiving channels are exploited, in order to analyse the effects of different channel calibration strategies in the considered DPCA scheme. Specifically, the channels associated to adjacent antenna pairs are employed. The reference signal is reconstructed from the signal collected at one of the surveillance channels.

An ultralight aircraft from Fraunhofer FHR (Delphin) has been employed as a cooperative target during the acquisition campaign (see Figure 2.4(d)). The considered case study is characterized by a bistatic geometry where the transmitter is located approximately in the direction opposite to the observed scene, with direct signal impinging on the antenna back-lobes (see Figure 2.5(a) for a sketch of the acquisition geometry).

(a)   (b)

(c)   (d)
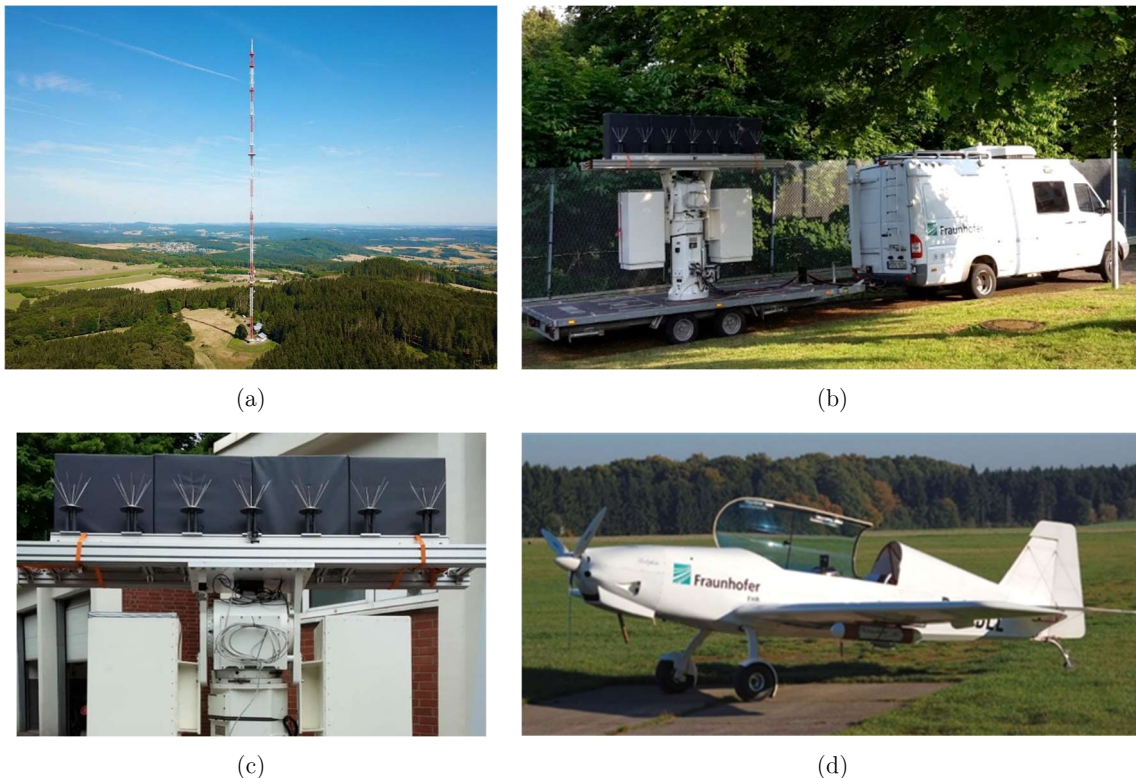
Figure 2.4: (a) The Eifel/Scharteberg transmitter of opportunity. (b) The experimental multi-channel receiver mounted on the back of a van in side-looking configuration. (c) A detailed view of the receiving antenna array. (d) The aircraft (Delphin) employed as cooperative aerial target.

Table 2.1

Parameters of experimental test

Symbol	Description	Value
DVB-T signal parameters		
	DVB-T Standard	8k 16QAM
f_c	Carrier frequency	690 MHz
N_c	Number of useful carriers	6817
T_u	Useful symbol duration	896 us
T_g	Guard interval duration	224 us
T_s	OFDM symbol duration	1120 us
B	Bandwidth	7.61 MHz
System and processing parameters		
v_p	Platform velocity	~13.8 m/s
d	Antenna spacing	0.36 m
CPI	Coherent processing interval	512 T_s

(a)   (b)
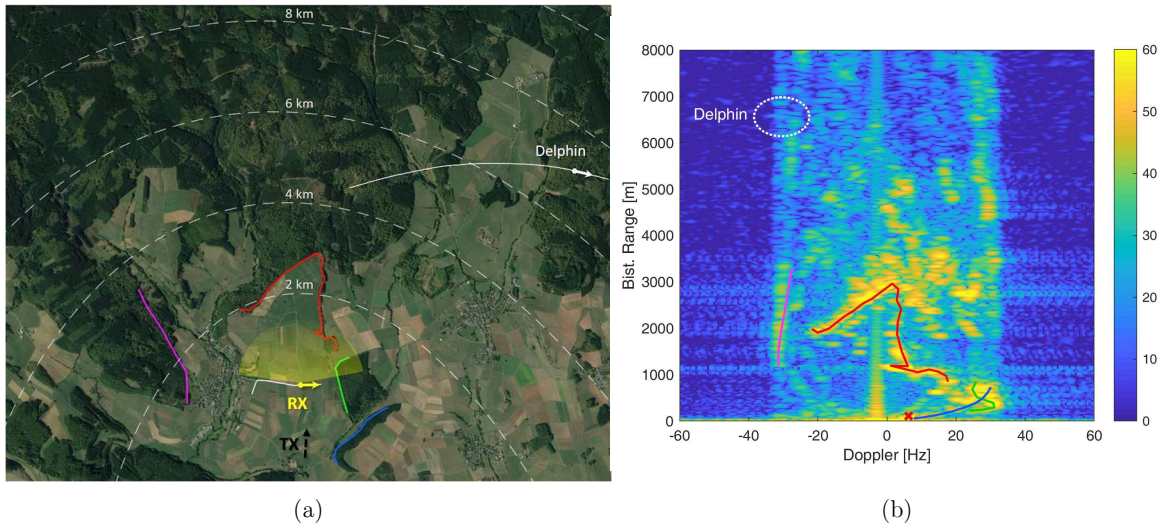
Figure 2.5: (a) Optical image showing the acquisition geometry. The receiver and aerial target position and direction of motion are indicated with yellow and white arrows, respectively. Black arrow indicates the transmittter direction of arrival. Dashed lines represent the bistatic iso-range curves. (b) Corresponding single channel range-Doppler map. Coloured lines indicate some distributions of strong scatterers from the area surrounding the passive radar during the acquisition and how they are mapped into the bistatic domain.

2.3.2 Analysis of the data

An example of range-Doppler map obtained from a single channel, namely before DPCA, is reported in Figure 2.5(b). Specifically, a coherent processing interval (CPI) of 512 $T_s \cong$ 0.57 s is considered and a Taylor windowing is applied in both range and Doppler domain,

in order to limit the sidelobes level of the ambiguity function down to $-40\ dB$ below its main peak. Notice that the resulting range-Doppler map is oversampled and scaled in amplitude to the estimated noise power level.

A strong DSI contribution appears at the first bistatic range bin and at Doppler frequency $-3.3\ Hz$; this low Doppler value is due to the angle formed by the Rx-Tx LOS and the platform velocity vector, which is close to 90° in the considered data file (see Figure 2.5(a)).

Given the platform velocity and the employed antennas, echoes from the stationary scene extend in Doppler frequency over a bandwidth of approximately $\pm v_p/\lambda \cong \pm 32\ Hz$ and are characterized by a strong heterogeneity in terms of power levels across the map (wide dynamic range); also, we observe the presence of large clutter discretes. In the reported map, the bistatic range is limited to the first 8 km, since in this acquisition few appreciable clutter contributions are present beyond that limit due to the terrain conformation (the passive radar system was operated in a hilly region).

By comparing the obtained range-Doppler map with the optical image in Figure 2.5(a), a few distributions of strong scatterers can be easily identified. Notice that, in Figure 2.5(b), these are indicated by coloured lines obtained by projecting onto the bistatic domain the curved lines in homologous colours in Figure 2.5(a). This analysis allows to better understand the characteristics of the clutter scene under consideration, as well as intrinsic limitations to the cancellation capability.

It is worth noting that the strong clutter contributions mainly arise from densely vegetated areas. In fact, the lines in Figure 2.5(a) typically lie on the perimeter of such areas, being the first line of trees responsible of the strongest returns.

Assuming, for the sake of simplicity, a Gaussian model for the power spectral density of the ICM due to windblown clutter, a typical RMS spectral width from 0.1 to 0.3 m/s is obtained [65], corresponding to wind speed from 1 to 30 mph. This would result in a clutter correlation coefficient in the order of $\rho(T_{DPCA}) = 0.975-0.997$ for the case under consideration. Therefore, to a first approximation, clutter attenuation performance of a single canceller is expected to be limited to $CA = [0.5/(1 - Re\{\rho(T_{DPCA})\}] \cong 13-22\ dB$ due to the sole effect of ICM [66].

Importantly enough, especially in the first kilometre, returns are affected by a superposition of front and back clutter echoes. Moreover, the area is characterized by the presence of wind turbines, located in the back-lobe direction and indicated with a red cross in Figure 2.5(b). The cooperative aerial target, whose expected position is indicated by a white ellipse in Figure 2.5(b), appears as buried into clutter background.

2.3.3 Results after channel calibration based on direct signal

In [15], the simplest approach was adopted for channel calibration, based on the direct signal coming from the exploited transmitter. A single complex coefficient is evaluated at the range-Doppler bin corresponding to the DSI, to compensate for channel imbalance, which is

assumed to be angle invariant, i.e. $\Gamma_q(\phi) = \Gamma_0$. Specifically, the complex correction coefficient is evaluated as:

$$\widehat{\Gamma}_0 = \frac{z^{(TA)}[l_{tx}, m_{tx}]}{z^{(LA)}[l_{tx}, m_{tx}]} \tag{2.5}$$

where $z^{(\gamma)}[l_{tx}, m_{tx}]$ is the complex value of range-Doppler map at location corresponding to the direct signal for the $\gamma = 'TA'/'LA'$ channel. This approach can rely on a strong and reliable source and proved to be effective in the analysis conducted in [15]-[16], where a dominant DSI contribution was present impinging on the main-lobe of the receiver antennas.

Unfortunately, under more general conditions, the direct signal is not representative of the overall clutter distribution in terms of amplitude and phase calibration requirements. This might be the case when the DSI DOA is not within the antenna main beam, but rather it impinges on the sidelobes or the back-lobes regions, where the patterns of the employed antennas are likely to differ.

This is shown in Figure 2.6 that reports the results of the application of the flexible-DPCA scheme to the selected data file, when adopting the DSI-based calibration strategy against a DSI signal impinging on the receiver antenna back-lobes. Notice that all range-Doppler maps are scaled so that 0 dB corresponds to the estimated noise power level, to allow a direct comparison of results. By comparing Figure 2.5(b) and Figure 2.6, it is evident how cancellation effectively occurs only for the DSI contribution, while echoes from stationary scene are only slightly attenuated or partially suppressed.

In order to measure the effectiveness of clutter suppression and compare the results of different approaches, we resort to the cancellation ratio (CR), which expresses the attenuation in clutter power provided by the DPCA stage. It is defined as:

$$CR[l, m] = \frac{P_c^{in}[l, m]}{P_c^{out}[l, m]} \tag{2.6}$$

where $P_c^{in}[l, m]$ is the clutter power measured at the generic delay-Doppler bin of maps obtained at the single channels (an average value is considered between the LA and TA channels) and $P_c^{out}[l, m]$ is that measured after the application of DPCA.

Figure 2.7 shows the CR map obtained for the result in Figure 2.6. As expected, perfect cancellation is obtained for the range-Doppler bin corresponding to DSI and high CR values are observed for the corresponding sidelobes contributions. Notice that the reported CR map has been upper limited to 20 dB, to facilitate the analysis of the small CR values; however, the CR values obtained at the DSI sidelobes are typically higher. Conversely, the average power reduction measured in the area corresponding to the overall endo-clutter region is less

than 6 dB, well below the predicted values according to the observed clutter characteristics, i.e., the expected ICM.

Such limitation could be in principle caused by a number of factors other than the ICM. However, in the following, it is shown that mostly residual channel imbalance prevents the clutter echoes from being effectively cancelled. This result can be mainly attributed to angle-dependent differences in the patterns of the employed surveillance antennas and gives evidence of the limits of a calibration approach based on the DSI and, more in general, of the simplified model of a uniform inter-channel imbalance.
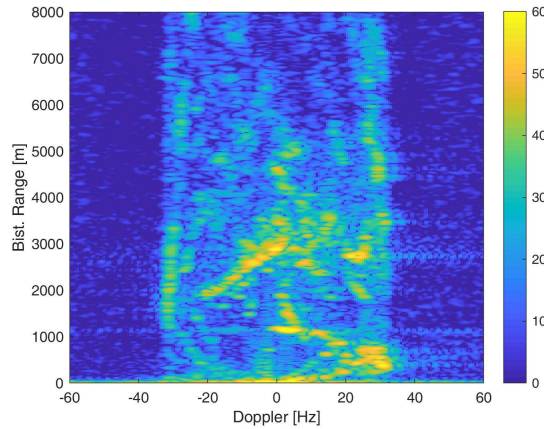
Figure 2.6: Range-Doppler map after DPCA with DSI-based calibration.
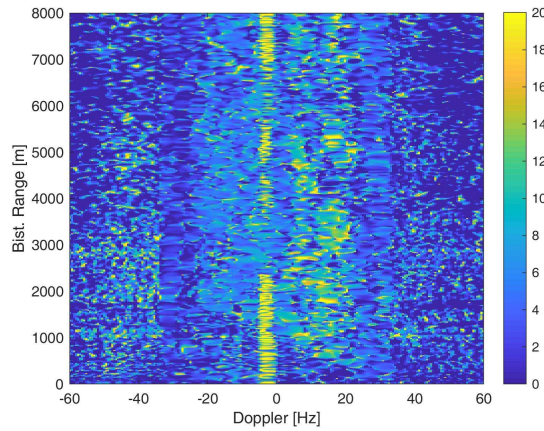
Figure 2.7: Cancellation Ratio obtained after DPCA with DSI-based calibration.

2.4 Two-stage cancellation approach

The analysis reported in the previous Section suggests the need for alternative calibration approaches based on the exploitation of clutter echoes instead of DSI. However, the direct-path component and related side-lobes are largely overlapped with clutter contributions in

the range-Doppler map. This may represent a major concern for imbalance estimation if the DSI is not effectively counteracted.

Therefore, in this Section, a two-stage cancellation approach is proposed, which allows for a combined suppression of DSI and clutter contributions. This approach was preliminarily considered in [17], where it was adopted in conjunction with a simple channel calibration strategy, as briefly summarized in the following. This two-stage approach is further extended in [20] to include more effective calibration strategies.

The idea is to firstly suppress the DSI on both surveillance channels in time domain, by resorting to extensive cancellation algorithm (ECA) techniques; then, clutter cancellation is performed in space-time domain via DPCA, after a clutter-based channel calibration. Accordingly, the resulting processing scheme is sketched in Figure 2.8.

ECA techniques [67]-[70] are able to remove DSI by projecting the surveillance signal into a subspace orthogonal to the direct signal. In this case the ECA-CD (ECA by carrier and Doppler) version of the algorithm is adopted, which operates carrier by carrier by exploiting the OFDM modulation of the considered waveforms [70]. Specifically, a proper Doppler shift is applied to the available reference signal, to centre the disturbance removal filter on the estimated DSI Doppler bin. Additionally, the filter spans over a couple of adjacent Doppler bins in order to improve the suppression of the DSI and the associated sidelobes.
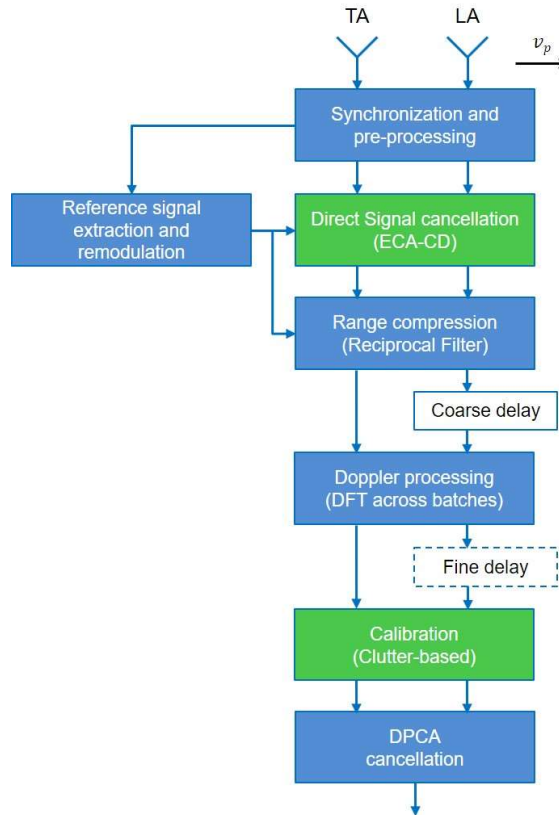
Figure 2.8: Modified processing scheme implementing the proposed two-stage cancellation approach.

It is assumed that a significant difference in amplitude and phase channel imbalance $\Gamma(\phi)$ exists between the DSI, typically dominant and coming from a specific direction, depending on the geometry, that might even correspond to the antenna back-lobes, and the main clutter background, mostly coming from a range of directions inside the antenna front lobe, where the imbalance is supposed to be almost invariant. Therefore, after DSI removal, channel calibration is performed based on clutter contributions appearing in the resulting range-Doppler maps, no longer affected by the direct signal component.

Aiming at preserving the paradigm of a simplified approach, it is initially considered the estimation of a single complex calibration coefficient maximizing the clutter cancellation at the subsequent DPCA stage for all the whole forward sector of the antenna patterns.

Starting from the model in (2.4), it is assumed that, after suppression of the DSI, the remaining clutter contributions are affected by an approximately uniform imbalance, i.e. $G_q^{(TA)}(\phi)/G_q^{(LA)}(\phi) = \Gamma_c$. Therefore, for clutter signal at the output of the two range-Doppler maps, the following relation holds: $z_c^{(TA)}[l, m] = \Gamma_c * z_c^{(LA)}[l, m]$.

Channel imbalance can then be estimated by resorting to a least square approach operated on the overall endo-clutter area. Specifically, we look for the calibration coefficient minimizing the power at the output of the DPCA subtraction:

$$\widehat{\Gamma_c} = \operatorname*{argmin}_{\Gamma} \left\{ E\{|z^{(TA)}[l,m] - \Gamma * z^{(LA)}[l,m]|^2\} \right\} = \frac{E\{z^{(TA)}[l,m]\, z^{(LA)*}[l,m]\}}{E\{|z^{(LA)}[l,m]|^2\}} \qquad (2.7)$$

where * indicates the complex conjugate and $z^{(\gamma)}[l, m]$ is the complex value of range-Doppler map at the $\gamma =$ "TA"/"LA" channel, including clutter and noise. In this case, the TA channel is arbitrarily taken as reference and the LA channel is adjusted by multiplying with $\widehat{\Gamma_c}$.

In practice, the expected values in (2.7) are replaced by their estimates obtained over proper clutter regions. For instance, by selecting a rectangular clutter area with range extent limited between indexes l1 and l2 and Doppler extent limited between indexes m1 and m2, the calibration coefficient can be evaluated as:

$$\widehat{\Gamma_c} = \frac{\sum_{l=l_1}^{l_2} \sum_{m=m_1}^{m_2} z^{(TA)}[l,m]\, z^{(LA)*}[l,m]}{\sum_{l=l_1}^{l_2} \sum_{m=m_1}^{m_2} |z^{(LA)}[l,m]|^2} \qquad (2.8)$$

The presented two-stage approach allows to achieve a combined suppression of both DSI and clutter, despite adopting a strategy based on a single calibration coefficient (SCC), provided that this is estimated based on clutter contributions. The advantages of this approach are not only due to the addition of a dedicated cancellation stage devoted to the removal of the DSI but also to the mitigation of the effects of the DSI on the subsequent calibration stage. In fact, it was shown that a poorer cancellation capability is obtained

against the stationary scene if the calibration coefficient is estimated before the removal of the DSI overlapping on the range-Doppler map.

Figure 2.9 shows the range-Doppler map obtained after applying the two-stage cancellation scheme against the data set under consideration in this work. Calibration is performed, according to (2.8), based on the overall endo-clutter region: bistatic range interval within [150;8000] m and Doppler frequency interval [-32;32] Hz. The first few range cells are skipped in order for the calibration not to be affected by additional back lobes clutter echoes and the aforementioned wind turbines. The corresponding CR maps are reported in Figure 2.10 (a) and (b), for the ECA-CD stage and the final DPCA stage respectively, in order to address the effects of each cancellation stage separately.

As expected, the DSI is largely cancelled by the ECA-CD stage and clutter power is significantly attenuated by the following DPCA stage. Focusing on cancellation performance of the DPCA stage, a remarkable clutter attenuation is now achieved, with an average power reduction in the endo-clutter region that exceeds 14 dB and CR values up to 25 dB at specific range-Doppler locations. The residual uncancelled clutter power in the final map highlights
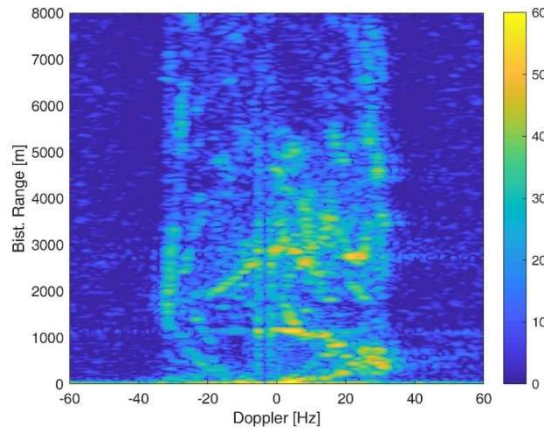
Figure 2.9: Range-Doppler map after two-stage cancellation scheme with SCC approach.

(a)   (b)
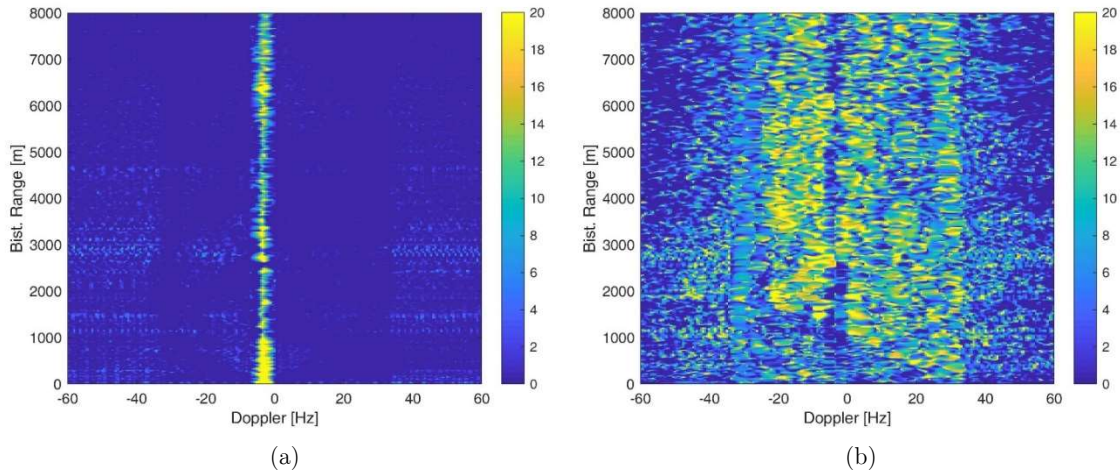
Figure 2.10: Cancellation Ratio obtained: (a) after ECA-CD stage only; (b) after DPCA stage with SCC approach.

the presence of further limitations to DPCA performance, potentially related to several effects, such as irregular platform motion, possible antenna misalignment and crabbing, mutual coupling effects, as well as the ICM.

However, by observing Figure 2.10 (b), one might notice that the CR values are much higher at specific Doppler intervals while they significantly reduce moving across the Doppler dimension. Unfortunately, this is the case of the Doppler region where the cooperative target Delphin lies and this does not allow to easily discriminate its echoes from the surrounding residual clutter.

As well known, for stationary scene echoes received by a moving radar, there is a direct mapping between Doppler frequency and azimuth angle of arrival. Based on this consideration, the above analysis suggests that additional angle-dependent channel imbalances should still be compensated for by resorting to more sophisticated calibration strategies, which will be introduced in the next Section.

2.5 Adaptive clutter-based calibration techniques

Several factors can influence the amplitude and phase response of receiving channels. Dissimilarities in antenna patterns, interaction with near-field obstacles, mutual coupling effect between array elements, and other potential sources of errors may cause non-negligible variations of channel imbalance as function of the angle of arrival. These variations can considerably limit DPCA cancellation performance even for clutter echoes coming from the front lobe region after a preliminary DSI suppression.

In order to investigate the effect of an angle-dependent channel imbalance on the clutter cancellation performance of the DPCA scheme, a simulated clutter scenario for a moving passive radar is considered. This also removes any other factor potentially affecting the experimental data.

Clutter returns are generated according to (2.1), for a scene spanning $N_R = 250$ range cells. Amplitudes $A_q(\phi)$ associated with different clutter patches are assumed independent and identically distributed complex gaussian variables, resulting in a homogeneous clutter scenario. Omnidirectional antennas are considered, within an angular sector $[0, \pi]$ (no back-lobe contributions). A DVB-T sequence is used as reference signal. Geometry, signal and system parameters are selected to match those of the experimental setup (see Table 2.1). The generated input signal includes clutter returns and thermal noise with an input clutter-to-noise-ratio (CNR) of 20 dB; to this purpose, the overall clutter contribution is scaled to have a power level of 20 dB above noise level (deliberately set to unity), at the input of each channel. Absence of ICM is assumed and a simulated angle dependent imbalance $\Gamma(\phi)$ between the two receiving channels is included. Specifically, a sinusoidal phase imbalance is assumed, both in azimuth and elevation angle, which maps onto the Doppler frequency axis as illustrated in Figure 2.11(a).

The range-Doppler map obtained from a single channel is reported in Figure 2.11(b). The corresponding range-Doppler map at the output of the DPCA scheme is shown in Figure 2.11(c), when a SCC strategy is applied for channel calibration. As expected, only the average component of the imbalance is corrected and an imperfect clutter cancellation is achieved, due to the uncompensated imbalance fluctuation. Therefore, a Doppler-dependent clutter cancellation performance is obtained, being the highest cancellation achieved where the phase imbalance is close to its average value.

In order to compensate for these effects and further improve clutter attenuation performance, more refined clutter-based channel calibration strategies are introduced and compared below. All the considered strategies rely on the two-stage cancellation scheme presented in Section 2.4, but they overcome the simplified approach based on a single calibration coefficient by looking for a set of coefficients to be applied across one dimension or two dimensions, namely Doppler or range/Doppler.
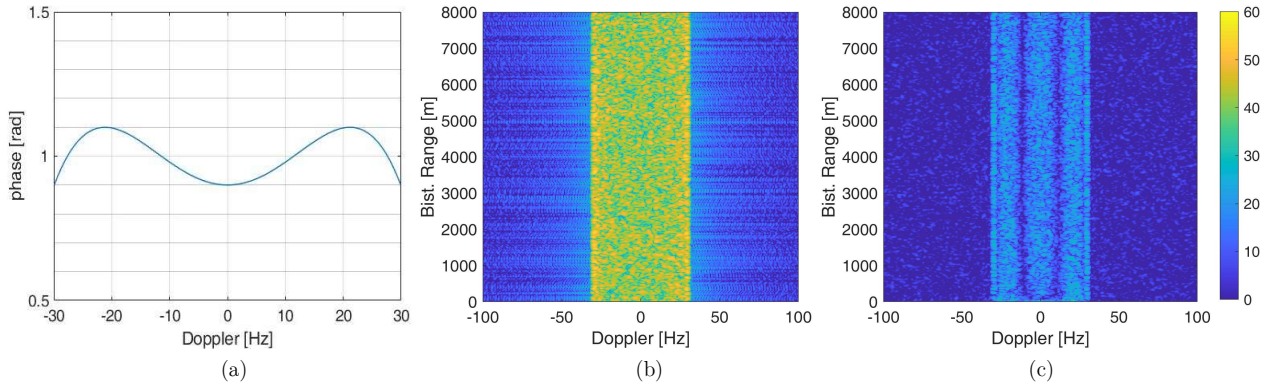
Figure 2.11: Effect of angle dependent channel imbalance in simulated clutter scenario: (a) simulated phase imbalance as a function of Doppler frequency; (b) single channel range-Doppler map; (c) range-Doppler map after DPCA with SCC approach.

2.5.1 Doppler dependent calibration (DDC)

Starting from the model in (2.4), we now consider the potential variation of channel imbalance as a function of the angle of arrival, i.e. $G_q^{(TA)}(\phi)/G_q^{(LA)}(\phi) = \Gamma(\phi)$. It is assumed that clutter returns at a generic Doppler bin m are dominated by the response of the scatterers belonging to the angular sector defined by the Doppler resolution, while contributions from different directions are negligible. This assumption holds when an appropriate windowing is adopted at the Doppler processing stage, which yields low sidelobes for the $g_d[m]$ function in (4). For the sake of clarity, the angular sector is centred at ϕ_m so that $\frac{v_p}{\lambda}\cos\phi_m = m\,\delta f$ and its width is given by $\delta\phi_m \cong \frac{\lambda}{v_p\sin\phi_m}\delta f$, δf being the Doppler resolution.

For sufficiently high Doppler resolution (narrow angular sector) and/or sufficiently slow variation of $\Gamma(\phi)$, the clutter contributions at the output of the two range-Doppler maps can be expressed as:

$$z_C^{(LA)}[l,m] = \sum_{q=1}^{N_R} G_q^{(LA)}(\phi_m) \ A_q(\phi_m) \ g_r\left[l - l_{\tau_q}\right] g_d[0] \ \delta\phi_m$$
$$z_C^{(TA)}[l,m] = \sum_{q=1}^{N_R} G_q^{(TA)}(\phi_m) \ A_q(\phi_m) \ g_r\left[l - l_{\tau_q}\right] g_d[0] \ \delta\phi_m \tag{2.9}$$

As a result, for clutter signal the following relation holds: $z_c^{(TA)}[l,m] \cong \Gamma(\phi_m) * z_c^{(LA)}[l,m]$.

This assumption allows us to exploit the one-to-one relationship between angle of arrival and Doppler frequency of stationary scatterers in order to provide an angle-dependent compensation of channel imbalance. Specifically, a Doppler dependent calibration (DDC) strategy is proposed, where we look for complex calibration coefficients to be separately applied at each Doppler bin so that the output clutter power after DPCA subtraction is minimized at that Doppler bin.

By proceeding as in (2.7)-(2.8), the correction coefficient at the m-th Doppler bin can be estimated as:

$$\hat{\Gamma}[m] = \frac{\sum_{l=l_1}^{l_2} z^{(TA)}[l,m] \ z^{(LA)^*}[l,m]}{\sum_{l=l_1}^{l_2} |z^{(LA)}[l,m]|^2} \tag{2.10}$$

where the average values at both the numerator and denominator are evaluated over consecutive range cells spanning indexes from l_1 to l_2.

This approach assumes that scatterers belonging to the same Doppler bin, and hence to the same angular direction, are characterized by analogous amplitude and phase channel imbalance, namely a nearly uniform imbalance in range.

It is worth noting that such Doppler dependent calibration technique is able to compensate not only for angle-dependent antenna pattern mismatch, but it also intrinsically compensates for any phase slope in Doppler, resulting from residual channel displacement, thus making unnecessary the fine delay compensation step in Figure 2.8 and adaptively establishing the DPCA condition.

A similar methodology for digital channel balancing was proposed in [60]-[61], in the context of multi-channel SAR-GMTI applications, where an iterative algorithm is operated in the 2-D frequency domain to calibrate spectral response of different channels. In our case, the relatively small bandwidth of exploited waveform, compared to typical SAR signals, allows to assume negligible difference in channel frequency response and to operate calibration only in the Doppler domain. Clearly, such data driven calibration strategies based on clutter

echoes are more effective when high values of CNR are present, which is the case of our experiment.

The idea of performing an angle/Doppler dependent calibration for multi-channel passive radar data has been also considered in [18] and [19], based on the estimation of the minimum variance power spectrum of clutter. This approach only allows an angle-dependent phase imbalance to be estimated and compensated for. Therefore, it requires additional stages devoted to a data-adaptive amplitude calibration.

Figure 2.12(a) shows the range-Doppler map obtained by applying the DPCA scheme combined with a DDC approach, for the same simulated clutter case of Figure 2.11. As expected, a significant improvement in terms of clutter cancellation capability is achieved, compared to the SCC case, thanks to the possibility to compensate also for the angle-dependent imbalance fluctuations.

Notice that the effectiveness of the channel calibration, and thus the cancellation performance, decreases when approaching the edges of clutter Doppler spectrum. This effect can be traced back to limited validity of the approximation made in (2.9). In fact, due to the non-linear relation between Doppler frequency and angle of arrival, in those regions Doppler resolution maps broader angular sectors, which may correspond to different values of channel imbalance, thus reducing the ability to compensate for local imbalance variations.

Figure 2.12(b) shows the average CR obtained, as a function of input CNR, for the same simulated clutter scenario. We notice that the CR initially improves as the input CNR increases, being the cancellation ideally limited only by thermal noise. However, when further increasing the CNR, the presence of uncancelled clutter residuals leads to a saturation of the cancellation performance. As expected, the DDC approach allows to achieve significantly higher values of cancellation, compared to the SCC approach, thanks to the adaptation capability in the Doppler dimension which compensates for imbalance variations.
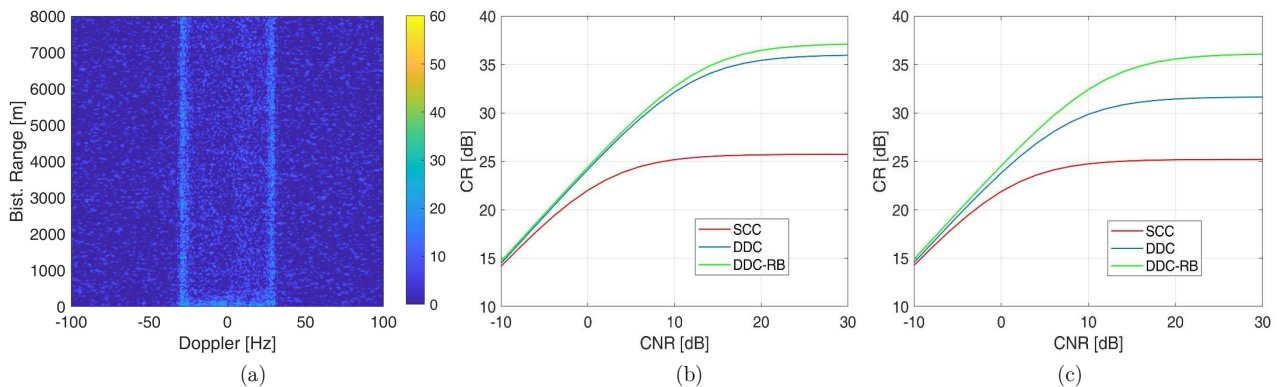
Figure 2.12: Analysis of adaptive clutter-based calibration techniques against simulated clutter scenario in the presence of angle dependent channel imbalance: (a) range-Doppler map after DPCA with DDC approach; (b) comparison of average CR obtained as a function of input CNR; (c) comparison of average CR in a different geometry with increased receiver altitude.

Figure 2.13 and Figure 2.14, respectively show the range-Doppler map after DPCA subtraction and the corresponding CR map, resulting from the application of the DDC approach in (2.10) to the experimental data set under consideration. Application is limited to Doppler frequency bins within the clutter bandwidth [-32;32] Hz and bistatic range interval [150;8000] m. The CR reported in Figure 2.14 takes into account the DPCA stage only, assuming that this is applied after the removal of the DSI by means of the ECA approach. By comparing these results with those in Figure 2.9 and Figure 2.10(b), a substantial improvement in clutter cancellation performance can be observed, with CR values increased by more than 10 dB at specific locations.

The amplitude and phase of the estimated calibration coefficients are shown in Figure 2.15 as a function of Doppler frequency (respectively solid blue and red lines). Their average values are consistent with the amplitude and phase imbalance estimated by means of the SCC strategy (reported in figure by dashed horizontal lines). However, a sensible variation of channel imbalance across Doppler frequencies can be noticed both in amplitude and in phase. Moreover, a slight phase slope is apparent, possibly due to a non-perfect delay compensation between LA and TA channels.
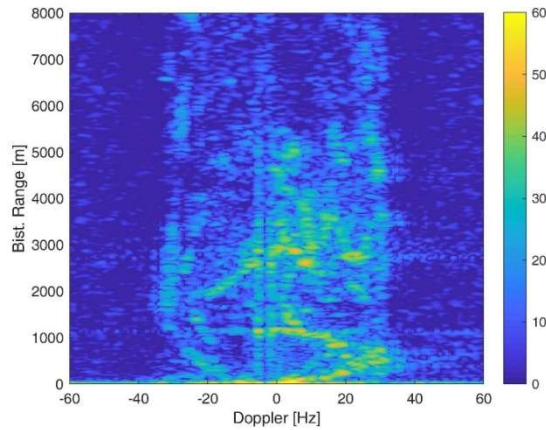
Figure 2.13: Range-Doppler map after two-stage cancellation scheme with DDC approach.
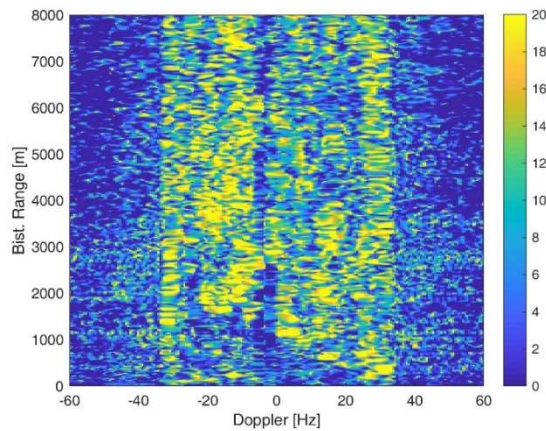
Figure 2.14: Cancellation Ratio obtained after the DPCA stage with DDC approach.

In order to assert with more confidence that the proposed digital calibration strategy is providing a reliable estimate of the actual angle-dependent channel imbalances, Figure 2.15 includes the corresponding curves obtained by averaging (2.10) over an acquisition time of 10 seconds (see dotted lines). Specifically, the average amplitude and phase calibration coefficients are evaluated based on subsequent non-overlapped CPIs, where the platform was verified to maintain constant motion parameters. The dotted curves clearly resemble the estimates obtained at the CPI under consideration, thus demonstrating that a reliable and stable information is extracted with the proposed approach.

As is apparent, the highest improvement in terms of CR between Figure 2.14 and Figure 2.10(b) is obtained at Doppler values where the largest deviations are observed in the estimated calibration coefficients (solid lines) with respect to the correction suggested by the SCC approach (dashed lines). This is the case of the Doppler region at about -30 Hz, where the enhanced clutter cancellation obtained after the DDC approach now yields an easier discrimination of the cooperative target Delphin, approximately at bistatic range 6600 m (see Section 2.6.2 for more details).
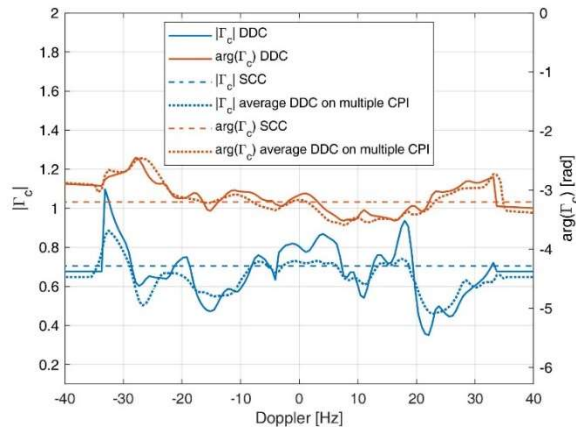
Figure 2.15: Amplitude and phase of the estimated calibration coefficients as a function of Doppler frequency: DDC on current CPI (solid line); DDC averaged over multiple CPIs (dotted lines); SCC value (dashed lines).

2.5.2 Doppler dependent calibration in range bands (DDC-RB)

Further performance improvement can be achieved by making the calibration technique adaptive also in the range dimension. The idea is to compensate for potential additional channel mismatch as a function of range, as this is largely related to antenna pattern differences in elevation.

In the considered experiment, this additional degree of freedom in the calibration process is not expected to give significant improvement, since a ground-based receiver experiences small variation in the elevation angle of observed clutter, mostly associated to changes in terrain height. Moreover, a relatively small extension in range has been considered in the

available data files. On the other hand, it is reasonably expected to be more beneficial for bistatic configurations exploiting an airborne receiver.

Adaptation capability in range can also be useful to mitigate the effects of clutter contributions coming from the antenna back-lobe, which typically affect the first range bins and might set different constraints on the calibration coefficients.

Starting from the simplified model in (2.9), the variation of imbalance in range is also taken into account, in addition to the variation in angle, i.e. $G_q^{(TA)}(\phi)/G_q^{(LA)}(\phi) = \Gamma_q(\phi)$. By proceeding as in Section 2.5.1, it is assumed that clutter returns at a generic range-Doppler bin $[l, m]$ are dominated by the response of the scatterers belonging to the clutter patch defined by the range and Doppler resolution. To guarantee the validity of this assumption, an appropriate windowing is adopted to achieve low sidelobes both in range and in Doppler, namely for both $g_d[m]$ and $g_r[l]$ functions in (4). Therefore, for clutter signal at the output of the LA and TA range-Doppler maps, the following relation holds: $z_c^{(TA)}[l, m] \cong \Gamma_{q_l}(\phi_m) * z_c^{(LA)}[l, m]$.

This assumption inherently requires compensating also for the range-dependent channel imbalance before applying DPCA stage. The simplest approach along this line, assuming a relatively slow variation of imbalance with range, is to subdivide the clutter area of interest in range bands and to apply a Doppler dependent calibration, according to (2.10), at each range band separately (DDC-RB).

In Figure 2.12(b) the SCC, DDC and DDC-RB approaches are compared in terms of average CR obtained for the simulated clutter scenario, as a function of the input CNR. We notice that the DDC-RB approach, applied by subdividing the clutter area into four non-overlapped range bands of 2000 m each, achieves the highest values of cancellation, thanks to the resulting adaptation capability in both Doppler and range dimensions. As expected, the improvement with respect to DDC approach is limited, since the effect of the imbalance variation in elevation is limited to the first few range bins due to the considered observation geometry (ground-based receiver). In Figure 2.12(c) a different geometry is considered, where assumed receiver altitude is increased from 3 m to 100 m. In this case the effect of imbalance variation in elevation is more significant and allows to better appreciate the advantages of the DDC-RB approach compared to the DDC.

In order to assess the achievable improvements in terms of cancellation performance and compare the different calibration techniques against the experimental data set, Figure 2.16 considers the curves of achieved CR as a function of Doppler frequency, which express the average power attenuation provided at each Doppler bin by the DPCA stage. Specifically, this is defined as in (2.6) where the power at the input and at the output of the DPCA stage at a given Doppler bin has been averaged over the available range gates.

Notice that values of CR also depend on the input CNR across Doppler bins, being the highest values expected at the Doppler bins where the strongest clutter contributions appear.

Besides this consideration, here we focus on the comparative analysis of the results obtained adopting the SCC, DDC and DDC-RB approaches for channel calibration.

As expected from previous Section, an appreciable improvement is achieved by applying a Doppler dependent calibration (blue dash-dot curve), compared to a single coefficient approach (red dashed curve). Apparently, the CR can then be further increased by few dBs, if calibration is applied in range bands (green solid curve). Specifically, in this case, the region of interest in bistatic range has been subdivided into five non-overlapped bands of 1600 m each. Obviously, a trade-off exists in selection of range bands dimension. On one hand, a smaller extension in range would result in a better cancellation performance; on the other hand, it might cause calibration process to be influenced by the presence of outliers, there including potential targets contributions.
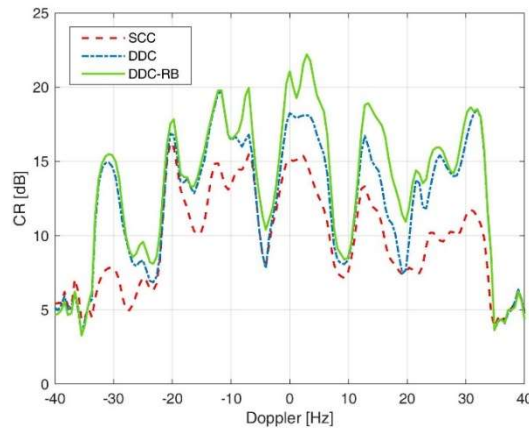
Figure 2.16: Comparison of average Cancellation Ratio given by the DPCA stage as a function of Doppler frequency for different calibration techniques.

2.5.3 Robust DDC-RB

When exploiting a Doppler dependent calibration strategy applied across range bands, the support (i.e. the number of bins in the range-Doppler map) used to estimate the required coefficients is deliberately reduced in order to track local changes of the channel imbalances over the considered area.

However, in such condition, the effectiveness of the proposed strategy could be jeopardized by the presence of potential outliers as their effect does not average out in the summation in (2.10). Such outliers might include:

- range-Doppler bins that are severely corrupted by noise;
- strong echoes from stationary scatterers impinging on the antenna back-lobes and affected by a different channel imbalance with respect to the scatterers lying in the area under consideration;
- sidelobes associated to strong scatterers belonging to a different area;
- potential strong moving targets in super clutter visibility condition.

If enough range bins are available for the estimation of a Doppler dependent channel imbalance, it is reasonable to assume that the presence of outliers has a negligible impact. Conversely, if few range bins are used, calibration becomes more sensitive to potential outlying values, preventing an effective clutter cancellation. In addition, targets with high signal to clutter ratio (SCR) may result in being partially suppressed.

In order to avoid this undesirable effect and improve robustness of the proposed adaptive calibration technique, we start from the following consideration. Clutter contributions belonging to same Doppler bin, and hence to same angular direction, within an appropriate extension in range, are presumably characterized by similar channel imbalance. Therefore, the values extracted at the corresponding bins, tend to be concentrated around the true local value, apart for an intrinsic fluctuation that depends on the local CNR. Specifically, we observed that the phase component of the sample estimates is typically quite stable across range cells. Therefore, when estimating the calibration coefficient, potential strong outliers could be in principle excluded based on their interferometric phase values.

The aim is to achieve a channel calibration ideally based on clutter contributions only and to avoid the influence of potential outliers. To this purpose, the calibration coefficient is evaluated for each Doppler frequency, according to (2.10), by exploiting only range bins whose phase difference between LA and TA channels does not deviate by more than an assigned threshold η from a median value estimated on that specific Doppler frequency:

$$\hat{\Gamma}[m] = \frac{\sum_{l \in \Lambda_{\mathrm{m}}} z^{(TA)}[l,m] \, z^{(LA)^*}[l,m]}{\sum_{l \in \Lambda_{\mathrm{m}}} |z^{(LA)}[l,m]|^2} \tag{2.11}$$

$$\Lambda_m = \{l : \, |\Delta\Phi[l,m] - \mathrm{median}(\Delta\Phi[l,m])| < \eta\} \quad \forall \, m$$

where $\Delta\Phi$ indicates the phase difference between co-registered channel maps:

$$\Delta\Phi[l,m] = \arg\{z^{(TA)}[l,m] \, z^{(LA)^*}[l,m]\} \tag{2.12}$$

In this way, by selecting a proper threshold value, potential strong moving targets, as well as echoes heavily corrupted by noise, can be excluded from the calibration process, thus improving its robustness. Median value is preferred to average value, since it is less sensitive to outliers. Moreover, to make estimation more robust against noise, only the first M bins with higher power level are considered.

To prove the effectiveness of the proposed solution, Figure 2.17 shows the results of channel calibration and DPCA on the cooperative aerial target. In particular, Figure 2.17(a) shows an enlarged view of a single channel range-Doppler map around the target position. Figure 2.17(b) and Figure 2.17(c) show the resulting maps after channel calibration and DPCA subtraction, respectively without and with the application of phase outliers exclusion
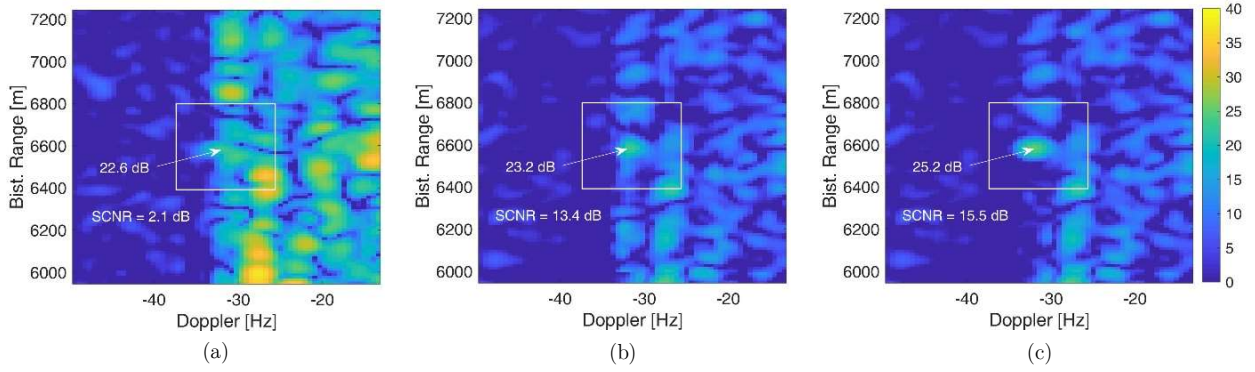
Figure 2.17: Results of cancellation scheme on real aerial target: (a) before DPCA subtraction; (b) after DPCA subtraction with DDC-RB; (c) after DPCA subtraction with Robust DDC-RB excluding outliers. Narrow range bands of 800m are used for calibration.

technique in (2.11). In the latter case, the threshold η is empirically set to 1 rad. DDC-RB approach is applied using narrow range bands of 800 m, in order to stress the effect of the presence of outliers.

A significant clutter attenuation is achieved in both cases, allowing the target echo to be easily detected. The estimated SCNR is increased by more than 10 dB in both Figure 2.17(b) and Figure 2.17(c) compared to Figure 2.17(a). However, we observe that the influence of moving target on calibration, appreciable in Figure 2.17(b), decreases the gain on target and the clutter cancellation capability on the corresponding Doppler bins. These effects are effectively mitigated in Figure 2.17(c) thanks to the proposed approach. This results in a further increase in terms of SCNR by 2.1 dB.

Notice that the exclusion of outliers can be applied also to the DDC approach, despite it is expected to be less sensitive to the presence of outliers. In the following, this will be referred to as Robust DDC. Benefits of excluding outliers from the calibration process will be further investigated in Section 2.6, where the effectiveness of the considered processing scheme and the proposed calibration strategies is analysed in terms of clutter suppression as well as moving target detection capability.

2.5.4 Computational effort

For the reader's convenience, the proposed channel calibration algorithms are summarized in Table 2.2, listing the adopted acronyms and their main characteristics. In addition, a comparison of required computational effort is also included, in terms of number of complex multiplications required for the estimation of corresponding calibration coefficients. In fact, the cost required for the application of calibration to one of the channels is the same for all techniques. N_d and N_r denote respectively the number of Doppler and range bins considered for calibration, corresponding to the selected clutter area of interest; n_r is the number of range bands in which the area is subdivided. Apart from DSI-based calibration (where a single complex multiplication is required), the other clutter-based techniques, namely SCC,

Table 2.2

Summary of considered channel calibration techniques

Technique	Reference	Description	Number of complex multiplications
DSI-based	Section 2.3.3, eq. (2.5)	Estimation of single calibration coefficient based on DSI	1
SCC	Section 2.4, eq. (2.8)	Estimation of single calibration coefficient based on clutter area	$2N_d N_r + 1$
DDC	Section 2.5.1, eq. (2.10)	Estimation of N_d coefficients as a function of Doppler frequency	$N_d(2N_r + 1)$
DDC-RB	Section 2.5.2	Estimation of N_d x n_r coefficients as a function of Doppler frequency and range band	$N_d(2N_r + n_r)$
Robust DDC	Section 2.5.3, eq. (2.11)	Robust version DDC to avoid the influence of strong outliers	$N_d(2N_r + 1) + N_d f(N_r)$
Robust DDC-RB	Section 2.5.3	Robust version of DDC-RB to avoid the influence of strong outliers	$N_d(2N_r + n_r) + N_d n_r f(N_r/n_r)$

DDC and DDC-RB, have a comparable computational effort, which depends on the range and Doppler extension of the considered clutter area. Notice that Robust versions of algorithms need an additional cost, indicated as a function of the number of range bins, due to operations required for exclusion of outliers. This additional cost cannot be easily expressed in terms of number of multiplications, since it requires sorting operations, and in any case it does not constitute a dominant contribution to the overall computational cost. Moreover, it is worth noting that the computational effort required by considered calibration approaches is substantially lower than that required for the evaluation of the range-Doppler maps.

2.6 Performance analysis against targets

In this Section, the performance of the considered processing scheme is investigated against real and synthetic moving targets. The effectiveness of the DPCA approach in suppressing clutter returns, while preserving moving target echoes, is verified when applying the different calibration strategies introduced in the previous Sections. The results are compared in terms of achievable improvement in signal-to-disturbance ratio.

A single cooperative aerial target was present in the experimental campaign and, due to its relatively high speed compared to the ground moving platform, it is rarely found within the clutter Doppler spectrum. Therefore, additional simulated moving targets are injected into real data, in order to have more chances for validating the proposed techniques.

2.6.1 Target model and effectiveness of the proposed approach

A synthetic target signal is generated from the reconstructed reference signal by applying specific delay and Doppler shift according to desired target bistatic range R_b and bistatic radial velocity v_b, according to the following model:

$$
\begin{aligned}
r_0^{(LA)}[l] &\cong A_0 \sum_n s_n\left[l - nL - l_{\tau_0}\right] e^{j2\pi f_{D_0} nT} \\
r_0^{(TA)}[l] &\cong \Gamma_c(\phi_0) \, A_0 \sum_n s_n\left[l - nL - l_{\tau_0}\right] e^{j2\pi f_{D_0} nT} e^{-j2\pi \frac{d}{\lambda}\cos\phi_0}
\end{aligned}
\tag{2.13}
$$

where A_0 is the target complex amplitude, $l_{\tau_0} = f_s R_b/c$ is the bistatic propagation delay (f_s being the sampling frequency), ϕ_0 is the angle between platform velocity vector and receiver to target line of sight and f_{D_0} is the target bistatic Doppler frequency given by:

$$
f_{D_0} = \frac{v_p}{\lambda}\cos\phi_0 - \frac{v_b}{\lambda}
\tag{2.14}
$$

Proper amplitude and phase imbalance coefficient $\Gamma_c(\phi_0)$ is also applied to the generated target echoes between LA and TA channels, according to the real imbalance estimated on clutter data at the same angular direction, in the absence of targets. Simulated target signal is then injected into the real acquired data.

The SCNR at the output of the DPCA stage is used in the following to compare the performance of different strategies. By definition, the SCNR improvement factor (IF) is equivalent to the product of disturbance CR and target gain (G), i.e. $IF = CR * G$. Notice that, in this case, the achievable target gain is limited to a maximum value of 3 dB.

Specifically, for the case of simulated targets, the target gain can be easily measured by comparing the power level of the input and output maps at the target range-Doppler location, when the processing scheme is fed with target echoes only. Correspondingly, the disturbance power level is estimated over a proper area surrounding the target location, by exploiting the maps containing just clutter and noise at the input and output of the DPCA stage. However, in both cases, the proposed channel calibration techniques are applied against data including both target echoes and disturbance contributions, in order to take into account the effects of targets on the calibration process.

In order to extensively investigate the effectiveness of the proposed calibration techniques, we focus on a single synthetic target, T1, whose parameters are listed in Table 2.3.

Results are reported in terms of disturbance cancellation ratio (Figure 2.18(a)) and output SCNR (Figure 2.18(b)), achieved after DPCA subtraction, as a function of the input SCNR used to generate the synthetic target echoes. Specifically, the obtained DPCA performance are compared after the application of the DSI-based calibration, the SCC, the DDC, and the

DDC-RB. Also, the robust versions of the latter two approaches, namely the Robust DDC and the Robust DDC-RB, are reported in order to understand the benefits of the exclusion of outliers.

As is apparent, when exploiting a DSI-based calibration strategy, a quite low CR value is obtained (see the grey curve in Figure 2.18(a)). This is well in line with the results in Figure 2.6 and Figure 2.7 and, in turn, results in a limited SCNR gain between the input and the output of the cancellation stage (see Figure 2.18(b)) so that, for instance, an input SCNR of 10 dB is required for the output SCNR to exceed 15 dB.

Despite still exploiting a single adaptive coefficient for the channel calibration, the SCC allows to significantly increase the CR and the subsequent SCNR gain with respect to the DSI-based approach. Moreover, thanks to the average performed across a wide region of the range-Doppler map, the SCC is not affected by the presence of the target up to very high values of the input SCNR. Therefore, the SCC could be regarded as a simple and effective approach in practical applications

However, the use of more sophisticated adaptive calibration strategies, compensating for Doppler and range dependent channel imbalance, allows to further improve the cancellation performance and, consequently, the SCNR gain. In particular, when exploiting the DDC or the DDC-RB (operating over range bands of 1600 m), the CR improves by 2 dB and 3 dB, respectively, compared to the SSC. Accordingly, in the considered case study, a remarkable input/output SCNR gain (slightly higher than 20 dB) is achieved with the DPCA applied after the DDC-RB, at least when the input SCNR is reasonably low.

As expected, localized adaptive calibration approaches are more sensitive to the presence of targets with high input SCNR values, as they represent outliers in the estimation of the calibration coefficients. This has non-negligible effects on both clutter cancellation performance, due to a corrupted channel imbalance estimation, and the resulting output SCNR, since this effect might yield a partial suppression of target signal. In fact, in the considered case study, both the DDC and the DDC-RB experience significant degradations as the input SCNR increase (see dashed lines in Figure 2.18(a-b)). Incidentally, we observe that this effect appears at lower SCNR values when exploiting the DDC-RB, since fewer range bins are used for estimating the calibration coefficients. In contrast, the DDC benefits from the average performed across a wider range extent so that the effect of outliers becomes apparent at higher SCNR values.

This undesirable effect can be avoided by making the calibration process robust against outliers, according to the strategy described in Section 2.5.3. Both the Robust DDC and the Robust DDC-RB allow to recover the CR loss due to the target influence on the calibration stage (see solid lines in Figure 2.18(a)). Accordingly, the moving target echoes are correctly preserved and a remarkably high SCNR gain is restored even when the target power level is several dBs above the disturbance background at the input of the DPCA. Nevertheless, it is
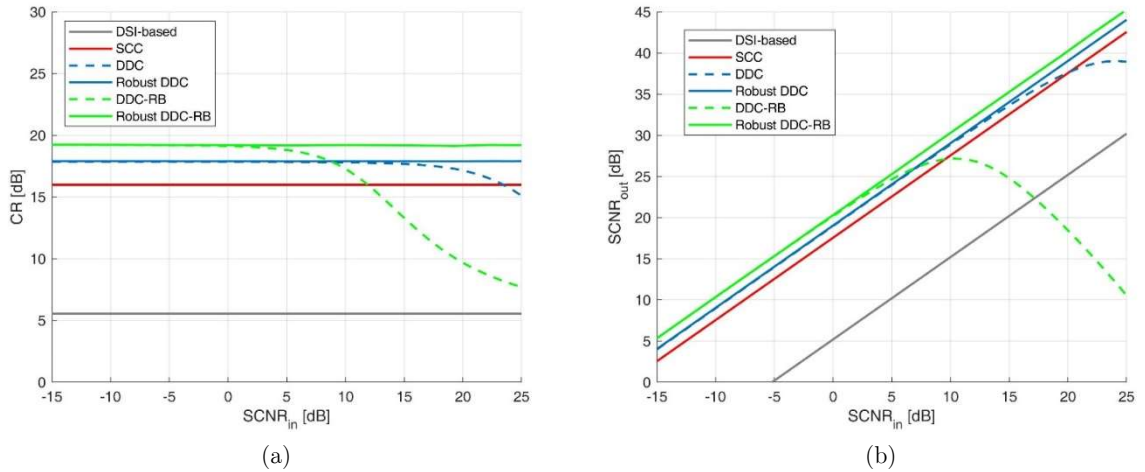
Figure 2.18: Performance analysis of DPCA adopting different channel calibration strategies, as a function of target SCNR in input: (a) disturbance Cancellation Ratio; (b) achieved target SCNR in output.
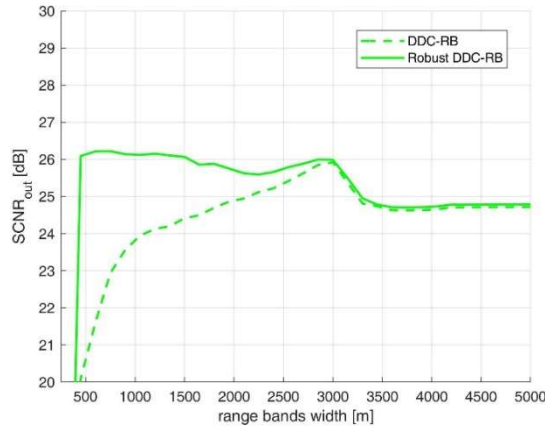
Figure 2.19: Performance analysis of DPCA adopting DDC-RB and Robust DDC-RB, as a function of range bands size: achieved target SCNR in output.

worth noting that such strong targets might be detected even before clutter suppression or by means of a less refined calibration strategy.

In order to understand the effect of the adopted range band size, Figure 2.19 reports the performance of the DPCA stage after the DDC-RB and the Robust DDC-RB as a function of the dimension of considered range band. In this case the input SCNR is set to a constant arbitrary value of 5 dB. As expected, the two approaches provide largely comparable results for large enough range bands. In contrast, the performance of the DDC-RB progressively degrades as the range band size decreases. When using the Robust DDC-RB, a limited reduction of range band extension can improve the cancellation ratio with respect to the results in Figure 2.18, thus providing a higher SCNR at the output of the DPCA stage. Clearly, beyond a certain limit, identification of outliers is no more feasible, and the performance rapidly degrades. This analysis also shows that the choice of range bands of 1600 m adopted so far allows a good trade-off between performance and robustness to outliers in

the case under consideration. This value will be also used for the analyses reported in the next Section.

2.6.2 Performance comparison

It is expected that the performance of the proposed approaches might vary across the range-Doppler map depending on the local clutter characteristics. Therefore, in order to further investigate the effectiveness of the considered strategies and to compare the achievable performance, results are reported below against multiple injected targets, as well as against the real cooperative target.

Parameters of real and simulated targets are listed in Table 2.3. Different angles of arrival are considered for injected targets and bistatic velocity values are set so that they do not coincide with the expected blind velocities $p\lambda/T_{DPCA}$ ($p \in \mathbb{Z}$).

The range-Doppler maps before and after DPCA subtraction are respectively shown in Figure 2.20(a-b). Specifically, the Robust DDC-RB approach is adopted for channel calibration. A significant reduction of clutter power is achieved, so that both real and simulated targets are clearly visible in the final map (see Figure 2.20(b)) and they could be easily detected by a conventional CFAR scheme.

Results in terms of disturbance cancellation ratio (CR), target gain (G) and corresponding SCNR improvement factor (IF), obtained for the different channel calibration strategies are reported in Table 2.4. As expected, a significant gap in DPCA performance is present between the DSI-based calibration and the other clutter-based calibration techniques.
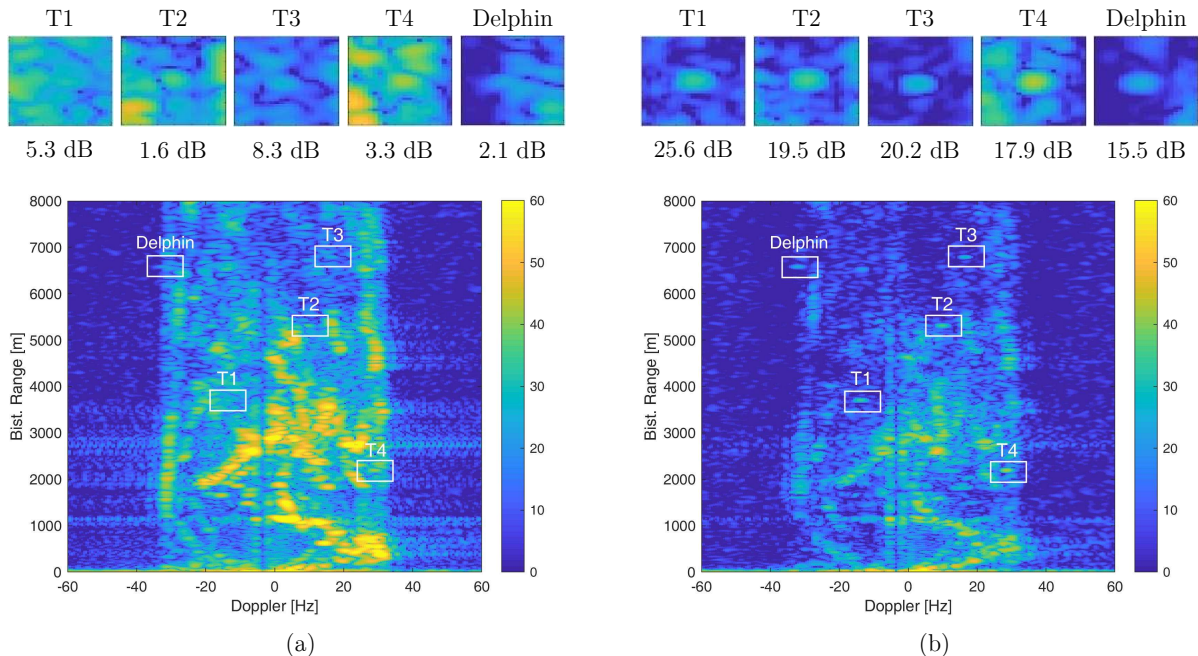
Figure 2.20: Range-Doppler map in presence of real and synthetic targets: (a) before DPCA subtraction; (b) after DPCA subtraction. DDC-RB approach is adopted over range bands of 1600 m. Enlarged views of targets and corresponding SCNR values are reported above.

Moreover, all targets, in different measure, benefit from the enhanced clutter cancellation capability given by the Robust DDC approach, compared to the SCC. In addition, the Robust DDC-RB allows a further improvement on specific targets (e.g. see T2). Notice that more localized calibration approaches do not significantly affect the target gain values. Finally, it is worth noting that analogous considerations can be made also for the real target (Delphin). This clearly proves the effectiveness of the considered processing scheme and the benefits of the proposed approaches for adaptive channel calibration.

Non-negligible clutter residuals are still visible in the final map. In particular, they are associated to backscattered echoes from forested areas close to receiver position and they are probably due to ICM limitations or potential additional error sources. However, these contributions have been considerably attenuated compared to their original power level. It is also worth recalling that a very simple architecture and undemanding processing have been

Table 2.3

Target parameters

	T1	T2	T3	T4	Delphin
R_b	3700 m	5300 m	6800 m	2200 m	6596 m
v_b	-6 m/s	9 m/s	6 m/s	10 m/s	-24.5 m/s
ϕ_t	90°	110°	85°	80°	37°

Table 2.4

Performance results

	T1	T2	T3	T4	Delphin
DSI-based Calibration					
G	-0.3 dB	1.2 dB	2.8 dB	1.5 dB	1.8 dB
CR	5.5 dB	9.7 dB	4.5 dB	4.9 dB	2.0 dB
IF	5.2 dB	10.9 dB	7.4 dB	6.4 dB	3.8 dB
Single Calibration Coefficient					
G	1.5 dB	1.9 dB	1.9 dB	2.5 dB	2.9 dB
CR	16.1 dB	12.1 dB	8.0 dB	10.8 dB	6.8 dB
IF	17.6 dB	14.0 dB	10.0 dB	13.2 dB	9.7 dB
Robust Doppler Dependent Calibration					
G	1.1 dB	1.4 dB	2.6 dB	2.4 dB	2.5 dB
CR	17.9 dB	12.6 dB	8.2 dB	12.4 dB	10.0 dB
IF	19.0 dB	14.0 dB	10.8 dB	14.8 dB	12.6 dB
Robust Doppler Dependent Calibration in Range Bands					
G	1.1 dB	1.5 dB	2.5 dB	2.5 dB	2.5 dB
CR	19.2 dB	16.3 dB	9.5 dB	12.0 dB	10.8 dB
IF	20.3 dB	17.8 dB	12.0 dB	14.6 dB	13.4 dB

used, based on just two receiving channels and DPCA approach, which limits the adaptivity only to the channel calibration stage.

2.7 Summary

This Chapter addressed the problem of direct signal interference and clutter cancellation for a passive radar system on moving platform, for the purpose of moving target indication (MTI). A processing scheme was adopted based on reciprocal filtering strategy and DPCA approach. Attention was mainly focused on the development of signal processing algorithms for digital channel calibration, in order to cope with the limitation deriving from the amplitude and phase inter-channel imbalance.

First, the limits of a channel calibration approach based on direct signal are highlighted, due to the effect of angle-dependent channel imbalance, for bistatic geometries where DSI and main clutter echoes have different directions of arrival.

Therefore, a two-stage strategy was proposed, aimed at achieving an effective cancellation of both DSI and clutter contributions and removing the influence of DSI on channel calibration. A preliminary suppression of DSI, typically representing the dominant contribution in the range-Doppler map, is provided at both receiving channels by means of an ECA algorithm. Then, a clutter-based channel calibration approach is applied prior to DPCA subtraction, in order to maximize clutter cancellation performance.

Different strategies for digital channel calibration were proposed, based on the criterion of minimizing the output power. Starting from the estimation of a single calibration coefficient (SCC), flexibility of calibration model has been gradually increased, in order to compensate for additional angle (DDC) and range dependent channel errors (DDC-RB). A robust version of these schemes was also introduced to avoid degradation due to the interference of strong targets.

Effectiveness of considered processing scheme and channel calibration approaches have been tested against simulated and experimental data from a DVB-T based mobile passive radar system. All the proposed strategies have been shown to provide a significant improvement, with respect to DSI-based calibration approach, both in terms of clutter cancellation performance and target detection capability. Specifically, among the proposed techniques, Robust DDC approach proved to yield very good performance against both real and synthetic targets. The Robust DDC-RB approach allowed limited additional improvements in the considered case study and this is mostly related to the adopted acquisition geometry, where a ground-based moving passive radar system was employed.

Chapter 3

Passive Radar STAP detection and DOA estimation under antenna calibration errors

This Chapter addresses the problem of clutter cancellation and slow-moving target detection and localization in multichannel passive radar onboard mobile platforms. A post-Doppler STAP approach is proposed, in the case of angle-dependent imbalances affecting the receiving channels. While the adaptivity of the space-time filter ensures an effective clutter suppression capability even in the presence of channel imbalance, different solutions are devised, aimed at mitigating the impact of channel calibration errors on target detection and localization performance. Section 3.1 introduces the addressed issues and the aims of the study. In Section 3.2, the signal model and the considered processing scheme for passive radar STAP are described. Then, Section 3.3 addressed the impact of channel calibration errors on target detection performance. In Section 3.4, two different schemes are proposed as potential solutions for target detection under imbalance conditions and their performance is analysed against a simulated clutter scenario in Section 3.5. Section 3.6 is concerned with the problem of target angular localization and the considered scheme is employed for accurate ML estimation of target DOA, against the impact of channel imbalance. In Section 3.7, the effectiveness of the proposed solutions is validated against experimental data from a DVB-T based mobile passive radar. Finally, conclusions are drawn in Section 3.8.

3.1 Introduction

In Chapter 2, a DPCA approach has been considered to provide GMTI capability in mobile passive radar. DPCA involves a simple system architecture and a limited computational load, which make it attractive for the passive radar application.

However, significant performance limitations may come from the presence of an amplitude and/or phase imbalance affecting the receiving channels, which can severely compromise the clutter cancellation capability of a DPCA scheme. Such imbalance can be in general function of the angle of arrival due to several factors (dissimilarities between the receiving antenna

patterns, mutual coupling effects, interaction with near-field obstacles) and its impact is made more severe by the characteristics of the passive bistatic scenario.

In fact, the low directivity of the typically available receiving antennas at VHF/UHF band, paired with a bistatic illumination from omni-directional broadcast transmitters, results in non-negligible clutter contributions simultaneously received from a very a wide angular sector and therefore easily affected by different amplitude and phase responses across the receiving channels, as also verified on experimental data in Chapter 2. On the other hand, the typical long integration time of passive radar provides a fine Doppler frequency resolution, which can be conveniently exploited.

In Chapter 2, effective ad-hoc solutions were developed for channel calibration in passive radar DPCA. The proposed strategies took advantage of the clutter angle-Doppler dependence for estimation of the angle-dependent imbalances. An accurate calibration of the received data proved to be largely required to preserve the clutter suppression capability. Moreover, the effects of channel errors on target signal had to be neglected, in favour of an effective clutter cancellation. In fact, target signal may experience a different imbalance compared to the clutter contributions appearing at same Doppler frequency, since belonging to a different angular direction, thus possibly affecting the detection performance despite an effective suppression of clutter. Finally, with two channels on receive, only the detection of target echoes can be sought whereas the problem of its angular localization within the broad antenna beam remains unsolved.

The intrinsic limitations of DPCA and its reliance on an adaptive calibration stage for the compensation of localized errors, suggest moving in the direction of a space-time adaptive processing (STAP) approach, [21]. At the expense of a higher computational load, STAP has more flexibility and adaptation capability, thanks to a higher number of adaptive degrees of freedom. The use of STAP for clutter rejection in passive radar was first considered in [24][25]. Preliminary experimental results of STAP in a DVB-T based mobile passive radar are presented in [26]. In [27], sparse Bayesian learning is employed for accurate estimation of clutter covariance matrix based on few secondary samples. In [28], a three-dimensional model is proposed to integrate clutter modelling and waveform impact in passive STAP. Further applications of STAP in passive radar are considered in [33], for improved target detection exploiting spatial diversity with OFDM waveforms, in [34], for direct signal interference suppression, and in [35] for clutter rejection in airborne bistatic Inverse-SAR (ISAR) imaging.

In this Chapter, a STAP scheme for mobile passive radar is proposed and its effectiveness is analysed in terms of clutter cancellation and moving target detection and localization, in the case of an unknown angle-dependent imbalance affecting the receiving channels. The set of adopted methodologies takes advantage of the characteristics of the passive radar scenario.

First, it is pointed out the fundamental role of a post-Doppler STAP approach in preserving clutter cancellation capability, also the in presence of channel calibration errors, identifying it as particularly suitable for mobile passive radar. It takes advantage of the long

48

integration time and the resulting fine Doppler resolution to considerably reduce the size of the adaptive problem and intrinsically compensate for the angle-dependent channel errors, by operating on a clutter subspace accounting for a limited angular sector.

Therefore, two detection schemes are proposed, aimed at mitigating the effects of the channel imbalance on target signal, whose direction of arrival (DOA) and related experienced imbalance may differ from those of clutter in the surrounding range/doppler cells, possibly affecting the detection and localization performance, despite the effective clutter suppression.

The first scheme consists of a partially non-coherent space-time generalized likelihood ratio test (GLRT), which performs a non-coherent integration of target signal across the receiving channels, to cope with losses due to spatial steering vector mismatch. Entirely excluding the presence of a calibration stage, it provides a simple but effective solution for target detection in systems featuring few receiving channels. The second scheme consists of a fully coherent space-time GLRT, where the echoes from the stationary scene are exploited to estimate the channel errors in the desired target search direction and calibrate the spatial steering vector, making use of the known relationship between angle of arrival and Doppler frequency of stationary scatterers. At the expense of an additional calibration stage, this solution provides slightly better detection performance and preserves target DOA estimation capability.

Finally, the target angular localization problem is addressed. The limited number and low directivity of receiving antennas, due to the typically exploited wavelengths, make the accurate estimation of target DOA a critical task. Such capability requires the availability of multiple spatial degrees of freedom, which must be properly exploited both for space-time clutter filtering and for target DOA estimation and can be severely compromised by presence of channel imbalance. To this purpose, the proposed STAP scheme is adopted for a maximum likelihood (ML) DOA estimation, assessing the key role of the steering vector calibration in mitigating the negative impact of the unknown channel errors.

Moving target detection and localization performances of the proposed solutions are analysed and compared, against a simulated clutter scenario. Moreover, some results are shown against experimental data collected by a DVB-T based multichannel passive radar mounted on a ground moving platform. The obtained results clearly demonstrate the effectiveness of the proposed strategies.

3.2 STAP scheme for passive radar

Let us consider a N channel passive radar receiver mounted on a moving platform and exploiting a stationary transmitter as illuminator of opportunity (see Figure 3.1). The platform moves at constant velocity v_p on a straight-line trajectory, assumed without loss of generality along the x-axis. Angles φ and ϑ indicate respectively the azimuth and depression angle of the receiver to scatterer line of sight.
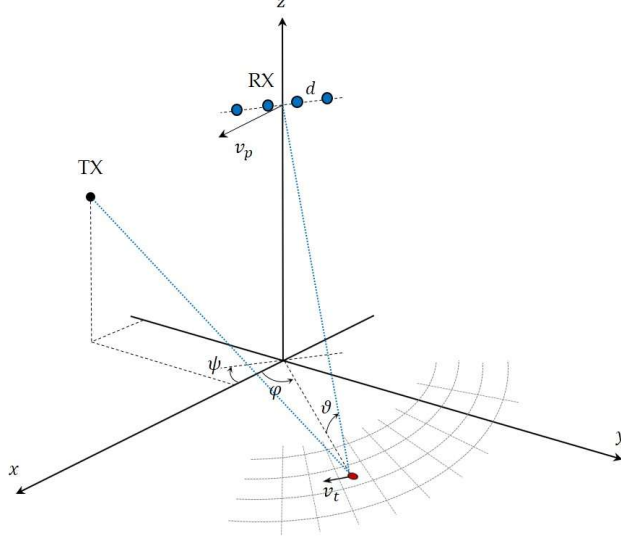
Figure 3.1: System geometry of a multichannel mobile passive radar exploiting a ground-based stationary transmitter as illuminator of opportunity.

Recalling the signal model adopted in Chapter 2 and extending it to a multichannel case, for a linear array of elements equally spaced by d in a side-looking configuration (crab angle ψ assumed equal to zero), the discrete time baseband signal received at the i-th antenna from a moving target at angles (φ_0, ϑ_0) and bistatic range R_b can be expressed as:

$$r_0^{(i)}[l] = G_i(\varphi_0, \vartheta_0)\, A_0 \sum_n s_n\big[l - nL - l_{\tau_0}\big] e^{j2\pi\, f_D\, nT}\, e^{-j2\pi\, i\, \frac{d}{\lambda}\cos\varphi_0 \cos\vartheta_0} \tag{3.1}$$

where the following notation is recalled (introduced in Chapter 2):

- l is the time index, denoting the l-th sample of the signal, sampled at frequency f_s;
- the transmitted signal is partitioned in batches of duration T and $s_n[l]$ denotes the n-th batch, including $L = T f_s$ samples; notice that the Doppler induced phase term within each batch has been neglected;
- $l_{\tau_0} = f_s R_b/c$ is the bistatic propagation delay, assumed constant during the CPI;
- A_0 is the target complex amplitude and $G_i(\varphi_0, \vartheta_0)$ is the complex gain of the i-th channel at target angular direction; the latter represents the overall receiver chains, including the antenna pattern, and accounts for possible imbalance between channels;
- f_D is the bistatic Doppler frequency, which can be expressed as the sum of two contributions:

$$f_D = \frac{v_p}{\lambda}\cos\varphi_0 \cos\vartheta_0 - \frac{v_b}{\lambda} \tag{3.2}$$

the first is related to the platform motion and the receiver to scatterer geometry, the second is due to the target intrinsic bistatic radial velocity v_b; λ denotes the signal carrier wavelength.

The signal representing the clutter contribution before range compression can be expressed as the superposition of echoes from a distribution of stationary scatterers ($v_b = 0$) at different bistatic ranges R_q ($q = 1, \ldots, N_R$) and different angles φ:

$$r_C^{(i)}[l] = \sum_{q=1}^{N_R} \int_\phi G_i(\varphi, \vartheta)\, A_q(\varphi) \sum_n s_n\left[l - nL - l_{\tau_q}\right]$$
$$\times\, e^{j2\pi \frac{v_p}{\lambda}\cos\varphi\cos\vartheta\, nT}\, e^{-j2\pi\, i\, \frac{d}{\lambda}\cos\varphi\cos\vartheta} d\varphi \tag{3.3}$$

where $A_q(\varphi)$ is the complex amplitude and τ_q the bistatic propagation delay of echo from clutter patch at angle φ and range R_q.

The adopted processing scheme for the application of STAP to the passive radar framework is sketched in Figure 3.2. It is obtained by extending the DPCA scheme presented in Chapter 2 to the general case of a N channel receiver. We recall that the scheme is based on a batch processing architecture, which recreates the conventional fast-time/slow-time framework of a pulsed radar system operating at an equivalent PRF given by the inverse of the batch duration ($PRF = 1/T$). The range compression stage is performed for each batch by means of a reciprocal filter, which has the dual role of controlling the signal ambiguity function and removing the temporal variability of the employed opportunity waveform (see [15] for more details). For this purpose, a perfect reconstruction of the reference signal is supposed available by means of a decode/recode approach. Notice that the use of the reciprocal filter, which was
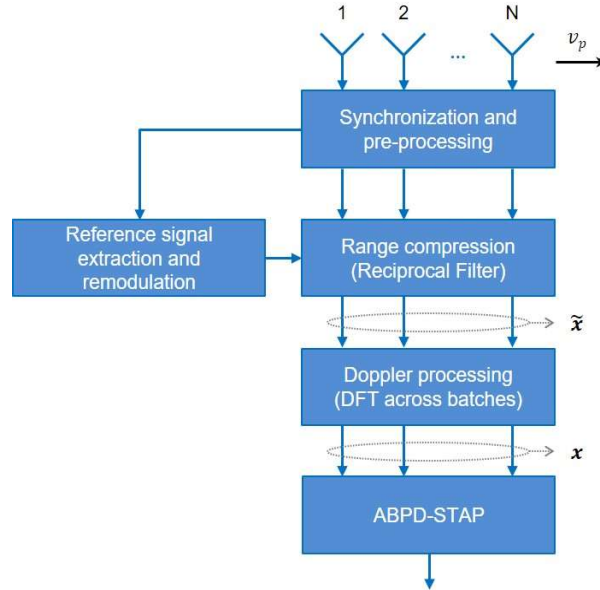
Figure 3.2: Sketch of the processing scheme of a post-Doppler STAP approach for passive radar.

fundamental in a non-adaptive approach like DPCA, also plays an important role in a STAP approach. By providing a time-invariant impulse response and improving the separation between range cells, it allows an ideal estimation of the adaptive filter.

After range compression stage, by collecting the samples associated to the range cell under test, from the N receiving channels and the M batches in the coherent processing interval (CPI), the $(NM \times 1)$ space-time data vector $\tilde{\boldsymbol{x}}$ is obtained. In the presence of a target with Doppler frequency f_D, DOA ϕ and complex amplitude $\bar{A}$, the data vector can be written as $\tilde{\boldsymbol{x}} = \bar{A}\,\tilde{\boldsymbol{s}} + \tilde{\boldsymbol{d}}$, where $\boldsymbol{d}$ represents the disturbance (clutter plus noise) component, assumed Gaussian with space-time covariance matrix $\widetilde{\boldsymbol{Q}} = E\left\{\tilde{\boldsymbol{d}}\tilde{\boldsymbol{d}}^H\right\}$. The space-time steering vector $\tilde{\boldsymbol{s}}$ can be expressed as $\tilde{\boldsymbol{s}}(f_D, \phi) = \boldsymbol{s}_t(f_D) \otimes \boldsymbol{s}_s(\phi)$, where $\boldsymbol{s}_t(f_D) = [1, e^{-j2\pi f_D T}, \dots,$ $e^{-j2\pi f_D MT}]^H$ is the temporal steering vector and $\boldsymbol{s}_s(\phi) = [1, e^{j2\pi d/\lambda \cos\phi}, \dots, e^{j2\pi Nd/\lambda \cos\phi}]^H$ is the spatial steering vector, $\otimes$ denoting the Kronecker product and H the Hermitian transpose. Notice that ϕ denotes the angle between the antenna end-fire and the receiver to scatterer line of sight $(\cos\phi = \cos(\varphi - \psi)\cos\vartheta)$.

As known, STAP adaptively combines spatial and temporal samples of the signal in order to suppress clutter in the angle-Doppler domain and maximize the detection probability of potential moving targets [46][47]. It is based on the inversion of the space-time disturbance covariance matrix $\widetilde{\boldsymbol{Q}}$, which is usually not available in practical applications and has to be estimated based on proper training data. In order to reduce the computational effort and the amount of training data required for an effective estimation of $\widetilde{\boldsymbol{Q}}$, a number of reduced-order STAP approaches have been suggested, where adaptive processing is applied after a non-adaptive projection of data in a proper subspace [50].

Particularly suitable for the passive radar case, characterized by relatively long integration times, are the post-Doppler STAP approaches, where adaptation occurs on a subset of Doppler-processed data. In fact, sufficiently long CPIs ensure proper decoupling of different clutter Doppler components. Specifically, an adjacent-bin post-Doppler (ABPD) approach is
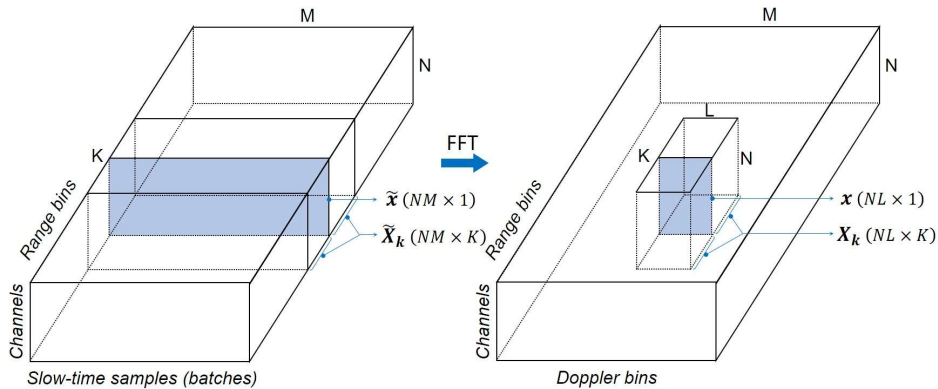
Figure 3.3: Graphical illustration of the formation process of data vectors $\tilde{\boldsymbol{x}}$, $\boldsymbol{x}$ and secondary data matrices $\widetilde{\boldsymbol{X}}_{\boldsymbol{k}}$, $\boldsymbol{X}_{\boldsymbol{k}}$, according to the ABPD approach. Notice that the FFT operation is performed in the slow-time domain, represented by the sequence of signal batches.

considered, which adaptively combines the N spatial samples from a subset of L adjacent Doppler bins centred at the cell under test.

Let $\boldsymbol{T}$ be a transformation matrix, which consists, in this case, of L adjacent columns of a discrete Fourier transform (DFT) matrix. The resulting vectors in the space-Doppler domain are given by $\boldsymbol{x} = \boldsymbol{T}^H \tilde{\boldsymbol{x}}$ and $\boldsymbol{s} = \boldsymbol{T}^H \tilde{\boldsymbol{s}} = \boldsymbol{s}_d \otimes \boldsymbol{s}_s(\phi)$ of size $(NL \times 1)$. The corresponding $(NL \times NL)$ space-Doppler disturbance covariance matrix will be $\boldsymbol{Q} = \boldsymbol{T}^H \widetilde{\boldsymbol{Q}} \boldsymbol{T}$.

Figure 3.3 offers a graphical illustration of the formation process of the data vector and the related training data, according to the adopted ABPD approach.

The well-known space-time GLRT detector can be easily derived following the approach in [71] and applied after the ABPD transformation:

$$\frac{\left| \boldsymbol{s}^H \widehat{\boldsymbol{Q}}^{-1} \boldsymbol{x} \right|^2}{\boldsymbol{s}^H \widehat{\boldsymbol{Q}}^{-1} \boldsymbol{s} \ (1 + \boldsymbol{x}^H \widehat{\boldsymbol{Q}}^{-1} \boldsymbol{x})} \gtrless \eta_1 \tag{3.4}$$

where matrix $\boldsymbol{Q}$ is substituted by its ML estimate $\widehat{\boldsymbol{Q}} = \boldsymbol{X}_k \boldsymbol{X}_k^H$, being $\boldsymbol{X}_k = [\boldsymbol{x}_1, \dots, \boldsymbol{x}_K]$ a set of training data of size $(NL \times K)$ from K adjacent range cells, assumed as statistically independent, identically distributed and target-free. The detection threshold η_1 is selected according to the desired value of false alarm probability (PFA), whose known analytical expression is:

$$PFA = \left(\frac{1}{l}\right)^{K-NL+1} \tag{3.5}$$

where $l = 1/(1 - \eta_1)$.

STAP solution can handle a higher number of degrees of freedom, offering more flexibility and adaptation capability compared to DPCA approach. On the one hand, it has a higher computational effort, since requires the estimation and inversion of a covariance matrix, potentially for each range-Doppler bin. However, the ABPD approach limits the computational cost and the number of required training data by significantly reducing the size of the covariance matrix. This also plays a key role in a real scenario, where the effectiveness of STAP would be subject to the potential non-homogeneity of clutter, which might not offer a sufficient number of homogeneous training data for matrix estimation.

3.2.1 Application against a simulated clutter scenario

To analyse the effectiveness of the considered scheme in a controlled environment, this is tested against a simulated clutter scenario for a multichannel moving passive radar.

A ground moving receiver is assumed exploiting a stationary transmitter in a quasi-monostatic geometry. An $8k$ mode DVB-T signal sequence is generated as a reference signal.

Details on the DVB-T signal parameters can be found in Table 2.1. Clutter returns are generated according to the model in (3.3), for a scene spanning $N_R = 1000$ range cells. Amplitudes $A_q(\varphi)$ associated with different clutter patches are assumed independent and identically distributed complex Gaussian variables, thus resulting in a homogeneous clutter scenario. We assume the availability of $N = 3$ perfectly balanced receiving channels, arranged in the along-track direction, in a side-looking configuration. Omnidirectional antennas are considered, within an angular sector $\varphi = [0, \pi]$ (no back-lobe contributions, supposed suppress by RAM). Carrier frequency is set to 690 MHz, platform velocity $v_p = 13$ m/s and antenna element spacing $d = \lambda/2$. We consider a CPI length of 512 OFDM symbols, corresponding to approximately half a second duration (~0.57 s), and we assume absence of internal clutter motion (ICM). Notice that, the DVB-T elementary period (7/64 µs) defines the fast-time sampling rate, while the batch duration, deliberately selected as equal to the OFDM symbol duration, defines the slow-time sampling rate (equivalent PRF $\cong 893$ Hz).

The generated input signal includes clutter returns and thermal noise and is scaled so that the overall clutter contribution has an assigned power level of 20 dB above the noise level, at the input of each Rx channel. The echo from a moving target is also included, with bistatic range $R_b = 4$ km, azimuth angle of arrival $\phi_0 = 90°$ and bistatic radial velocity $v_b = 5$ m/s. Target signal-to-noise ratio (SNR), defined as the ratio of target signal power level with respect to noise, at the input of each channel before range compression, is set to -43 dB.

The range-Doppler map obtained from a single channel is reported in Figure 3.4(a). As apparent, clutter returns appear across a Doppler extension of approximately $\pm v_p/\lambda \cong \pm 30$ Hz, while target signal-to-clutter-plus-noise ratio (SCNR) is -26 dB. In the simulation, the target SCNR is measured by taking the power level at the target range-Doppler location, when the processing is fed with target echoes only, and disturbance power level estimated over a proper area surrounding target location, in the maps containing only clutter and noise.

Applying the ABPD-STAP scheme in Figure 3.2, the resulting range-Doppler map at the output of the adaptive filter (numerator in (3.4)) is shown in Figure 3.4(b). In particular,
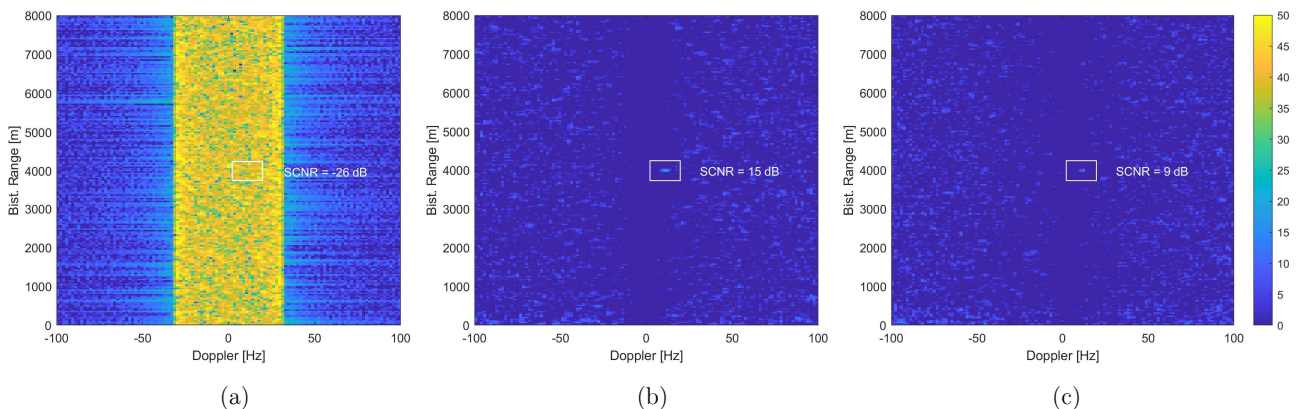
Figure 3.4: Range-Doppler maps from simulated clutter scenario: (a) single channel map; (b) after ABPD-STAP with perfectly balanced channels; (c) after ABPD-STAP in the presence of channel imbalance.

$L = 3$ adjacent Doppler bins are used, for a total on $NL = 9$ degrees of freedom. The number L of Doppler bins is generally selected as small as possible, to reduce the computational complexity, but sufficient to guarantees good clutter cancellation capability. In our case, the value $L = 3$ proved to be a suitable trade-off between required cost and effectiveness of the adaptive filter. The number of training data is set to $K = 6NL = 54$. This large sample support is selected in order to minimize the undesirable adaptivity losses.

Notice that all the range-Doppler maps are scaled to provide unitary processing gain for thermal noise, thus allowing a direct comparison of results. As expected, the clutter background is effectively cancelled and the resulting target SCNR is 15 dB, with an overall improvement of 41 dB.

3.3 Limitations due to channel calibration errors

To analyse the effects of channel imbalance, the simulation process includes the presence of a deterministic but unknown angle-dependent imbalance between the receiving channels. We denote by $\Gamma_{ij}(\phi) = G_i(\phi)/G_j(\phi)$ the complex imbalance between channel i and j. Specifically, a sinusoidal phase imbalance is assumed as illustrated in Figure 3.5, where channel 1 is arbitrarily taken as reference. Notice that, channel error is modelled as a function of the angle ϕ between the array line and the receiver to scatterer line of sight.

It is worth noting that the level of the simulated phase imbalance in Figure 3.5 is of the same order of magnitude of the imbalance experienced on experimental data in Chapter 2.

The range-Doppler map resulting at the output of the STAP scheme in presence of channel imbalance is reported in Figure 3.4(c). ABPD approach with $L = 3$ and $K = 54$ is again applied. As expected, the adaptation capability of the STAP filter allows to intrinsically compensate for the angle dependent channel errors and keeps providing an effective cancellation of clutter echoes. In fact, the known one-to-one relationship between angle of arrival and Doppler frequency of stationary scatterers, as well as the fine Doppler resolution guaranteed by the long integration times of passive radar, allow the ABPD approach to
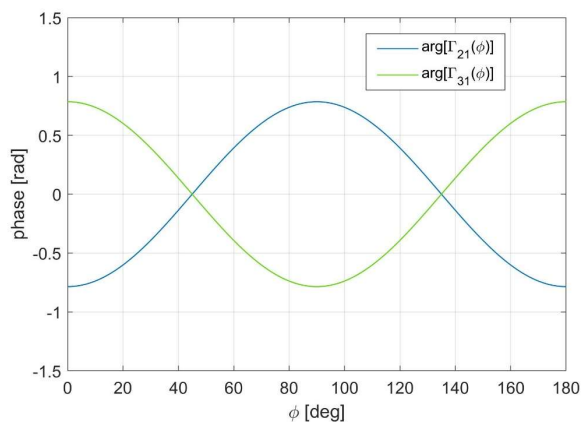
Figure 3.5: Simulated phase imbalance between receiving channels as a function of the angle of arrival.

55

operate on a clutter subspace accounting for a limited angular sector. This allows to significantly reduce the number of degrees of freedom of the adaptive filter, by still being able to compensate for the local variation of the angle-dependent channel imbalance.

However, although STAP proves robust against channel imbalance for what concerns clutter suppression capability, the same cannot be said for the corresponding target steering vector used in the adaptive filter. In fact, the presence of unknown channel errors may cause a mismatch between the nominal spatial steering vector $\boldsymbol{s}_s(\phi)$ and the actual target vector affected by channel imbalance, which can be modelled as $diag\{[1, \; \Gamma_{21}(\phi),...,\Gamma_{N1}(\phi)]\} \; \boldsymbol{s}_s(\phi)$, by taking channel 1 as reference without loss of generality. This may result in target signal gain losses. In the case of Figure 3.4(c), the final target SCNR is in fact limited to 9 dB, with a loss of 6 dB with respect to the case without channel imbalance.

Figure 3.6 shows the target signal response in the angle-Doppler domain at the output of the optimum space-time filter, without (a) and with (b) the effect of channel imbalance. Such result is evaluated in absence of noise and known covariance matrix case and can be seen as the theoretical output SCNR achievable, normalized to its maximum, as a function of target DOA and Doppler frequency. In both cases we recognize the typical clutter ridge of a side-looking configuration, but the presence of channel imbalance produces a slight deformation and an enlargement of the clutter notch. Moreover, we notice a dispersion of the clutter energy in the angle-Doppler domain, due to the angle-dependent imbalance. This results in losses also far from clutter notch, as an effect of the adaptive cancellation filter.

In order to evaluate the performance losses associated to the presence of channel imbalance in terms of target detection capability, a Monte Carlo analysis is performed (1000 runs) assuming the same simulated scenario and processing parameters adopted in the previous example. The space-time GLRT detector in (3.4) has been considered, with a desired PFA set to 10^{-6}. A Swerling 0 target model has been assumed.

(a)   (b)
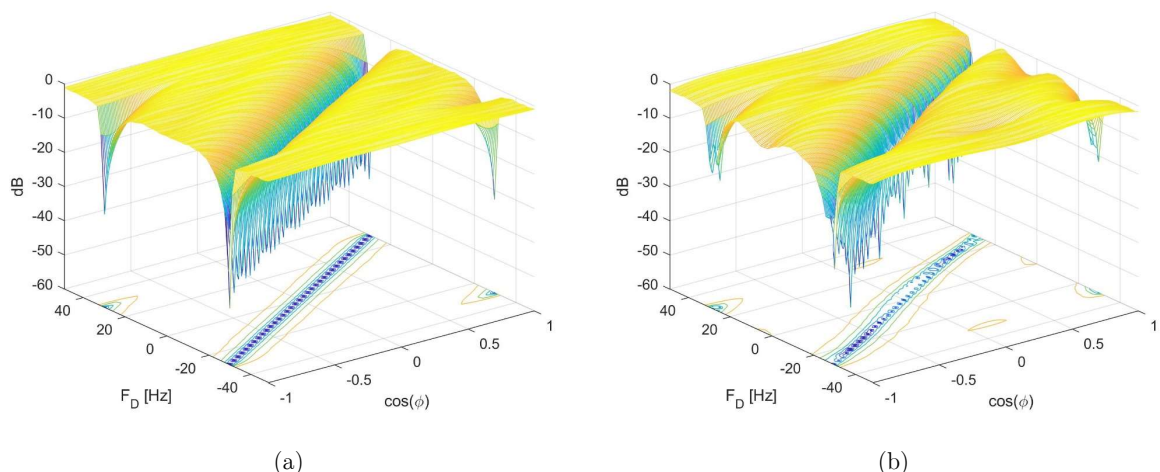
Figure 3.6: Target signal response in the angle-Doppler domain at the output of the optimum space-time filter in absence of noise and for known covariance matrix: (a) in the case of perfectly balanced channels; (b) in the presence of channel imbalance.

In Figure 3.7, the results are shown in terms of probability of detection (PD) as a function of target input SNR. Two targets are considered, a DOA $\phi_0 = 90°$ and with bistatic velocity 7 m/s and 3 m/s. They are representative of target condition sufficiently far and close to the clutter notch, respectively. The dashed curves in figure represent the detection performance achievable in absence of channel imbalance, while the solid curves show the corresponding performance when receiving channels are affected by the imbalance modelled in Figure 3.5.

A significant loss can be observed, especially for target velocity 3 m/s, corresponding to a slow target close to clutter notch. This indicates that the presence of channel mismatch may increase the clutter rank and produce an enlargement of clutter notch (as from [47]), thus raising the target minimum detectable velocity (MDV). This is also confirmed by looking at Figure 3.8, where PD is evaluated as a function of target bistatic velocity, for a fixed SNR of -45 dB. Notice that a decrease in PD performance is present also for higher velocity values. This is mostly caused by the mentioned dispersion of clutter energy in the angle-Doppler domain, which has to be cancelled by the adaptive filter (see depressions in Figure 3.6(b)).
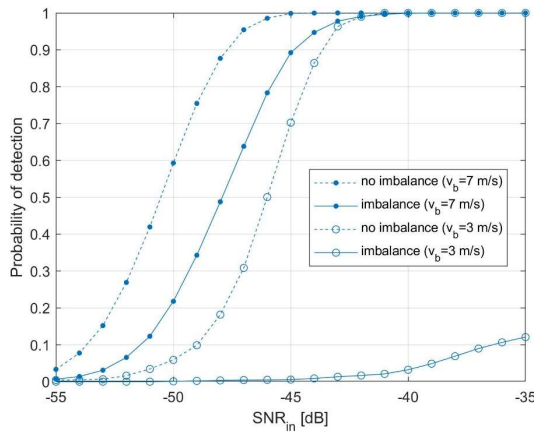
Figure 3.7: Probability of detection as a function of target input SNR, for target bistatic velocities 3 m/s and 7 m/s, in absence and in presence of channel imbalance. Desired false alarm probability is set to 10^{-6}.
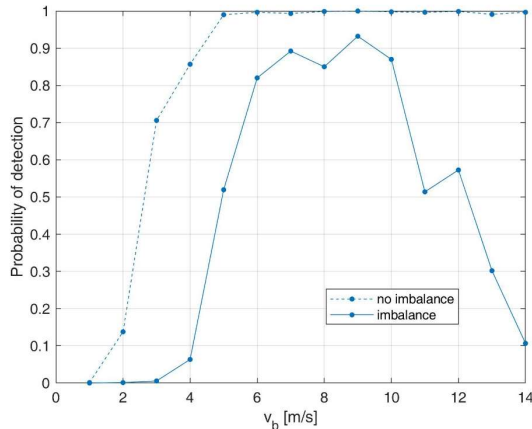
Figure 3.8: Probability of detection as a function of target bistatic velocity, for target input SNR=-45 dB, in absence and in presence of channel imbalance. Desired false alarm probability is set to 10^{-6}.

3.4 Solutions for target detection

It has been shown how the presence of an unknown imbalance affecting the receiving channels can impact on moving target detection performance of a mobile passive radar. In particular, when adopting a STAP approach on a multichannel system, the mismatch of target steering vector, as well as the coefficients estimated for the cancellation of clutter, may result in undesirable gain loss or even partial suppression of target signal at the output of the adaptive filter.

It is worth noting that applying digital channel calibration techniques, like those proposed in Chapter 2, to the received data is crucial to guarantee clutter cancellation in a non-adaptive approach like DPCA, while it is not strictly required in the STAP case. In fact, the adaptation capability of STAP can intrinsically compensate for localized channel errors, thus preserving clutter suppression capability. Moreover, in case of angle-dependent channel errors, target signal may experience a different imbalance compared to clutter contributions appearing at same Doppler frequencies, since belonging to a different angular direction. As a result, a Doppler-based calibration strategy like those in Chapter 2 would not be effective against target steering mismatches.

In the following, two possible strategies for target detection are proposed, aimed at recovering the performance losses associated to channel calibration errors in a mobile passive radar exploiting a STAP scheme.

3.4.1 Spatially non-coherent GLRT (NC-GLRT)

If the knowledge of channel imbalance in each desired steering direction is not possible, a simple potential solution can be to renounce to a coherent integration in the spatial domain. If a small number of receiving channels is available, typically true in passive radar systems, this would produce a limited loss in terms of final signal to disturbance ratio.

A partially non-coherent space-time GLRT detector (referred to as NC-GLRT) is proposed, where the steering vector is specified in the Doppler domain but not specified in the spatial domain, resulting in a non-coherent integration of the spatial target echoes.

Such detector, firstly introduced in [21], can be derived along the line of [72], where a polarimetric adaptive detection scheme is addressed. Considering the spatial component of the steering vector $\boldsymbol{s}_s$ as a vector of unknown parameters, this is replaced with its maximum likelihood estimate during the derivation process. By defining the $(NL \times N)$ matrix $\boldsymbol{\Sigma} = \boldsymbol{s}_d \otimes \boldsymbol{I}_N$, where $\boldsymbol{I}_N$ is the N-dimensional identity matrix, the resulting GLRT detector is given by:

$$\frac{\boldsymbol{x}^H \widehat{\boldsymbol{Q}}^{-1} \boldsymbol{\Sigma} \left(\boldsymbol{\Sigma}^H \widehat{\boldsymbol{Q}}^{-1} \boldsymbol{\Sigma} \right)^{-1} \boldsymbol{\Sigma}^H \widehat{\boldsymbol{Q}}^{-1} \boldsymbol{x}}{\left(1 + \boldsymbol{x}^H \widehat{\boldsymbol{Q}}^{-1} \boldsymbol{x} \right)} \gtrless \eta_2 \tag{3.6}$$

This detector keeps the CFAR property and the expression of the PFA follows (see [72]):

$$PFA = \frac{(1 - \eta_2)^{K-NL+1}}{(K - NL)!} \sum_{j=1}^{N} \frac{(K - NL + N - j)! \ \eta_2^{N-j}}{(N - j)!} \tag{3.7}$$

This approach still performs an adaptive space-time filtering of data, aimed at whitening of clutter returns. While, at the expense of a limited loss in terms of maximum integration gain (and directivity), it is robust against losses due to spatial steering vector mismatches, thanks to a non-coherent integration of target echoes across the receiving channels.

3.4.2 GLRT with steering vector calibration (Cal-GLRT)

An alternative and more sophisticated approach consists in maintaining a fully coherent detection scheme and exploiting the information from stationary scene echoes to estimate the angle-dependent channel errors and define the correct spatial steering vector towards desired target search direction.

The basic idea is to make use of the Doppler spread that characterizes clutter returns seen from a moving receiver and the corresponding relationship between angle of arrival and Doppler frequency. In a similar fashion to the approaches in Chapter 2, the Doppler frequency resolution can be exploited to isolate the contributions from scatterers belonging to specific angular directions, thus allowing an estimation of the angle-dependent imbalance affecting the receiving channels. In this regard, the fine Doppler resolution provided by the typically long integration times of passive radar is an additional asset.

This principle has been exploited also in some previous works, for array calibration in airborne radar [52]-[54], [60],[61]. The estimation of channel errors and the correct spatial steering vector in a specific direction can be made in different ways: for instance, by selecting principal eigenvector from clutter sample covariance matrix formed at corresponding Doppler bin [53],[61]; or by least square estimation comparing returns of co-registered range-Doppler maps at same Doppler bin [20],[60]. In this work, the latter approach is adopted.

Let us assume $z^{(i)}[l, m]$ to be the complex value at generic range-Doppler bin of the range-compressed and Doppler-processed channel i, after proper temporal co-registration. The imbalance estimated at the m-th Doppler bin between channels i and j (the latter assumed as reference) is given by:

$$\hat{\Gamma}_{ij}[m] = \frac{\sum_{l=l_1}^{l_2} z^{(i)}[l, m] \ z^{(j)^*}[l, m]}{\sum_{l=l_1}^{l_2} |z^{(j)}[l, m]|^2} \tag{3.8}$$

where the average is evaluated over consecutive range cells spanning indexes from l_1 to l_2.

The imbalance at specific direction of interest $\hat{\Gamma}_{ij}(\phi_0)$, can be obtained by selecting or interpolating the imbalance values estimated as a discrete function of Doppler bins in (3.8), at Doppler frequency $f_D = v_p/\lambda \cos \phi_0$.

Defining $\mathbf{\Lambda}(\phi_0) = \boldsymbol{I}_L \otimes diag\{[1, \hat{\Gamma}_{21}(\phi_0), \dots, \hat{\Gamma}_{N1}(\phi_0)]\}$, the space-time coherent GLRT detector with calibrated steering vector (referred to as Cal-GLRT) is given by:

$$\frac{\left|\boldsymbol{s}^H \mathbf{\Lambda}^{\mathrm{H}} \widehat{\boldsymbol{Q}}^{-1} \boldsymbol{x}\right|^2}{\boldsymbol{s}^H \mathbf{\Lambda}^{\mathrm{H}} \widehat{\boldsymbol{Q}}^{-1} \mathbf{\Lambda} \boldsymbol{s} \ (1 + \boldsymbol{x}^H \widehat{\boldsymbol{Q}}^{-1} \boldsymbol{x})} \gtrless \eta_1 \tag{3.9}$$

At the expense of the additional cost required for steering vector calibration, this solution is expected to maximise the spatial integration gain on target signal, provided that a good estimation of channel imbalance can be achieved. In addition, as will be shown in the following, this scheme preserves phase information between receiving channels, being suitable for target DOA estimation purpose.

3.5 Detection performance analysis

In order to test and compare the performance of the proposed detection strategies in a controlled environment, the same simulated clutter scenario of the previous Section is considered, with $N = 3$ receiving channels affected by the simulated angle-dependent imbalance in Figure 3.5. The ABPD-STAP approach is applied, with $L = 3$ Doppler bins and the number of training data is set to $K = 54$.

Detection performance is analysed by means of Monte Carlo analyses for moving targets in the endo-clutter region. The NC-GLRT scheme in (3.6) and the Cal-GLRT scheme in (3.9) are compared with the standard GLRT detector in (3.4), where a mismatched steering vector is considered due to channel imbalance. This latter case is referred to as mismatched GLRT. The case without imbalance is also considered as a reference. Specifically, in Figure 3.9(a), the results are shown in terms of estimated PD as a function of target input SNR, for the same target parameters of Figure 3.7. The desired PFA is set to 10^{-6}.

As expected, both the solutions proposed in Section 3.4 allow to mostly prevent the partial suppression of target signal due to the channel imbalance and the resulting steering vector mismatch, largely recovering the detection performance losses with respect to the case of no imbalance. A significant difference can be noticed, compared to the mismatched GLRT case (see solid blue curves), in terms of minimum SNR required for a given PD, especially for lower target velocity. The performances of the ideal case (see blue dashed curves) are almost restored. Note that, although the considered solutions largely recover the performance losses caused by imbalance, the condition of perfectly balanced channels in all directions cannot be completely re-established.

The above considerations are also confirmed by looking at Figure 3.9(b), where the PD is shown as a function of target bistatic velocity, for a fixed SNR of −45 dB. Both NC-GLRT and Cal-GLRT allow a considerable reduction of target MDV, by reducing the width of clutter notch. The performance at higher velocity values is also considerably improved.

The Cal-GLRT detector (see green dash-dot curves) yields the best performance. In fact, the steering vector calibration allows to maximise the coherent integration gain of target signal in the spatial domain.

Confirmation of the above can be found by looking at the target signal response at the output of the optimum filter, shown in Figure 3.10. As evident, a narrow clutter ridge is restored, thanks to the steering vector calibration. Small losses far from clutter notch are still present (see depressions in Figure 3.10), due to the mentioned dispersion of clutter energy in

(a) (b)
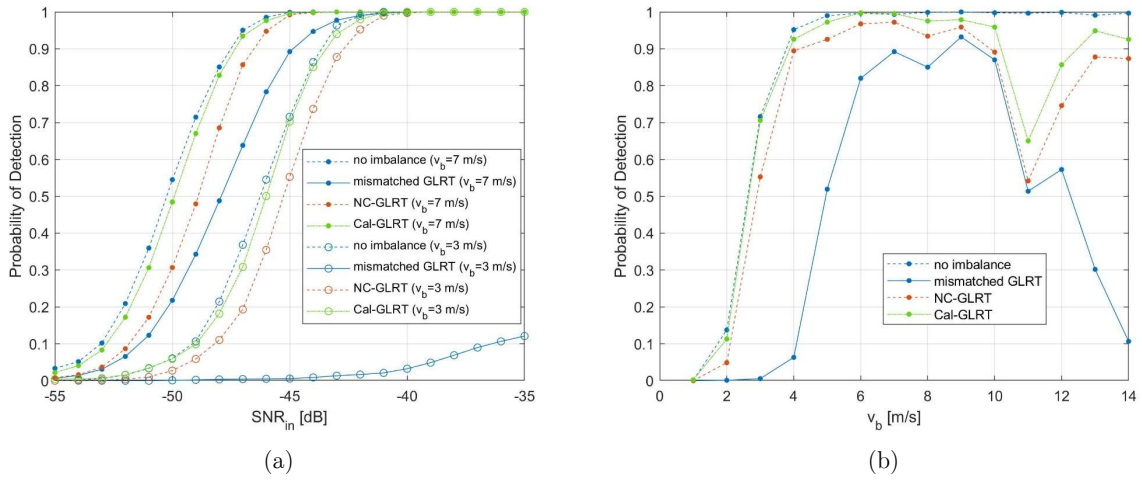
Figure 3.9: Performance comparison of the considered detection schemes, in presence of channel imbalance. (a) Probability of detection as a function of target input SNR, for target bistatic velocities 3 m/s and 7 m/s. (b) Probability of detection as a function of target bistatic velocity, for target input SNR=-45 dB. False alarm probability is set to 10-6.
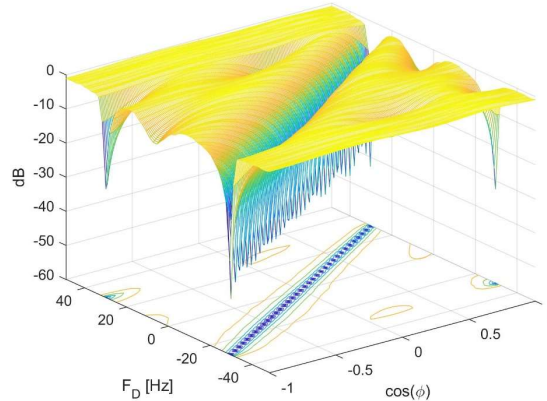
Figure 3.10: Target signal response in the angle-Doppler domain at the output of the optimum space-time filter in absence of noise and for known covariance matrix, when considering the steering vector calibration.

the angle-Doppler domain. They are mostly associated to side-lobe residual clutter contributions and depends on the specific angular behaviour of the considered imbalance. They are responsible for the losses observable around 11 m/s in Figure 3.9(b).

Notice that, in the considered simulated scenario, the homogeneous distribution of clutter facilitates the estimation of channel imbalance and the corresponding steering vector correction at desired angular direction. In a real environment, strategies accounting for potential variation of imbalance as a function of range or for robustness of estimation against outliers, like those described in Chapter 2, could be adopted.

The NC-GLRT approach (see red dashed lines in Figure 3.9) only shows slight losses (in the order of 1-2 dB) compared to the Cal-GLRT case. These are mostly associated to a minor loss of non-coherent integration in the spatial domain (when using a small number of receiving channels). Nevertheless, it proves that an effective disturbance rejection capability is still preserved, despite the lower complexity due to the absence of an online calibration stage.

Therefore, this last approach proves to be a suitable and simple solution for the purpose of target detection in mobile passive radar with few receiving channels, being robust against significant imbalance possibly affecting the channels.

3.6 Target DOA estimation

Typically, passive radar exploiting VHF/UHF bands are characterized by broad antenna beams and a limited number of array elements. Therefore, an accurate target localization represents a critical task and interferometric approaches are commonly used to estimate target DOA, by exploiting the phase information across the available receiving channels.

Specifically, an ML DOA estimation approach for radar employing STAP is assumed (see [73]). Like the detection schemes in previous Sections, DOA estimation can be performed after a non-adaptive transformation, aimed at containing the adaptivity losses and the required computational complexity.

By operating in the space-Doppler domain after the ABPD transformation of Figure 3.2, the target angle estimate is obtained by maximizing the log-likelihood function with respect to ϕ:

$$\hat{\phi}_t = \arg \max_{\phi} \left\{ \frac{\left| \boldsymbol{s}^H(\phi) \widehat{\boldsymbol{Q}}^{-1} \boldsymbol{x} \right|^2}{\boldsymbol{s}^H(\phi) \widehat{\boldsymbol{Q}}^{-1} \boldsymbol{s}(\phi)} \right\} \tag{3.10}$$

where the unknown ϕ_t represents the actual target DOA.

In practice, the ML estimate can be viewed as the location of the peak in a dense grid of adaptive matched filters (AMF) [74]. Typically, the radar performs detection tests over a bank of filters coarsely spaced by the nominal beamwidth in angle. Once a target is detected,

refined angle measurement is achieved through (3.10). The desired level of RMS error is typically chosen to be about a tenth or twentieth of beamwidth (BW).

The presence of an unknown imbalance affecting the receiving channels is a major problem for target detection but even more for their accurate angular localization. Inter-channel imbalance is expected to produce a significant degradation of DOA estimation accuracy. Although a non-coherent integration strategy in the spatial domain represents an effective solution for target detection, a coherent approach paired to a proper calibration of spatial steering vector is required when interested in target DOA estimation.

The same strategy adopted in Section 3.4.2 for calibration of target steering vector based on returns from stationary scene can be exploited to achieve a corrected ML DOA estimator.

By defining $\mathbf{\Lambda}(\phi) = \boldsymbol{I}_L \otimes diag\{[1, \hat{\Gamma}_{21}(\phi), ..., \hat{\Gamma}_{N1}(\phi)]\}$, $\hat{\Gamma}_{ij}(\phi)$ being the estimated imbalance between channels i and j for each angle ϕ in a dense grid around the direction of target detection, the ML DOA estimator with calibrated steering vector (referred to as calibrated MLE) is given by:

$$\hat{\phi}_t = \arg \max_\phi \left\{ \frac{\left|\boldsymbol{s}^H(\phi)\mathbf{\Lambda}^{\mathrm{H}}(\phi)\widehat{\boldsymbol{Q}}^{-1}\boldsymbol{x}\right|^2}{\boldsymbol{s}^H(\phi)\mathbf{\Lambda}^{\mathrm{H}}(\phi)\widehat{\boldsymbol{Q}}^{-1}\mathbf{\Lambda}(\phi)\boldsymbol{s}(\phi)} \right\} \tag{3.11}$$

Imbalance $\hat{\Gamma}_{ij}(\phi)$ for each test direction can be obtained by interpolating the imbalance estimated as a function of Doppler bins $\hat{\Gamma}_{ij}[m]$, at Doppler frequency $f_D = v_p/\lambda \cos \phi$.

The DOA estimation accuracy of the standard ML estimator in (3.10), referred to as mismatched MLE, and of the calibrated version in (3.11) is evaluated by means of a Monte Carlo analysis (1000 runs), against the same simulated scenario of the previous Sections. An ABPD-STAP approach is again applied, with $N = 3$ receiving channels, possibly affected by the angle-dependent imbalance shown in Figure 3.5, and $L = 3$ Doppler bins. The number of training data for disturbance covariance matrix estimation is set to $K = 54$. Both the estimators operate with a bank of filters equally spaced in angle by $\delta\phi = 1°$ within the array nominal BW ($\sim$57°), centred at $\phi_0 = 90°$. The simulated target DOA is set to $\phi_t = 85°$.

First, in order to appreciate the effect of a steering vector calibration on DOA estimation performance when in the presence of channel imbalance, Figure 3.11 shows the likelihood function of (3.10) and (3.11), obtained in the ideal case of known covariance matrix and in absence of noise. Notice that the phase imbalance generates a bias error in the mismatched case (blue curve), which is instead removed by the steering vector calibration (green curve). Moreover, especially for slower targets, also the width of the clutter notch plays a fundamental role.

In Figure 3.12, the accuracy of the DOA estimators is compared as a function of target input SNR, for bistatic velocities 7 m/s and 3 m/s. Results are shown in terms of standard deviation and bias of the estimation, both normalised to the nominal BW.
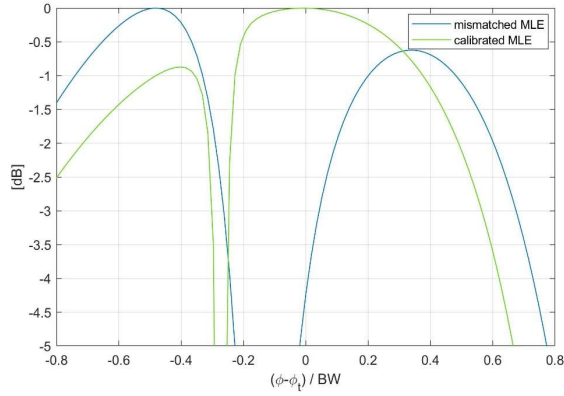
Figure 3.11: Example of the likelihood functions of the ML DOA estimators, in the known covariance matrix case, when in presence of channel imbalance. Target set at DOA 85° with bistatic velocity 3 m/s.

First, we notice that the presence of channel imbalance significantly degrades the accuracy of the mismatched MLE (see solid blue curves), by increasing both the standard deviation and the bias error, with respect to the case where no imbalance is present (see dashed blue curves). In particular, the resulting mismatch tends to polarize the DOA estimate, as clearly visible in Figure 3.12(b), for high SNR values.

Conversely, it is evident that the calibrated MLE (see dash-dotted green curves) is able to mostly prevent the performance losses due to the channel imbalance, almost recovering the estimation accuracy of the ideal case (namely in absence of imbalance).

To provide an additional reference for the DOA estimation accuracy of the considered scheme in the ideal case and to better evaluate the impact of channel errors and of the proposed calibration approach, the Cramér-Rao bound (CRB) is also considered.

Following [75][76], and assuming known target Doppler frequency and covariance matrix Q, the CRB after the non-adaptive ABPD transformation can be expressed as:

(a)   (b)
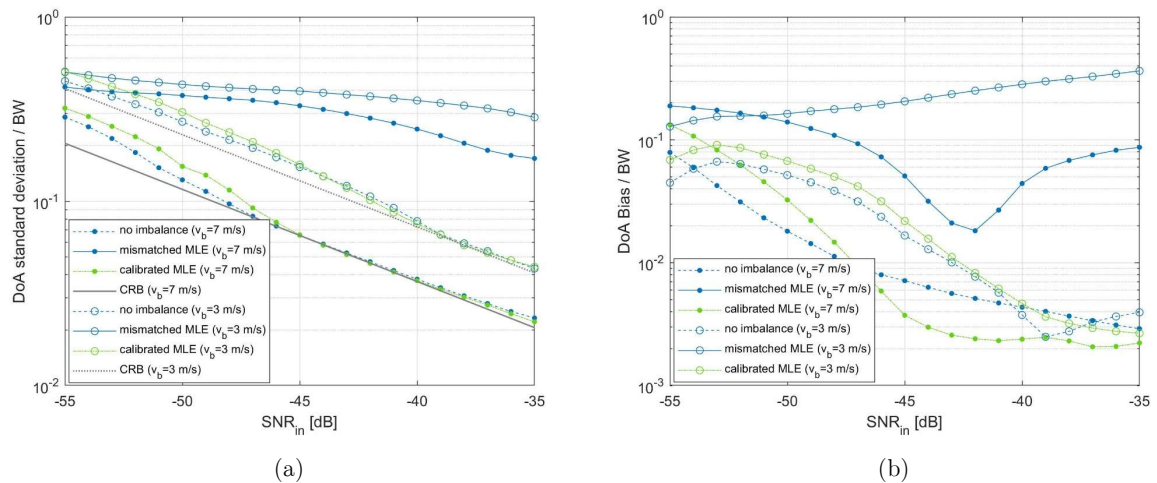
Figure 3.12: Comparison of ML DOA estimation accuracy as a function of target input SNR: (a) standard deviation normalized to BW; (b) bias error normalised to BW.

$$\sigma_\phi^2 = [\boldsymbol{J}^{-1}] = \left\{ 2|\bar{A}|^2 \left[\left(\dot{\boldsymbol{s}}^H(\phi)\boldsymbol{Q}^{-1}\dot{\boldsymbol{s}}(\phi) \right) - \frac{|\dot{\boldsymbol{s}}^H(\phi)\boldsymbol{Q}^{-1}\boldsymbol{s}(\phi)|^2}{\boldsymbol{s}^H(\phi)\boldsymbol{Q}^{-1}\boldsymbol{s}(\phi)} \right] \right\}^{-1} \tag{3.12}$$

where σ_ϕ is the standard deviation of the DOA estimation error, $\boldsymbol{J}$ is the Fisher information matrix, $\overline{A}$ is the resulting target complex amplitude and $\dot{\boldsymbol{s}}(\phi) = \partial\boldsymbol{s}(\phi)/\partial\phi$.

In Figure 3.12(a), the corresponding CRB is reported for both the considered target velocities (solid and dotted grey curves). For high SNR values there is a good match between theoretical results and simulation. This is due to the ML nature of the estimator, which guarantees the condition of asymptotic efficiency. A little departure of the simulated results from the theory occurs for low SNR, when the standard deviation of the estimate becomes comparable with the BW. This is however a case of limited interest. Also notice that, for higher SNR, the ML estimator is subject to a saturation effect due to the use of a discrete set of angles (bank of filters) for DOA estimation.

3.7 Experimental results

In this Section, the effectiveness of the proposed strategies for target detection and DOA estimation is demonstrated against a set of experimental data from the DVB-T based multichannel mobile passive radar from Fraunhofer FHR.

Specifically, the same set of data employed in Chapter 2 is considered. In this case, the signal acquired by all the four available receiving channels is exploited. The four channels serve as surveillance channels and are arranged to form a uniform linear array (ULA) in side-looking configuration (see Figure 2.4). The reference signal is reconstructed from one of them.

The parameters of the exploited DVB-T signal and the main acquisition and processing parameters are the same reported in Table 2.1. Refer to Figure 2.5(a) for a sketch of the bistatic acquisition geometry.

The four receiving channels are affected by a considerable angle dependent imbalance, as thoroughly described in Chapter 2. However, differently from the DPCA case analysed before, such imbalance is not expected to compromise the clutter suppression capability when the ABPD-STAP approach is adopted. Nevertheless, it can have an impact on moving target detection and localization performance, as described in the previous Sections.

To prove the effectiveness of the proposed solutions in preventing the performance degradation due to steering vector mismatch, four simulated moving targets are injected into the real data, according to the model in (3.1), in addition to the real cooperative aerial target Delphin. Proper imbalance is applied to the generated target echoes across the receiving

Table 3.1

Target parameters

	T1	T2	T3	T4	Delphin
R_b	4700 m	3700 m	6850 m	2500 m	6596 m
v_b	-6 m/s	6 m/s	11 m/s	4 m/s	-24.5 m/s
ϕ_t	37°	157°	109°	70°	~ 37°
$SCNR_i$	-1 dB	-6 dB	-2 dB	-12 dB	2 dB
$SCNR_o$	17 dB	16 dB	12 dB	17 dB	15 dB

channels, according to the imbalance estimated at the corresponding target DOA. The parameters of the real and the simulated targets are reported in Table 3.1. Notice that the direction of Delphin target is known only with a certain approximation.

Figure 3.13 shows the range-Doppler maps resulting from the considered experimental data set plus the simulated targets. Specifically, Figure 3.13(a) represents the range-Doppler map obtained from a single channel, namely before STAP processing, scaled to the estimated noise power level. As evident, the clutter returns from the stationary scene extend over a Doppler bandwidth compatible with the platform velocity ($v_p/\lambda \cong \pm 32\ Hz$) and are characterized by a strong heterogeneity in terms of power levels across the map. Moreover, a strong direct signal contribution appears at first bistatic range bin and low Doppler frequency, being the angle between the Rx-Tx line of sight and the platform velocity vector close to 90°.

The considered moving targets, due to their bistatic radial velocity and DOA, fall within the clutter Doppler bandwidth and appear as buried into clutter, being hardly detectable. Their positions are indicated by white boxes and the corresponding SCNR values are reported.
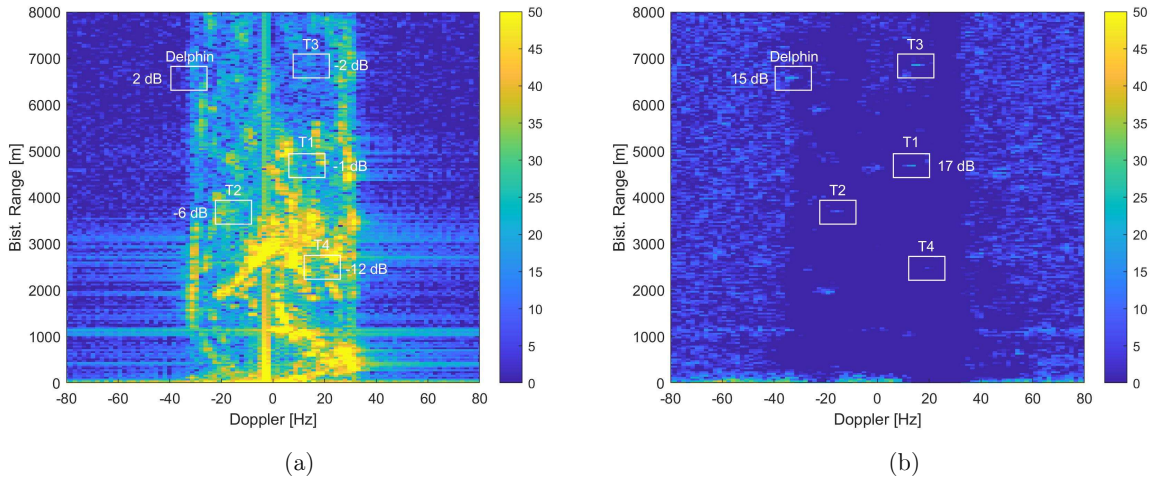
Figure 3.13: Range-Doppler maps obtained from the experimental data: (a) single channel map; (b) map after ABPD-STAP with calibrated steering vector towards direction of targets T1 and Delphin. Target positions are indicated by white boxes and the corresponding SCNR values are reported. SCNR after STAP filtering is reported only for targets belonging to the selected steering direction.

Figure 3.13(b) shows the resulting range-Doppler map at the output of the space-time adaptive filter (numerator of (3.9)). The ABPD-STAP scheme is applied, with $N = 4$ channels and $L = 3$ Doppler bins. In this case, the number of training data is limited to $K = 3NL = 36$, in order to account for the heterogeneity of the real clutter scenario. In fact, this can limit the number of available homogeneous secondary data, thus reducing the effectiveness of STAP.

The steering vector of the adaptive filter is selected towards the DOA of targets T1 (i.e. $\varphi_0 = 37°$) and calibrated based on the imbalance estimated from clutter, at the corresponding Doppler bin. With such steering, also the real target Delphin is expected to be included in the BW. For this reason, the SCNR values after STAP filtering are reported in the figure only for pointed targets T1 and Delphin. The other targets do not reach their maximum SCNR, since belonging to different DOAs, however they are still visible in the final map. The output SCNR values achievable when the proper steering vector is applied for each target are reported in Table 3.1.

The above result clearly demonstrates the effective clutter suppression capability of the proposed STAP approach, which proves to be robust against the presence of angle dependent calibration errors affecting the receiving channels.

To analyse more in detail the role of the solutions proposed in Section 3.4 for target detection and to compare their performance, Figure 3.14(a) and (b) report the results obtained with the NC-GLRT detector in (3.6) and with the Cal-GLRT detector in (3.9), respectively.

Specifically, for each solution, the test statistics is reported over the bistatic range-Doppler map before the application of a proper threshold, selected according to a desired value of nominal PFA. For a fair comparison, the test statistic is mapped into the PFA setting that

(a)   (b)
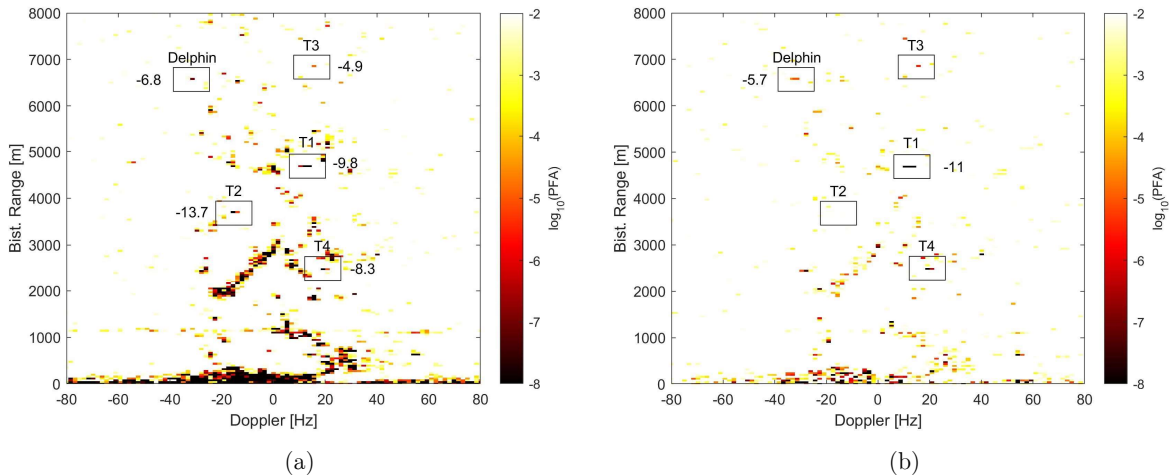
Figure 3.14: Minimum nominal PFA to be set to detect each bin, using (a) the NC-GLRT scheme; (b) the Cal-GLRT scheme with steering towards direction of targets T1 and Delphin. Values are expressed as $\log_{10}(\text{PFA})$. Target positions are indicated by black boxes. PFA values for the Cal-GLRT case are reported only for targets belonging to the selected steering direction.

Table 3.2

Minimum nominal PFA for target detection [$\log_{10}$(PFA)]

	T1	T2	T3	T4	Delphin
mismatched GLRT	-1.4	-1.9	-3.4	-3.2	-1.8
NC-GLRT	-9.8	-13.7	-4.9	-8.3	-6.8
Cal-GLRT	-11.1	-15.3	-6.2	-9.7	-5.7
Cal-GLRT @+5°	-8.9	-14.7	-5.6	-9.4	-5.3
Cal-GLRT @+10°	-6.3	-13.5	-4.9	-5.2	-4.9

would allow to exceed the corresponding threshold. In other words, each pixel in the map has been scaled so that it represents the minimum value of nominal PFA to be set for that pixel to yield a detection. Notice that results are reported as $\log_{10}$(PFA).

Target positions are indicated on maps by black boxes. Notice that, for the Cal-GLRT scheme in Figure 3.14(b), the calibrated steering vector is again steered towards the DOA of targets T1 and Delphin. For this reason, the PFA values are compared in the figure only for the two targets belonging to the steering direction.

For a complete comparison, Table 3.2 reports the minimum nominal PFA values to detect each target with the different detection schemes. Specifically, for the Cal-GLRT scheme, the case where the selected direction for steering and calibration is coincident with each target DOA and the cases where it deviates by 5° or 10° with respect to target angular positions, with targets still included in the array nominal BW (~23°), are considered. This in order to simulate realistic detection conditions of a target search stage. Notice that such different target steering conditions are not considered for the NC-GLRT detector, which does not include a spatial steering vector component, due to the non-coherent integration in the spatial domain. Finally, for comparison, the results obtained in the mismatched GLRT case are also reported.

From the results in Figure 3.14 and Table 3.2, the following considerations are in order:

- The NC-GLRT scheme allows us to detect targets in all directions simultaneously (depending on the antenna element pattern), while the fully coherent scheme normally requires proper beam steering.
- The non-coherent integration yields a higher number of false alarms for the same PFA compared to the Cal-GLRT scheme, even at low PFA values, due to the enhancement of persistent clutter structures. However, notice that the NC-GLRT tends to integrate the false alarms accounting for all different angular directions.
- It is also worth noting that the presence of additional non-cooperative moving targets in the scene during the acquisition cannot be excluded.

- The Cal-GLRT scheme yields better results with respect to the NC-GLRT, when steering is aligned with target DOA, allowing target detection until lower values of PFA. The only exception is Delphin target, where a slightly better result is achieved with the non-coherent approach. This is mostly because for simulated targets the imbalances were generated based on clutter data, therefore a perfect calibration can be reached with the adopted technique. While the real target, whose DOA may not exactly match the nominal one and which also features an elevation angle, may deviate from the imbalance estimated from clutter.

- Accordingly, when target DOA does not exactly coincide with steering direction (last two rows of Table 3.2), but still falls within the BW and therefore detection is desirable, the NC-GLRT approach may outperform the Cal-GLRT also for the simulated targets. In this case, in fact, the estimated calibration may differ from that required by the target, due to the angular variation of channel imbalance. Nevertheless, both the considered solutions yield significantly better results compared to the mismatched GLRT case.

- Selecting a PFA of 10^{-4} all the considered targets would be detected by both the proposed detection approaches; conversely, none of them would be detected in the mismatched case.

In the coherent approach, the array nominal BW is in the order of 23°, thus offering poor target localization capability. An appropriate estimation of target DOA is then required.

To estimate the target angular position and verify the role of steering vector calibration in the target localization process, the space-time ML DOA estimation approach proposed in Section 3.6 is considered. Specifically, it is applied for each target after the same ABPD transformation used for detection, exploiting the $N = 4$ receiving channels, $L = 3$ Doppler bins and $K = 36$ training data. A bank of filters equally spaced by $\delta\phi = 0.1°$ within the nominal BW is adopted.

The results of DOA estimation for each target are reported in Table 3.3, for the mismatched MLE in (3.10) and the calibrated MLE in (3.11). The errors with respect to the corresponding true DOA values in Table 3.1 are reported in brackets.

It is evident that the steering vector calibration allows to significantly improve the estimation accuracy, preventing the negative impact of channel imbalance on target

Table 3.3

Target DOA estimation results

	T1	T2	T3	T4	Delphin
mismatched MLE	32.1° (-4.9°)	145.5° (-11.5°)	106.3° (-2.7°)	81.5° (+11.5°)	46.9° (+9.9°)
calibrated MLE	35.7° (-1.3°)	157.1° (+0.1°)	108.6° (-0.4°)	70.2° (+0.2°)	35.4° (-1.6°)

localization performance. In fact, a correct DOA estimated is achieved for all targets, with an average error below one thirtieth of the nominal BW. Notice that a slightly less accurate estimation is achieved for T1 and Delphin targets, whose DOA is far from the broadside direction.

The above results clearly demonstrate the effectiveness of the proposed strategies, both in terms of target detection and DOA estimation, in the presence of channel calibration errors.

From the above considerations, for a mobile passive radar equipped with a limited number of receiving channels, it seems reasonable to suggest the following operational strategy. A less demanding spatially non-coherent approach like in (3.6), which does not require an online calibration stage, could be adopted for the purpose of target detection. While an additional calibration stage could be applied in a fully coherent space-time scheme for DOA estimation like in (3.11), once target has been detected.

3.8 Summary

This Chapter addressed the problem of clutter rejection and slow-moving target detection and localization from multichannel mobile passive radar in the presence of antenna calibration errors. Specifically, it considered the application of a post-Doppler STAP scheme and discussed the impact of channel calibration issues, proposing some practical solutions.

An ABPD-STAP was suggested as a suitable approach for mobile passive radar and its effectiveness was analysed in terms of clutter cancellation and moving target detection, against both simulated and real clutter scenarios. The scheme is especially tailored to address the case of an angle-dependent imbalance affecting the receiving channels. In this case, the clutter cancellation capability is guaranteed by the adaptive degrees of freedom of the STAP filter. Nevertheless, it was shown that the effects of target steering vector mismatch and of filter coefficients estimated for clutter suppression may result in gain losses and partial suppression of target signal at the output of the adaptive filter, as well as in its inaccurate angular localization.

To address these points, the proposed ABPD-STAP scheme includes solutions aimed at recovering the target detection losses and performing an accurate DOA estimation.

First, a spatially non-coherent space-time GLRT (NC-GLRT) scheme was considered, where steering vector is not specified in the spatial domain, resulting in a non-coherent integration of target echoes across the receiving channels. Our analysis showed that, at the expense of a limited loss in terms of maximum integration gain, this approach is robust against a significant imbalance affecting the received signals, thus preventing large detection losses. By entirely excluding the presence of a calibration stage, it represents a simple but effective solution for moving target detection, especially when few receiving channels are available.

Then, a calibrated space-time GLRT (Cal-GLRT) scheme was considered, where the echoes from the stationary scene are exploited for an estimation of the angle-dependent channel errors and a proper correction of the spatial steering vector mismatch, making use of the clutter spread in Doppler and of the one-to-one relationship between angle of arrival and Doppler frequency of stationary scatterers. This approach is specifically devised for the case of passive radar STAP, where it is customary to operate with long coherent integration intervals and wide antenna beams, which allows the proposed calibration approach to operate effectively. Our analysis showed that, at the expense of an additional calibration stage, this solution can provide slightly better detection performance and allows to preserve target DOA estimation capability. Alternatively, it can be applied only to the potential targets detected by a first stage based on the NC-GLRT scheme, to enable DOA estimation capability.

Finally, the problem of target angular localization by DOA estimation was addressed, which represents a critical task in mobile passive radar featuring few wide beam antennas. We capitalized on the introduced steering vector calibration, by assessing the key role that it plays in providing an accurate space-time ML estimation of target DOA, by mitigating the negative impact of the unknown channel errors.

The effectiveness of the proposed solutions has been tested, in terms of moving target detection and localization, against both simulated and experimental data from a DVB-T based multichannel mobile passive radar, showing an effective operation.

Chapter 4

Dual Cancelled Channel STAP for target detection and DOA estimation in Passive Radar

In this Chapter, a dual cancelled channel STAP scheme is proposed for slow-moving targets detection and DOA estimation in multi-channel mobile passive radar, aimed at reducing the system computational complexity, as well as the number of required training data, compared to a conventional full-array solution. The proposed scheme, in conjunction with an ABPD approach, yields comparable performance with respect to the equivalent full array case, both in terms of target detection and DOA estimation accuracy, despite the lower computational cost. Moreover, it offers more robustness against adaptivity losses, operating effectively even in the presence of a limited set of training data, as often available in highly non-homogeneous clutter scenarios experienced in bistatic passive radar. In Section 4.1, the addressed issues and the aims of the study are introduced. Section 4.2 recalls the processing scheme for passive radar STAP proposed in Chapter 3. Section 4.3 describes the processing steps of the dual cancelled channel STAP for passive radar. Its performance is then analysed in Section 4.4, in terms of target detection and DOA estimation, against a simulated clutter scenario and compared with that of the corresponding full array solution. In Section 4.5, the effectiveness of the proposed scheme is validated against a set of experimental data from a DVB-T based multi-channel mobile passive radar. Finally, conclusions are drawn in Section 4.6.

4.1 Introduction

The use of multiple channels on receive and the adoption of STAP techniques for GMTI in mobile passive radar was shown to overcome the intrinsic limitations of a DPCA approach. A complete processing scheme has been proposed in Chapter 3, as particularly suitable for mobile passive radar. By resorting to an adjacent-bin post-Doppler (ABPD) STAP approach, it easily fits into the typical passive radar processing chain and takes advantage of the long integration times to reduce the size of the adaptive cancellation problem and intrinsically compensate for potential angle-dependent channel errors. Target detection is then based on

a space-time detection scheme where a calibrated spatial steering vector can be exploited to prevent accidental target rejection arising from severe channel imbalance. Finally, a space-time maximum likelihood estimator (MLE) is employed to also provide the accurate target angular localization.

The passive radar STAP scheme in Chapter 3 showed to enables effective GMTI capability. A much larger flexibility is gained compared to DPCA thanks to the adaptive use of a higher number of spatial degrees of freedom (DOF). In fact, clutter cancellation, target detection and DOA estimation are performed according to a full-array strategy, i.e., by jointly exploiting all the N available channels on receive. This is paid in terms of increased complexity for the resulting system, since it requires: (i) the estimation and inversion of a $NL \times NL$ space-time disturbance covariance matrix, L being the number of temporal DOF; (ii) the availability of a number of training data greater than $2NL$ in order to limit the adaptivity loss [47], which might be difficult to be guaranteed in the considered bistatic passive radar scenario; and (iii) the implementation of computationally expensive algorithms for the maximization of the DOA MLE likelihood function, being the computational burden dependant on the desired estimation accuracy.

In this Chapter, the above limitations are addressed, and an alternative approach based on a dual cancelled channel STAP scheme is proposed. This approach takes inspiration from a family of sub-optimal STAP schemes reported in the active radar literature [77]-[80], where an adaptive transformation is first applied on the received data to reduce the number of spatial DOF, which are then directly exploited for both target detection and DOA estimation. For instance, the solution in [78] exploits the generalised monopulse estimator (GME), which relies on the sum and difference channels obtained after adaptive clutter cancellation. However, in order to also limit the computational cost of the preliminary adaptive transformation, we resort to the AB-STAP technique presented in [79].

This technique is first integrated into the ABPD-STAP scheme proposed in Chapter 3. Accordingly, the output of the first processing stages, separately applied at each receiving channel, are grouped into two spatially displaced antenna sub-apertures and the same STAP technique is applied to each sub-aperture, thus obtaining two clutter cancelled channels. These channels are then properly recombined for the purpose of target detection, while target DOA is estimated via a simple closed-form expression from the two outputs by exploiting their displaced phase centres. The AB-STAP approach allows us to further reduce the computational complexity of the system, by reducing the number of the adaptive DOF in the space-time clutter filtering (namely the size of the covariance matrices to be estimated and inverted). Despite the lower computational cost, the proposed scheme does not suffer from significant performance losses with respect to the conventional full-array solution. Moreover, due the smaller number of adaptive DOF, it is more robust against adaptivity losses, operating effectively even in the presence of a limited sample support. This plays a key role in a real passive radar scenario, where the effectiveness of STAP is subject to the potential

non-homogeneity of clutter, which may limit the number of relevant training data. Lastly, the estimation of target DOA does not require a functional maximisation, thanks to the closed form expression of the estimator, thus requiring a lower computational cost, which in turn is independent of the desired estimation accuracy.

The moving target detection and localization performance of the proposed strategy are analysed and compared with those of the equivalent full array solution (assumed as a benchmark), against a simulated clutter scenario. Moreover, results are shown against experimental data collected by a DVB-T based multi-channel passive radar mounted on a ground moving platform. The obtained results clearly demonstrate the effectiveness of the considered strategy.

4.2 Passive radar STAP scheme

Let us consider again the system configuration illustrated in Figure 3.1. A multichannel passive radar receiver, mounted on a moving platform and exploiting a stationary transmitter as illuminator of opportunity, moves at constant velocity v_p on a straight-line trajectory. The N spatial receiving channels are arranged in the along-track direction with spacing d and form a uniform linear array (ULA) in side-looking configuration. We denote by ϕ the angle between the antenna end-fire and the receiver to scatterer line of sight.

The same signal and clutter model adopted in Chapter 2, for a dual channel system, and in Chapter 3, for the corresponding multi-channel case, is considered. For convenience, this Section briefly recalls the processing scheme proposed in Chapter 3 for passive radar STAP (see Figure 3.2), here referred to as full array STAP scheme, since jointly exploiting all the N available spatial DOF.

After a preliminary stage, including synchronization and reconstruction of the reference signal, the range compression is performed by means of reciprocal filter. A batch processing architecture is separately applied at each receiving channel, establishing the conventional fast-time/slow-time framework of a pulsed radar. After range compression, the samples associated to the range cell under test, coming from the N receiving channels and the M batches in the CPI, are arranged into the $(NM \times 1)$ space-time data vector $\tilde{\boldsymbol{x}}$. In the presence of target with complex amplitude $\bar{A}$, Doppler frequency f_D, and DOA ϕ, the data vector can be written as $\tilde{\boldsymbol{x}} = \bar{A}\,\tilde{\boldsymbol{s}} + \tilde{\boldsymbol{d}}$, where $\tilde{\boldsymbol{d}}$ is the disturbance (clutter plus noise) component, assumed Gaussian with space-time covariance matrix $\widetilde{\boldsymbol{Q}}$. The space-time steering vector $\tilde{\boldsymbol{s}}$ can be expressed as $\tilde{\boldsymbol{s}}(f_D, \phi) = \boldsymbol{s}_t(f_D) \otimes \boldsymbol{s}_s(\phi)$, where $\boldsymbol{s}_t(f_D) = [1, e^{-j2\pi f_D T}, ...\,, e^{-j2\pi f_D MT}]^H$ and $\boldsymbol{s}_s(\phi) = [1, e^{j2\pi d/\lambda \cos\phi}, ...\,, e^{j2\pi Nd/\lambda \cos\phi}]^H$ are respectively the temporal and spatial steering vector, $\otimes$ denoting the Kronecker product, H the Hermitian transpose and λ the signal carrier wavelength.

Adopting an ABPD approach, the adaptive filter is applied on a subset of Doppler-processed data, specifically on the N spatial samples from L adjacent Doppler bins centred

at the cell under test. Denoting by $\boldsymbol{T}$ the non-adaptive transformation matrix, consisting of L adjacent columns of a DFT matrix, the transformed data vector in the space-Doppler domain is $\boldsymbol{x} = \boldsymbol{T}^H \widetilde{\boldsymbol{x}} = \bar{A}\,\boldsymbol{s} + \boldsymbol{d}$, of size $(NL \times 1)$, where $\boldsymbol{s}(\phi) = \boldsymbol{s}_d \otimes \boldsymbol{s}_s(\phi)$. The corresponding $(NL \times NL)$ disturbance covariance matrix is $\boldsymbol{Q} = \boldsymbol{T}^H \widetilde{\boldsymbol{Q}} \boldsymbol{T}$.

The well-known adaptive matched filter (AMF) detector [74], applied after the ABPD transformation, is given by:

$$\frac{\left|\boldsymbol{s}^H \widehat{\boldsymbol{Q}}^{-1} \boldsymbol{x}\right|^2}{\boldsymbol{s}^H \widehat{\boldsymbol{Q}}^{-1} \boldsymbol{s}} \gtrless \eta \tag{4.1}$$

where matrix $\boldsymbol{Q}$ is replaced by its ML estimate $\widehat{\boldsymbol{Q}} = \boldsymbol{X}_k \boldsymbol{X}_k^H$, being $\boldsymbol{X}_k = [\boldsymbol{x}_1, \dots, \boldsymbol{x}_K]$ a set of training data of size $(NL \times K)$ from K adjacent range cells, assumed as independent, identically distributed and target-free. The detection threshold η is selected according to the desired value of PFA.

As seen in Chapter 3, an asymptotically efficient estimate of target DOA can be achieved by exploiting the MLE. This is obtained by taking the maximum of the log-likelihood function with respect to ϕ:

$$\hat{\phi}_t = \arg \max_{\phi} \left\{ \frac{\left|\boldsymbol{s}^H(\phi) \widehat{\boldsymbol{Q}}^{-1} \boldsymbol{x}\right|^2}{\boldsymbol{s}^H(\phi) \widehat{\boldsymbol{Q}}^{-1} \boldsymbol{s}(\phi)} \right\} \tag{4.2}$$

Typically, the radar performs detection tests over a bank of filters coarsely spaced in angle by the nominal beamwidth (BW). Once a target is detected, a refined angle measurement is achieved through (4.2).

The above STAP scheme proved effective for passive radar GMTI, but it involves a non-negligible level of complexity. It requires the estimation and inversion of a $(NL \times NL)$ disturbance covariance matrix, potentially for each range-Doppler bin. The implementation of (4.2) requires finding the maximum of a non-linear function, either by using fast converging techniques or by evaluating it for a set of discrete values and selecting the one providing the maximum. This can be expensive in terms of computational load, the latter being proportional to the required estimation accuracy. Such cost may not be in line with the usual low complexity of passive radar, especially in the case of mobile systems providing onboard processing.

Moreover, the availability of a sufficient number of uniform training data, to limit the adaptivity loss, may be difficult to be guaranteed in a passive bistatic radar scenario. In fact, the typical ground-based transmitters of opportunity are likely to produce a non-uniform illumination of the ground due to the masking effects of terrain. Also, the typical long wavelengths might be affected by anomalous propagation. In addition, due to its covert

operation and potentially limited coverage, passive radar might be operated also at short range, where non-uniform clutter distributions occur, especially for airborne geometry.

To mitigate the above limitations, in the next Section, an alternative STAP approach for target detection and DOA estimation in an operational mobile passive radar is proposed.

4.3 Dual cancelled channel STAP for passive radar

The dual cancelled channel approach is based on the idea of adaptively forming two clutter cancelled channels which could be directly exploited for both target detection and DOA estimation. Specifically, the AB-STAP technique, originally presented in [79], is considered. This approach is particularly suitable for the passive radar case, thanks to its low complexity architecture, reduced computational cost and its robustness against highly non-homogeneous clutter scenarios.

The adopted processing scheme is sketched in Figure 4.1. This is obtained by modifying the scheme proposed in Chapter 3 for passive radar STAP, so as to integrate the considered dual cancelled channel approach.

The antenna array is split into two spatially displaced (possibly overlapped) sub-apertures. The same ABPD-STAP technique is applied to each sub-aperture, thus obtaining two clutter cancelled channels, namely channels A and B. These channels are then coherently recombined for the purpose of target detection. For range-Doppler cells where detection is declared, target
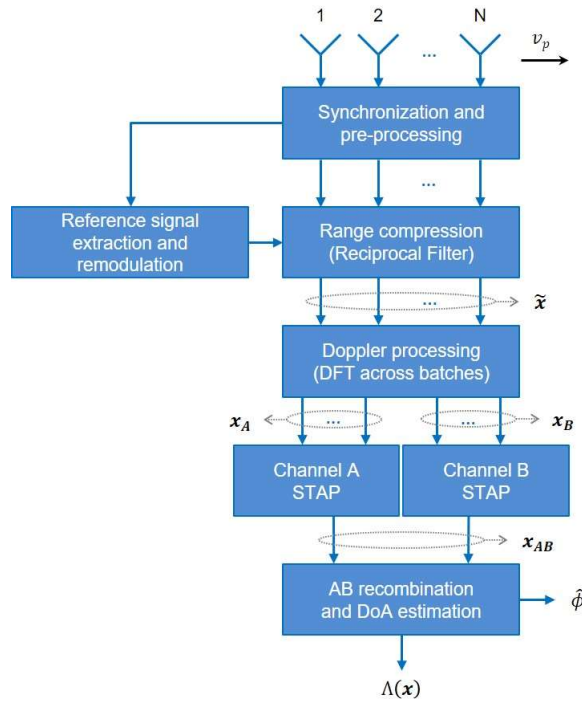

Figure 4.1: Processing scheme for post-Doppler AB-STAP in passive radar.

DOA estimation can be performed from the A and B channel outputs by exploiting their different phase centres.

The processing steps are described in the following:

(i) *Creation of two spatially displaced channels*: the $(NL \times 1)$ data vector $\boldsymbol{x}$ is split into two $(N_0 L \times 1)$ subvectors $\boldsymbol{x}_A$ and $\boldsymbol{x}_B$, corresponding to channels A and B, respectively. $\boldsymbol{x}_A$ contains the data collected from the first N_0 antennas ($N/2 \leq N_0 < N$), while $\boldsymbol{x}_B$ contains those collected from the last N_0 antennas.

(ii) *Cancellation of clutter on each channel*: the subvectors $\boldsymbol{x}_A$ and $\boldsymbol{x}_B$ are filtered with a sample matrix inverse scheme, giving outputs y_A and y_B

$$y_{A(B)} = \boldsymbol{w}_{A(B)}^H \boldsymbol{x}_{A(B)} = \boldsymbol{s}_{A(B)}^H(\phi_L) \widehat{\boldsymbol{Q}}_{A(B)}^{-1} \boldsymbol{x}_{A(B)} \tag{4.3}$$

where $\boldsymbol{s}_{A(B)}(\phi_L)$ and $\widehat{\boldsymbol{Q}}_{A(B)}$ are the steering vector and the estimated covariance matrix of channel A (B), respectively. Notice that, while ϕ represents the generic unknown target DOA, we denote by ϕ_L the array look direction.

Since $\boldsymbol{s}_B(\phi_L) = \boldsymbol{s}_A(\phi_L) \exp\{j2\pi(N - N_0)d/\lambda \cos\phi_L\}$, in a uniform array, channels A and B exhibit disturbance with the same structure. As a result, a better estimate can be obtained averaging the estimates made on the two channels, that is $\widehat{\boldsymbol{Q}}_A = \widehat{\boldsymbol{Q}}_B = \frac{1}{2}(\boldsymbol{X}_{kA}\boldsymbol{X}_{kA}^H + \boldsymbol{X}_{kB}\boldsymbol{X}_{kB}^H)$, being $\boldsymbol{X}_{kA}$ and $\boldsymbol{X}_{kB}$ the $(N_0 L \times K)$ set of training data for channels A and B, respectively. Although not totally independent (if $N_0 > N/2$), averaging the two estimates yields a more stable estimate of the true covariance matrix.

(iii) *Recombination of channels for target detection*: using only one of the two channels to detect targets, may result in significant performance degradation in terms of cancellation capability, since the equivalent antenna length and the employed spatial DOF have been reduced. To recover this degradation and avoid detection losses, an optimal coherent recombination of the two channels is performed.

Arranging the two outputs in the (2×1) vector $\boldsymbol{x}_{AB} = [y_A \ y_B]^T$ and applying the AMF detection scheme, we obtain

$$\frac{\left|\boldsymbol{s}_{AB}^H \widehat{\boldsymbol{Q}}_{AB}^{-1} \boldsymbol{x}_{AB}\right|^2}{\boldsymbol{s}_{AB}^H \widehat{\boldsymbol{Q}}_{AB}^{-1} \boldsymbol{s}_{AB}} \gtrless \eta_{AB} \tag{4.4}$$

where η_{AB} is the detection threshold. The steering vector $\boldsymbol{s}_{AB}$ in the detector is given by

$$\boldsymbol{s}_{AB}(\phi_L) = \begin{bmatrix} \boldsymbol{w}_A^H \boldsymbol{s}_A(\phi_L) \\ \boldsymbol{w}_B^H \boldsymbol{s}_B(\phi_L) \end{bmatrix} = \boldsymbol{w}_A^H \boldsymbol{s}_A(\phi_L) \begin{bmatrix} 1 \\ 1 \end{bmatrix} \tag{4.5}$$

where $\widehat{\boldsymbol{Q}}_{AB}$ is the (2×2) estimated covariance matrix at the output of channels A and B, being $\boldsymbol{Q}_{AB}$ expressed as:

$$\boldsymbol{Q}_{AB} = \begin{bmatrix} \alpha & \rho \\ \rho^H & \alpha \end{bmatrix} \tag{4.6}$$

Notice that $\boldsymbol{Q}_{AB}$ is a Toeplitz Hermitian matrix having elements α (average disturbance power at the output of each channel) and ρ (cross-correlation between the two outputs). This can also be used to obtain a more stable estimate from the data.

As shown in [79] and [80], the optimal recombination of the two channels allows to mostly recover the detection losses with respect to the full array case. Moreover, due to the smaller number of adaptive DOF used by each step of AB-STAP, smaller adaptivity losses are expected compared to full array STAP. This plays a fundamental role in a real scenario, where the potential non-homogeneity of clutter may limit the number of relevant training data usefully exploitable.

(iv) *Estimation of target DOA from the two cancelled channels*: once a target is detected, its DOA can be estimated by applying the MLE to the two cancelled channels A and B. This results in

$$\hat{\phi}_{t,AB} = \arg \max_{\phi} \left\{ \frac{\left| \boldsymbol{s}_{AB}^H(\phi) \widehat{\boldsymbol{Q}}_{AB}^{-1} \boldsymbol{x}_{AB} \right|^2}{\boldsymbol{s}_{AB}^H(\phi) \widehat{\boldsymbol{Q}}_{AB}^{-1} \boldsymbol{s}_{AB}(\phi)} \right\} \tag{4.7}$$

The maximization is performed only with respect to the last stage of the processing chain, which only involves 2-dimensional quantities. This allows to find a closed form expression for the ML estimate of target DOA.

Considering that steering vector $\boldsymbol{s}_{AB}$, as a function of unknown angle ϕ, can be written as

$$\boldsymbol{s}_{AB}(\phi) = \begin{bmatrix} \boldsymbol{w}_A^H(\phi_L) \boldsymbol{s}_A(\phi) \\ \boldsymbol{w}_B^H(\phi_L) \boldsymbol{s}_B(\phi) \end{bmatrix} = \boldsymbol{w}_A^H(\phi_L) \boldsymbol{s}_A(\phi) \begin{bmatrix} 1 \\ e^{j\psi} \end{bmatrix} \tag{4.8}$$

where $\psi = 2\pi(N - N_0)d/\lambda(\cos\phi - \cos\phi_L)$, and defining the following quantities

$$\boldsymbol{z} = \begin{bmatrix} z_1 \\ z_2 \end{bmatrix} = \boldsymbol{Q}_{AB}^{-1} \boldsymbol{x}_{AB} \tag{4.9}$$

$$v = z_1 z_2^H / |\boldsymbol{z}|^2 \tag{4.10}$$

$$u = \rho/\alpha \tag{4.11}$$

we obtain (see [79][80] for more details)

$$\hat{\psi} = \arcsin\left(\frac{2\text{Im}\{vu^H\}}{|2v + u|}\right) - \angle(2v + u) \tag{4.12}$$

where $\text{Im}\{\zeta\}$ and $\angle(\zeta)$ are the imaginary part and the phase of the complex number ζ, respectively. Finally, the ML estimate of target DOA is obtained as

$$\hat{\phi}_{t,AB} = \arccos\left\{\frac{\lambda}{2\pi d(N - N_0)}\hat{\psi} + \cos\phi_L\right\} \tag{4.13}$$

As evident, the target DOA estimation does not require a functional maximisation and yields a simple formula to be implemented, thus requiring a reduced computational cost.

It is worth noting that the value of N_0 defines the number of spatial DOF reserved for clutter cancellation on both channels A and B, but it also affects the displacement of their phase centres. Better DOA estimation could be achieved with large phase centres displacement (i.e. small N_0), but this would be paid in lower clutter cancellation capability on both channels A and B. In other words, a trade-off exists between the theoretical sensitivity for DOA estimation and the signal-to-clutter plus noise ratio (SCNR) measured at the output of the channels. Appropriate choices should be made according to the specific scenario. Notice that the SCNR at the output of A and B channels, responsible for DOA estimation accuracy, is always lower than the SCNR available for target detection after channel recombination.

4.4 Performance analysis

In this Section, the effectiveness of the AB-STAP approach for a multi-channel mobile passive radar is analysed and its performance is compared with respect to the corresponding full array solution, both in terms of target detection and DOA estimation capability. To this purpose the considered schemes is tested against a simulated clutter scenario.

We consider the case of a moving receiver at an altitude of 1000 m exploiting a ground-based transmitter. An $8k$ mode DVB-T signal sequence is assumed as a reference signal. Clutter returns are generated according to the model in (3.3), for a scene spanning 1000 range cells. The complex amplitudes associated with different clutter patches are assumed independent and identically distributed Gaussian variables. We assume the availability of $N = 4$ receiving channels, arranged in the along-track direction, forming a side-looking configuration. The antennas are assumed omnidirectional in the frontal region (no back-lobe contributions). The signal carrier frequency is set to 690 MHz, the platform velocity to $v_p = 13$ m/s and the antenna element spacing to $d = \lambda/2$. We assume a CPI of 512 OFDM symbols (approximately 0.57 s), and absence of internal clutter motion (ICM).

The generated signal includes clutter echoes and thermal noise. Clutter power is scaled so that the overall clutter-to-noise ratio (CNR) has an assigned level of 20 dB at the input of each channel, before range compression. The echoes of two identical moving targets are also included, with bistatic range $R_b = 2$ km and 5 km, azimuth angle of arrival $\phi_t = 90°$ and bistatic radial velocity $v_b = 8$ m/s ($f_D \cong 18$ Hz). The signal-to-noise power ratio (SNR), at the input of each channel before range compression, is set to -50 dB for both targets.

In Figure 4.2(a), the range-Doppler map obtained from a single channel is reported. As evident, the non-negligible receiver altitude causes a non-uniform distribution of clutter in the near range region, where the first target is located. In contrast, in the far range region of the second target, clutter distribution is uniform, spreading over a Doppler extension of approximately $\pm v_p/\lambda \cong \pm 30\ Hz$. The resulting target SCNR (after range compression and Doppler processing) is -27 dB and -26 dB, respectively, so that both targets are completely buried into clutter returns. Target SCNR is measured by taking the power level at the target range-Doppler location, when the processing is fed with target echoes only, and the disturbance power level estimated over a proper area surrounding target location, when the map contains only clutter and noise.
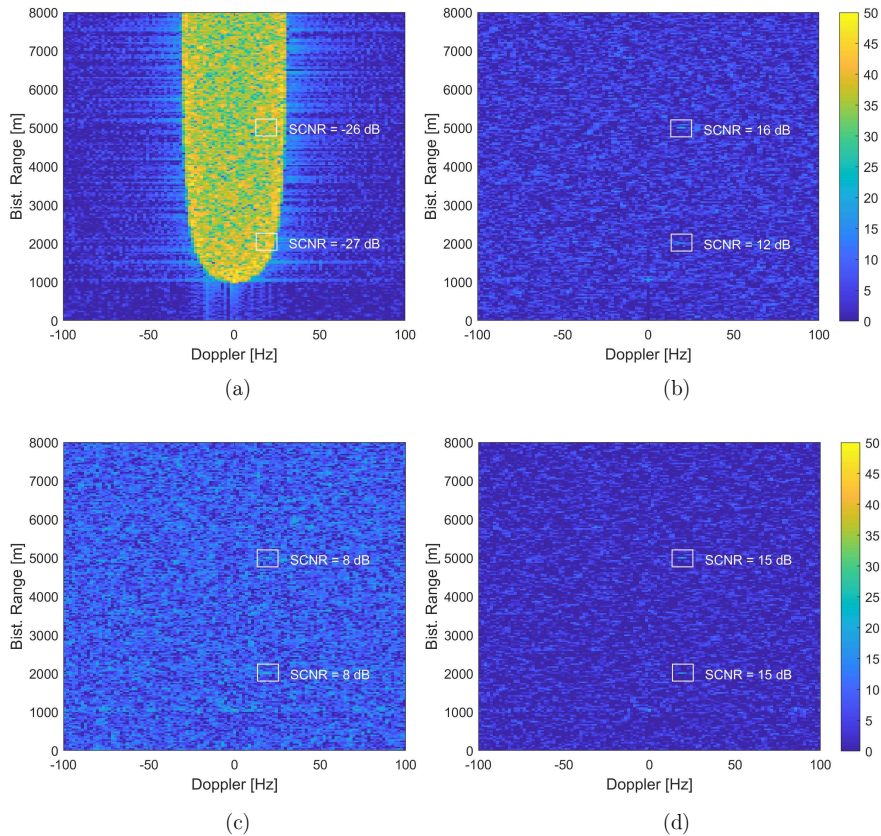

Figure 4.2: Range-Doppler maps from a simulated clutter scenario assuming receiver altitude 1000 m: (a) single channel map; (b) map after full array STAP with K=24 training data; (c) map after full array STAP with K=16 training data; (d) map after AB-STAP with K=16 training data.

Figure 4.2(b) shows the range-Doppler map obtained when applying the full array STAP scheme, using $N = 4$ channels, $L = 3$ adjacent Doppler bins and $K = 2NL = 24$ training data. The clutter is effectively cancelled and the SCNR of the target at far range is brought to 16 dB, with an improvement of 42 dB. For the near range target instead, the achievable SCNR is limited to 12 dB, due to the inhomogeneity of clutter data. To avoid this, in Figure 4.2(c), the sample support is reduced to $K = 16$. In this case however, the small number of training data yields higher adaptivity losses, rising the residual disturbance background and limiting the final SCNR to 8 dB for both targets.

The result obtained when applying the AB-STAP scheme with $K = 16$ training data is shown in Figure 4.2(d). The array is split into two (non-overlapped) sub-arrays of $N_0 = 2$ antennas, forming the A and B channels. In this case, the clutter is still effectively suppressed, and the limited number of secondary data counteract the effect of non-homogeneous clutter at near range, without introducing undesirable adaptivity losses. As a result, a final SCNR of 15 dB is obtained for both the far and the near range targets.

4.4.1 Target detection performance

To compare the full-array and the AB-STAP schemes in terms of detection performance, a Monte Carlo analysis is carried out (1000 runs), under different conditions of availability of secondary data. The same parameters adopted in the previous example are assumed and, for simplicity, a uniform clutter scenario. The space-time AMF detectors in (4.1) and (4.4) are considered, with a desired PFA level of 10^{-4}. Swerling 0 target model is assumed.

In Figure 4.3, the resulting probability of detection (PD) is shown as a function of the target input SNR. The target bistatic radial velocity $v_b = 7$ m/s is representative of slow target condition, sufficiently close to clutter notch. Two cases are considered, with different number of available training data. Specifically, $K = 24$ represents the case of enough training data for the full array solution (twice the number of the adaptive DOF), while $K = 16$ represents a condition of limited sample support.

When $K = 24$ training data are available (dashed curves), AB-STAP performs very closely to full array STAP. Although clutter cancellation is performed by means of only two spatial DOF on the A and B channels, their optimal coherent recombination allows to avoid considerable detection losses. Notice that the slight remaining advantage of the full array case ($<$1dB), might be further reduced when considering target velocities further from clutter notch or by adopting overlapped solutions for A and B channels (e.g. $N_0 = 3$).

When the number of training data is reduced to $K = 16$ (solid curves), a significant performance degradation is observed in the full array case, due to the adaptivity losses. Conversely, the AB-STAP only shows a limited performance drop, thanks to the smaller number of adaptive DOF used in each step (half of the full array case). As a result, in this case, AB-STAP outperform full array STAP by approximately 5 dB.
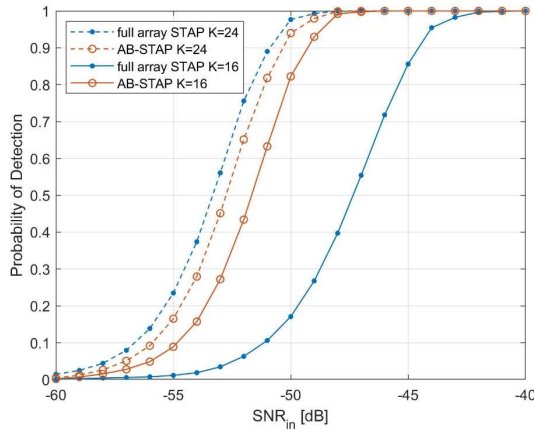
Figure 4.3: Detection performance comparison as a function of target input SNR. Target bistatic velocities is set to 7 m/s and desired PFA to 10^{-4}.
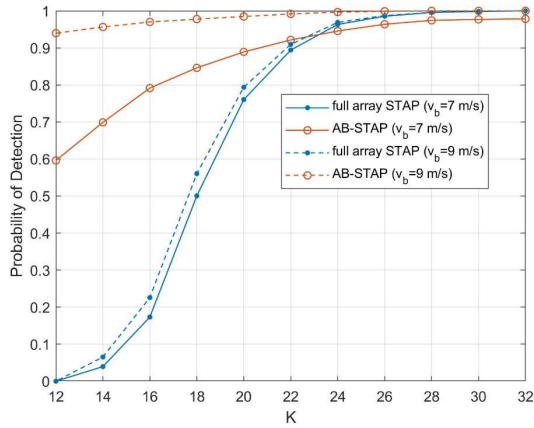
Figure 4.4: Detection performance comparison as a function of the number of training data. Target input SNR is set to -50 dB and desired PFA to 10^{-4}.

The above considerations find confirmation also in Figure 4.4, where PD is evaluated as a function of K, for a fixed target SNR of -50 dB. As expected, the performance decreases significantly more in the full array case, as the number of training data reduces, while losses associated to the AB-STAP approach are remarkably smaller. Moreover, even for larger values of K, AB-STAP shows minor differences in performance, compared to full array STAP, only for targets close to clutter notch, in favour of lower complexity and computational cost.

4.4.2 DOA estimation performance

As discussed in Section 4.3, once target is detected, AB-STAP is able to perform the target DOA estimation via the closed form expression in (4.12)(4.13) by exploiting the outputs of the A and B channel. The DOA estimation accuracy provided by this approach is evaluated and compared with the full array STAP estimator in (4.2), by means of a Monte Carlo analysis (1000 runs) applied against the same simulated scenario. Specifically, the full array

MLE is operated with a bank of filters equally spaced in angle by $\delta\phi = 0.1°$ within the array nominal BW (~38°), corresponding to a step smaller than BW/100. The AB-STAP scheme employs $N_0 = 2$ elements in the A and B channels. With $N = 4$ elements at disposal, this choice ensures the largest phase centre displacement. Both the estimators are applied after the ABPD transformation with $L = 3$ Doppler bins. The bistatic velocity and DOA of the simulated target are respectively $v_b = 7$ m/s and $\phi_t = \phi_L = 90°$.

In Figure 4.5, the resulting estimation accuracy is shown as a function of the target input SNR. Results are compared in terms of standard deviation in Figure 4.5(a) and bias error in Figure 4.5(b), both normalised to the nominal BW.

We notice that, for $K = 24$ training data (dashed curves), the accuracy of AB-STAP and full array STAP estimators are comparable, showing an almost identical standard deviation. Conversely, when the number of training data is led to $K = 16$ (solid curves), the standard deviation and bias error increase in the full array case. Instead, the AB-STAP shows negligible adaptivity losses even for small sample support. In this specific case, the AB-STAP allows to improve the standard deviation by 20% with respect to the full array STAP. The above considerations are also supported by results in Figure 4.6, where the DOA estimation accuracy is represented as a function of K, for a fixed target SNR of -45dB.

In Figure 4.5(a) and Figure 4.6, the Cramér-Rao bound (CRB) is also reported for both the considered estimators (dash-dotted curves). This gives a useful reference for the DOA estimation accuracy and allows to better assess the effect of the selected strategies on the ideal estimation performance.

Following [75][76], and assuming a known target Doppler frequency, the CRB for the full array STAP estimator in (4.2) can be expressed as in (3.12). The corresponding CRB for the AB-STAP scheme is obtainable by replacing s, $\dot{s}$ and Q with their corresponding 2-dimensional quantities, s_{AB}, $\dot{s}_{AB}$ and Q_{AB}.

Figure 4.5: Comparison of DOA estimation accuracy as a function of target input SNR: (a) standard deviation in BW units; (b) bias error in BW units. Target bistatic velocity is set to 7 m/s.
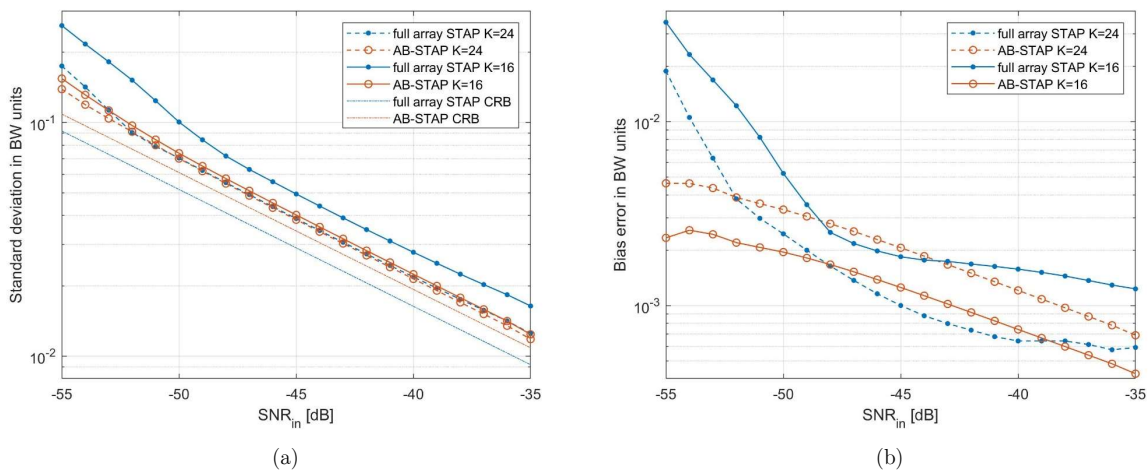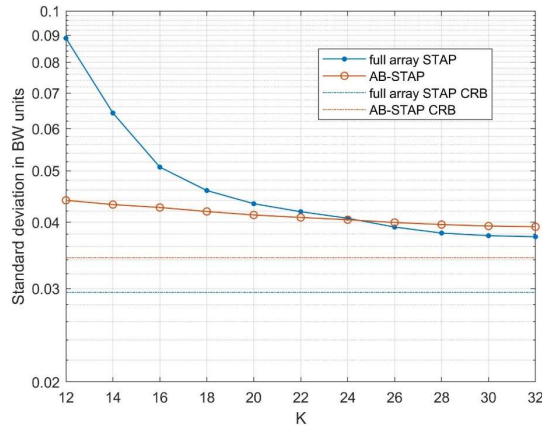
Figure 4.6: DOA estimation accuracy as a function of the number of training data. Target input SNR is -45 dB.

Both the estimators appear as asymptotically unbiased and efficient, due to their ML nature. The amount of loss of the simulated results with respect to the CRB is a measure of the adaptivity loss, due to the number of training data. Again, this confirms the robustness of the AB-STAP approach. In fact, despite its slightly worse asymptotic performance (see the difference in the CRB curves), it performs better that the full array scheme, as the availability of training data reduces.

Finally, it is worth recalling that the full array estimator requires finding the maximum among a discrete set of angles (bank of filters) for DOA estimation. Therefore, it can be subject to performance saturation effects and involves a non-negligible computational load, proportional to the required estimation accuracy. In contrast, owing to the closed form expression of the estimator, the AB-STAP approach does not suffer from saturation and offers a reduced complexity and computationally attractive solution.

4.5 Experimental results

In this Section, the effectiveness of the AB-STAP scheme for slow-moving targets detection and localization in mobile passive radar is demonstrated against a set of experimental data. The data are acquired by a multichannel receiver mounted on a ground moving platform and based on DVB-T transmissions.

The experimental setup and the considered data set correspond to those formerly used in Chapter 3, where a full array STAP scheme was successfully applied for target detection and DOA estimation. In this Chapter, the full array scheme is compared with the AB-STAP approach, in order to verify the benefits of this latter solution in a real scenario.

It is recalled that the system features four receiving channels, arranged to form a uniform linear array (ULA) in side-looking configuration (see Figure 2.4). The parameters of the exploited DVB-T signal and the main acquisition and processing parameters are the same reported in Table 2.1. Refer to Figure 2.5(a) for a sketch of the bistatic acquisition geometry.

Table 4.1

Target parameters

	T1	T2	T3	T4	Delphin
R_b	4700 m	3600 m	6850 m	2400 m	6596 m
v_b	-6 m/s	6 m/s	11 m/s	7 m/s	-24.5 m/s
ϕ_t	37°	157°	109°	70°	$\sim 37°$
f_D	11.7 Hz	-14.9 Hz	15.9 Hz	26.7 Hz	-31.1 Hz

In addition to the cooperative aerial target Delphin, four simulated moving targets have been injected into the acquired data. The parameters of the real and simulated targets are reported in Table 4.1.

It is also worth noting that the same strategy presented in Chapter 3 for calibration of the spatial steering vector component has been adopted here, in order to mitigate the impact of the angle-dependent inter-channel imbalances on the target detection and localization performance. Specifically, this is applied to vector s in the full array STAP scheme and to vectors s_A and s_B in the AB-STAP scheme.

Figure 4.7 reports the range-Doppler maps resulting from the considered experimental data set. In particular, Figure 4.7(a) shows the map obtained from a single channel, namely before STAP processing. The map is scaled to the estimated noise power level. As apparent, the clutter echoes from the stationary scene spread over a Doppler bandwidth compatible with the platform velocity $(v_p/\lambda \cong \pm 32\ Hz)$. Moreover, the strong direct signal contribution appears at zero bistatic range and Doppler frequency close to zero, being the Rx-Tx line of sight approximately orthogonal to the platform velocity vector.

The radial velocities and DOAs of the real and simulated moving targets are such that they fall within Doppler bandwidth of clutter, being mostly buried into it and therefore not easily detectable. The target positions are indicated by white boxes in the map and their corresponding SCNR values are reported. Notice that these values are higher compared with those of the simulated case, since targets compete with lower local clutter power.

The observed clutter scenario is characterized by a large heterogeneity, associated to the presence of densely vegetated and rural areas. This aspect is exacerbated by the bistatic acquisition geometry of passive radar, typically exploiting ground-based transmitters, prone to non-uniform illumination and shadowing phenomena, due to the terrain orography. In this context, the AB-STAP approach represents a suitable solution, since operating effectively even with a limited sample support.

Figure 4.7(b), shows the range-Doppler map obtained when applying the full array STAP scheme, jointly using the $N = 4$ channels, with $L = 3$ Doppler bins and $K = 16$ training data. As expected, the large adaptivity losses result in a high residual disturbance background, which lower the achievable SCNR and may hinder the detection of targets.
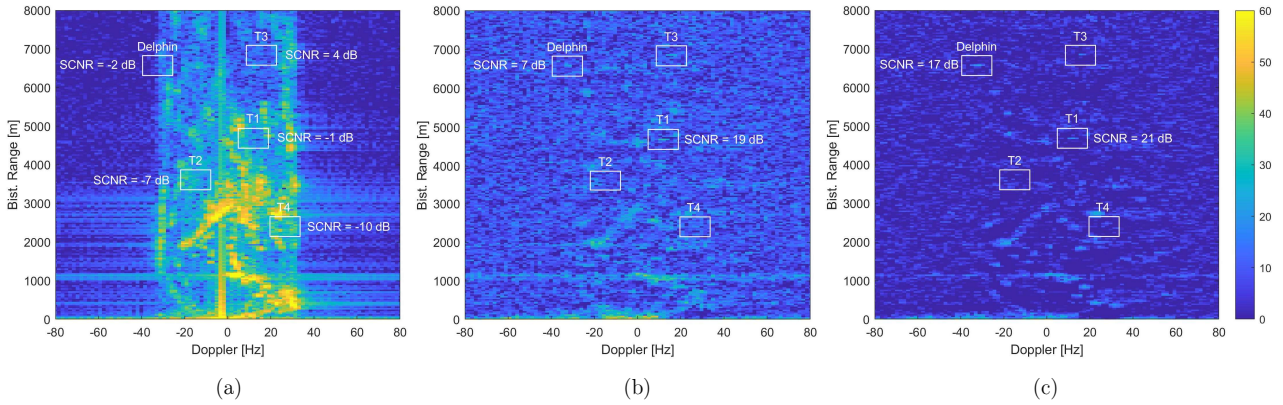
Figure 4.7: Range-Doppler maps obtained from the experimental data: (a) single channel map; (b) map after full array STAP; (c) map after AB-STAP. Number of training data is set to K=16. Steering is towards direction of targets T1 and Delphin. Target positions are indicated by white boxes. SCNR values are reported after STAP only for targets included in the resulting main beam.

For comparison, Figure 4.7(c) shows the corresponding range-Doppler map at the output of the adaptive filter, when applying the AB-STAP scheme, employing $N_0 = 2$ elements for the A and B channels and using the same amount of training data.

In both cases, the spatial steering vector is oriented in a direction ($\phi_L = 37°$) such as to include in the main beam the real target Delphin and target T1, which both appear clearly visible in the final maps. For this reason, the SCNR after STAP is reported in figure only for these targets. The other targets, whose DOAs are not included in the main beam, are less visible. The theoretical array pattern is shown in Figure 4.8, with the corresponding target angular positions. Notice that, due to element spacing larger than $\lambda/2$, a grating lobe appears for steering directions far from broadside. In the considered case, target T3 is also visible in the final map since located in direction of grating lobe.

The above result clearly demonstrates the effective clutter suppression and moving target detection capability of the AB-STAP approach, also in the presence of a limited sample support for the adaptive filter estimation.

For a more comprehensive analysis and comparison of the detection performance, Figure 4.9 reports the results obtained with the full array STAP detector in (4.1) and with the AB-
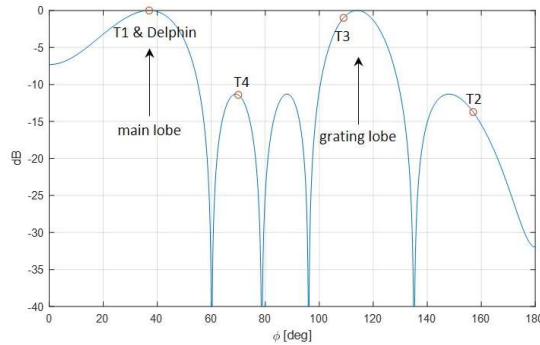
Figure 4.8: Theoretical array pattern with steering at ϕ=37° and target positions, indicated by red circles.

STAP detector in (4.4). For each solution, the test statistics is reported over the bistatic range-Doppler map before the application of a proper threshold, selected according to a desired value of nominal PFA. For a fair comparison, the test statistic is mapped into the PFA setting that would allow to exceed the corresponding threshold. Basically, each pixel in the map has been scaled so that it represents the minimum value of nominal PFA to be set for that pixel to yield a detection. Notice that the results are reported as $\log_{10}(\text{PFA})$.

Specifically, the two detectors are compared in Figure 4.9 (a) and (b) for $K = 24$ training data and, similarly, in Figure 4.9 (c) and (d) for $K = 16$ training data. Target positions are indicated on maps by black boxes. Notice that also in this case the spatial steering vector is oriented towards the DOA of targets T1 and Delphin.

For a full comparison, Table 4.2 reports the minimum nominal PFA values which allow us to detect each target with the different detection schemes, when an appropriate spatial steering includes the target in the man beam.

From the results in Figure 4.9 and Table 4.2, the following considerations are in order:

Figure 4.9: Minimum nominal PFA to detect each bin: (a) full array STAP with K=24; (b) AB-STAP with K=24; (c) full array STAP with K=16; (d) AB-STAP with K=16. Values are expressed as $\log_{10}(\text{PFA})$. Steering is towards direction of targets T1 and Delphin. Target positions are indicated by black boxes.

Table 4.2

Minimum nominal PFA for target detection [$\log_{10}(\text{PFA})$]

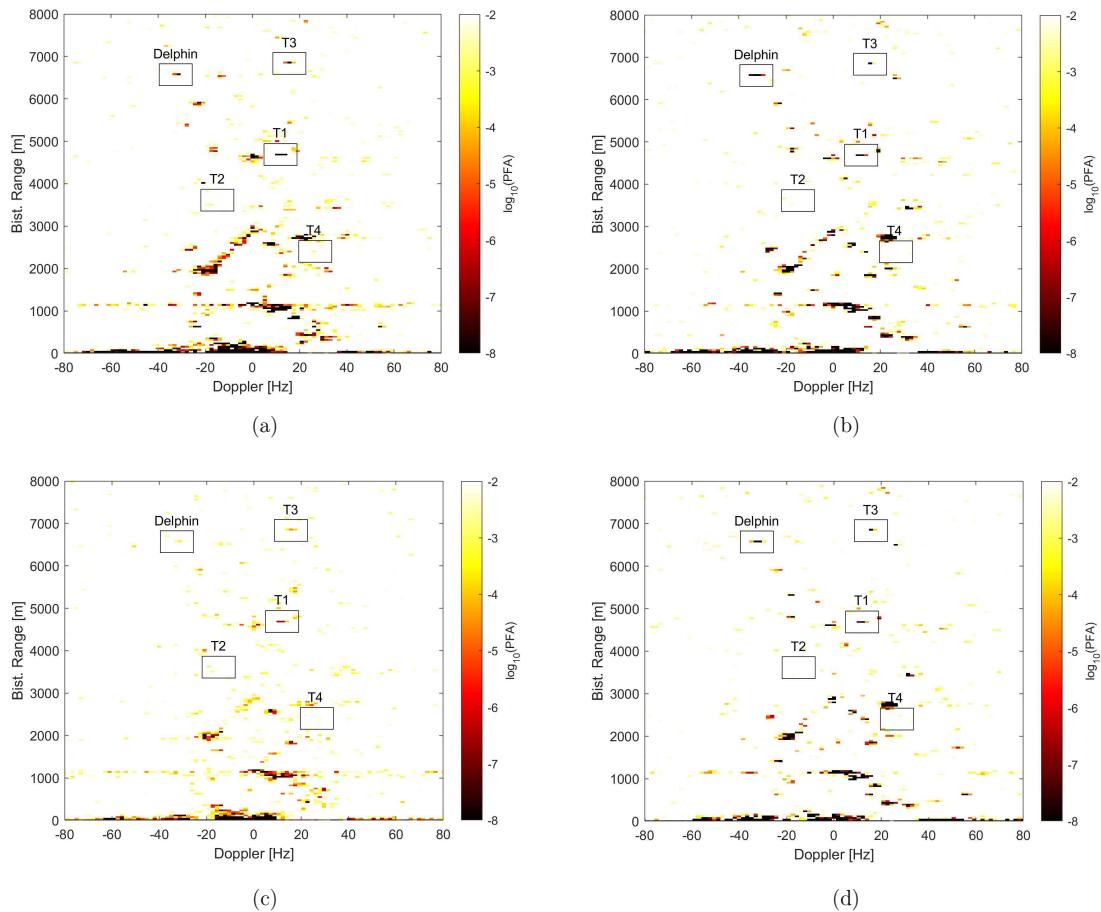|	full-array STAP					AB-STAP				
	T1	**T2**	**T3**	**T4**	**Delphin**	**T1**	**T2**	**T3**	**T4**	**Delphin**
K=24	-11.6	-6.7	-10.5	-4.8	-7.5	-9.3	-7.0	-7.8	-5.1	-9.6
K=16	-6.6	-2.2	-4.6	-3.3	-3.1	-8.6	-8.0	-6.5	-6.6	-9.3

- Comparing Figure 4.9 (a) and (b), the full array STAP scheme seems yielding a higher number of false alarms compared to the AB-STAP scheme, for given PFA. False alarms are mostly associated to persistent clutter structures, especially in those areas where clutter power shows abrupt variations and filter adaptivity is more likely to fail.

- It is worth mentioning that the presence of additional non-cooperative moving targets in the observed scene during the acquisition cannot be excluded.

- When the training data are reduced to $K = 16$, Figure 4.9(c) and (d), the more localized adaptation capability allows the AB-STAP scheme to better handle the clutter discrete and reduce the number of false alarms, without compromising target detection. Conversely, in the full array STAP scheme this is paid in terms of higher adaptivity loss, which raises the detection threshold to prevent a general increase of the false alarms, thus compromising the detection capability.

- Looking at Table 4.2, when enough training data are available, both the detection schemes yield remarkable results, allowing target detection until low values of PFA. In the case of limited sample support, instead, the detection performance of the full array STAP drastically decreases, while the AB-STAP approach is able to mostly preserve or even improve its outcomes (see for example T2 and T4). As a result, the AB-STAP largely outperform the full array STAP for all targets in this case.

- By selecting a PFA of 10^{-4}, with $K = 24$ training data all the considered targets would be detected by both the detection schemes. For $K = 16$, the AB-STAP would still detect all the targets, while the full array scheme would miss the detection of three out of five targets.

After target detection, an appropriate estimation of target DOA is worthwhile for target localization purpose. In fact, the array nominal BW is in the order of 23° (when steered at broadside), thus offering poor target localization capability. This is achieved by resorting to the space-time ML DOA estimation strategies formerly presented.

Specifically, in the full array STAP case, the target angular position is estimated by finding the maximum of (4.2) over a bank of filters equally spaced by $\delta\phi = 0.1°$ within the array nominal BW, corresponding to a step smaller than BW/100. In the AB-STAP approach instead, the closed form expression in (4.12)(4.13) is exploited. In both cases, the estimation is achieved after the ABPD transformation, using $N = 4$, $N_0 = 2$ and $L = 3$. For the purpose of our analysis, the angular ambiguity resulting from the antenna spacing larger than $\lambda/2$

Table 4.3
Target DOA estimation results

	full-array STAP					AB-STAP				
	T1	T2	T3	T4	Delphin	T1	T2	T3	T4	Delphin
K=24	36.3° (-0.7°)	158.1° (+1.1°)	108.1° (-0.9°)	69.2° (-0.8°)	34.3° (-2.7°)	37.4° (+0.4°)	157.8° (+0.8°)	109.7° (+0.7°)	69.1° (-0.9°)	35.3° (-1.7°)
K=16	32.8° (-4.2°)	161.1° (+4.1°)	110.5° (+1.5°)	68.6° (-1.4°)	48.6° (+11.6°)	38.1° (+1.1°)	156.2° (-0.8°)	110.1° (+1.1°)	68.5° (-1.5°)	37.2° (+0.2°)

was neglected and, in the estimation process, the known target position was used to identify the non-ambiguous angular sector. Please note that this strategy does not affect our results as we are mostly interested in small estimation errors around the true target DOA.

The results of DOA estimation for each target are reported in Table 4.3, for a number of training data equal to $K = 24$ and $K = 16$. The error with respect to the true DOA values in Table 4.1 is reported in brackets.

Analysing the results, we can notice that, for a large sample support, both the AB-STAP and the full array STAP provide an accurate DOA estimation for all targets, with an average error below one twentieth of the nominal BW. When the sample support is limited to $K = 16$ instead, the estimation accuracy of the full array STAP is considerably reduced. On the other hand, the AB-STAP approach is able to mostly preserve its good localization performance, while requiring a lower computational complexity.

Finally, Figure 4.10 shows the DOA estimation results obtained for the real target Delphin over consecutive CPIs. Specifically, 24 subsequent CPIs, each of length 512 OFDM symbols and overlapped by 256 symbols, were considered, for an overall observation time of approximately 7 s. The results clearly show the advantage of the AB-STAP scheme compared to the full array scheme, both in terms of accuracy and stability of the estimation, especially in the case of a limited sample support.

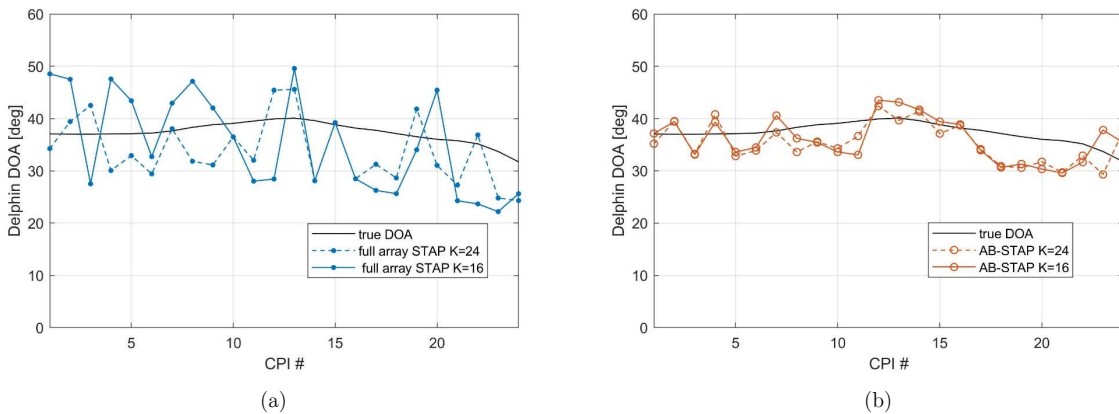(a)   (b)

Figure 4.10: DOA estimation results for real target Delphin over consecutive CPIs: (a) using full array STAP scheme; (b) using AB-STAP scheme.

The results reported in this Section prove the capabilities of the AB-STAP strategy against a real clutter scenario and its advantages over the full array scheme. The AB-STAP represents a suitable and convenient solution for target detection and DOA estimation in mobile passive radar equipped with multiple channels on receive.

4.6 Summary

In this Chapter, a dual cancelled channel STAP scheme was proposed for clutter rejection and slowly moving target detection and localization in multi-channel mobile passive radar. The proposed scheme is aimed at reducing the computational complexity, as well as the number of required training data, compared to a conventional full-array solution.

Specifically, the AB-STAP technique was considered, combined with an adjacent-bin post-Doppler (ABPD) strategy, and proved to be a suitable solution for multi-channel mobile passive radar. The reduction of computational complexity is obtained both by reducing the number of adaptive DOF in the space-time processing steps and by providing a simple closed-form expression for target DOA estimation.

Despite its lower computational load, the proposed scheme was shown to yield comparable target detection and DOA estimation performance with respect to the equivalent full array solution. Moreover, it proved to be more robust against adaptivity losses, operating effectively even in the presence of a limited sample support. This plays a fundamental role in a practical passive bistatic scenario, where the potential non-homogeneity of the clutter returns may easily compromise the performance of STAP, by limiting the number of training data usefully exploitable.

The effectiveness of the proposed scheme has been demonstrated against simulated and experimental data from a DVB-T based multichannel mobile passive radar.

Chapter 5
Conclusion and future work

The goal of this thesis was to contribute to research on passive radar on moving platforms by addressing the main issues connected to the use of space-time processing methodologies for GMTI applications. The research performed has led to the development of *ad hoc* signal processing techniques and operational strategies to tackle the limitations deriving from the passive bistatic framework to the capability of clutter cancellation and slow-moving target detection and localization. In this Chapter, the main novelties brought about by this work are summarised, followed by some recommendations for future research.

5.1 Results and novelties

Firstly, the adoption of a processing scheme based on the DPCA approach was considered, combined with reciprocal filtering, in dual-channel mobile passive radar. Specifically, the problem of direct signal interference and clutter cancellation for the purpose of slow-moving target detection was addressed. Attention was mainly focused on the development of signal processing algorithms for digital channel calibration, in order to cope with the limitations deriving from amplitude and phase inter-channel imbalance.

- The strict connection between mobile passive radar framework and channel imbalance problem has been highlighted. The low directivity of typical receiving antennas, paired with a bistatic broadcast illumination, results in the simultaneous reception of non-negligible clutter contributions from a very wide angular sector, as well as in a strong direct path interference. Such contributions are likely to suffer from an angle-dependent imbalance across the receiving channels, made more severe by the use of commercial low-cost components. Our analysis showed how these effects can severely compromise the cancellation performance of DPCA and complicate the calibration strategy.

- Evidence was given of the limits of a channel calibration approach based on the direct signal, due to the effect of the angle-dependent channel imbalance, especially for bistatic geometries where DSI and main clutter echoes have different directions of arrival.

- A two-stage cancellation approach was proposed, aimed at achieving effective rejection of DSI and clutter returns and removing the influence of DSI on the subsequent channel

calibration. A preliminary suppression of DSI is provided at both receiving channels by resorting to an ECA filtering. Then, an effective clutter cancellation is performed via DPCA subtraction, enabled by an accurate clutter-based channel calibration stage.

- Different strategies for digital channel calibration were developed, based on the criterion of minimization of the output power. The proposed strategies exploit the one-to-one relationship between angle of arrival and Doppler frequency of stationary scatterers and the fine Doppler resolution provided by the typical long integration times of passive radar, to provide an angle-dependent compensation of channel imbalance. Starting from the estimation of a single calibration coefficient (SCC), the flexibility of the calibration model has been gradually increased, in order to compensate for additional angle (DDC) and range dependent channel errors (DDC-RB). A robust version of these schemes was also introduced to avoid the degradation due to the interference of strong targets.

- The effectiveness of the proposed processing scheme and channel calibration strategies has been demonstrated via an experimental validation against the data acquired by a DVB-T based passive radar system mounted on a ground moving platform.

The DPCA solution offers a simple system architecture and a reduced computational cost for passive radar GMTI. However, an accurate localized calibration of the received data was shown to be largely required to guarantee an effective suppression of clutter. Moreover, the effects of channel errors on target signal are neglected, in favour of an effective disturbance cancellation. In fact, target signal may experience a different imbalance compared to the surrounding clutter in the range/Doppler map, since belonging to a different DOA. This may affect the detection performance despite an effective suppression of clutter. Finally, with two channels on receive, only the detection of target echoes can be sought, whereas the problem of its angular localization within the broad antenna beams remains unsolved.

The second part of the thesis was focused on the development of STAP techniques, exploiting more than two receiving channels. This on the one hand allowed to improve the disturbance cancellation and moving target detection performance, on the other hand it also enabled the target angular localization capability. Moreover, the clutter cancellation capability relies on the adaptivity of the space-time filter. Therefore, the effects of channel calibration errors on target signal can be addressed, mitigating the negative impact on target detection and localization performance.

- An ABPD-STAP approach was proposed, which plays a key role in preserving the clutter cancellation capability also in the presence of an angle-dependent imbalance affecting the receiving channels. This approach proved particularly suitable for mobile passive radar. It takes advantage of the typical long integration times and the resulting fine Doppler resolution to: (*i*) significantly reduce the size of the adaptive problem, by exploiting the decoupling of the clutter Doppler components; (*ii*) allow the adaptive filter to intrinsically compensate for the angle-dependent channel errors, by operating on a clutter subspace accounting for a limited angular sector.

- Two novel detection schemes were developed, aimed at mitigating the effects of the channel imbalance on target signal:

  (*i*) A partially non-coherent space-time GLRT (NC-GLRT) scheme, where the steering vector is not specified in the spatial domain, resulting in the non-coherent integration of target echoes across the receiving channels. At the expense of a limited loss in terms of maximum integration gain, this approach proved to prevent large detection losses. By entirely excluding a calibration stage, it represents a simple but effective solution for moving target detection, especially when few receiving channels are available

  (*ii*) A calibrated space-time GLRT (Cal-GLRT) scheme, where the clutter echoes are exploited for estimation and correction of the spatial steering vector mismatch, making use of the fine Doppler resolution and of the one-to-one relationship between angle of arrival and Doppler frequency of stationary scatterers. At the expense of an additional calibration stage, it provides slightly better detection performance and preserves DOA estimation capability. Alternatively, it can be applied only to the potential targets detected by a first stage based on the NC-GLRT scheme, for target DOA estimation.

- The problem of target angular localization in mobile passive radar has been addressed. The limited number and the low directivity of antennas make it a critical task and require an accurate estimation of target DOA. The multiple spatial degrees of freedom available must be properly exploited both for space-time clutter filtering and for target DOA estimation. To this purpose, the proposed STAP scheme was adopted, capitalizing on the introduced steering vector calibration to provide accurate ML DoA estimation, by mitigating the negative impact of the unknown channel errors.

- After performance assessment against simulated data, the effectiveness of the developed strategies in terms of moving target detection and localization has been demonstrated by an experimental validation, against the data acquired by a multichannel mobile passive radar exploiting DVB-T signal.

Finally, attention has been focused on further reducing the computational complexity of passive radar STAP in multichannel configurations, as well as on increasing its robustness against adaptivity losses. In fact, the heterogeneity of a real clutter scenario, exacerbated by the bistatic acquisition geometry of passive radar exploiting ground-based illuminators, may limit the availability of homogeneous training data, decreasing the effectiveness of STAP.

- A dual cancelled channel STAP scheme was developed, aimed at reducing the system computational complexity, as well as the number of required training data, compared to a conventional full-array solution. Specifically, the AB-STAP technique was considered, combined with an adjacent-bin post-Doppler strategy. The reduction of computational cost is obtained both by reducing the number of adaptive DOF in the space-time processing steps and by providing a simple closed-form expression for target DOA estimation. The proposed scheme showed to yield comparable performance with

respect to the equivalent full array case. Moreover, it proved to be more robust against adaptivity losses, operating effectively even in the presence of a limited sample support.

- The performance of the developed strategy in target detection and DOA estimation has been analysed against simulated data and an experimental validation of its benefits was given by exploiting a DVB-T based multi-channel mobile passive radar.

5.2 Future Outlook

During this work, the following key points and areas of further research were identified.

- The reliability and the performance of the system could be improved by resorting to the exploitation of information diversity. Among this, the multi-frequency operation, namely the joint use of signals received at different carrier frequencies, typically available from broadcast transmitters, in conjunction with the spatial diversity, is expected to provide interesting and unexplored perspectives for mobile passive radar. The impact of the exploitation of this information diversity on clutter cancellation performance and its integration with STAP could be investigated and specific optimization criteria for the design of the receiving system could be derived.

- In addition to the multi-frequency and spatial diversity, also the information diversity conveyed by the temporal dimension could be investigated, by exploring the impact of using the reciprocal range compression filter with signal fragmentations different from the OFDM symbols for DVB-T. The reciprocal filtering strategy would allow the normalization of the signal ambiguity function by removing the temporal variability associated to waveform information content, without being bounded to the symbol structure of the OFDM signal. This would further increase the flexibility of the system with respect to the characteristics of the waveform of opportunity.

- The possibility to exploit polarimetric information diversity could also be considered. As known, a proper combination of the signals received at different polarizations can enhance the clutter cancellation and target detection capability of passive radar. In the case of mobile passive radar, multi-dimensional detection schemes exploiting space-time-polarimetric observations could be investigated. These schemes would adaptively exploit the polarimetric differences between the target and the competing disturbance to improve the target discrimination capability.

- The effectiveness of the strategies proposed in this thesis, and of those foreseen for the future, will be extensively tested and validated against larger experimental datasets. For this purpose, new acquisition campaigns will be carried out, also considering different system configurations. Specifically, passive radar receivers installed on other categories of carrying platforms, e.g. airborne platforms, as well as different bistatic acquisition geometries and clutter environments can be explored. This would give the opportunity to confirm the results of this dissertations and might put in evidence new

aspects to investigate. Furthermore, other types of illuminators of opportunity could also be considered, to be exploited by a moving receiver. In particular, DVB-S transmissions might offer a very wide coverage and more convenient geometry, compared to terrestrial illuminators.

The results and the strategies presented in this thesis, and the ones expected for the near future, will hopefully contribute to paving the way for a full operational capability of passive radar system onboard moving platforms in the next future.

Bibliography

[1]   H. D. Griffiths and C. J. Baker, "An Introduction to Passive Radar," Norwood, MA, USA: Artech, Mar. 2017.

[2]   H. D. Griffiths, "Passive and bistatic radar," chapter in book edited by W. L. Melvin and J. A. Scheer, "Principles of Modern Radar: Radar Applications," SciTech Publishing, Inc., 2014.

[3]   P. Lombardo, F. Colone, "Advanced processing methods for passive bistatic radar systems", chapter in book edited by W. L. Melvin and J. A. Scheer, "Principles of Modern Radar: Advanced Radar Techniques," SciTech Publishing, Inc., 2012, pp. 739-821.

[4]   J. Palmer, D. Cristallini, and H. Kuschel, "Opportunities and current drivers for passive radar research" in Proc. IEEE Radar Conf., Johannesburg, South Africa, 2015, pp. 145–150.

[5]   R. Klemm et alii (Eds.), "Novel radar techniques and applications", Part III: Passive and multistatic radar, IET Publisher, 2017.

[6]   L. M. H. Ulander, P. Frölind, A. Gustavsson, R. Ragnarsson and G. Stenström, "VHF/UHF bistatic and passive SAR ground imaging," 2015 IEEE Radar Conference (RadarCon), Arlington, VA, 2015, pp. 0669-0673.

[7]   D. Gromek, K. Kulpa and P. Samczyński, "Experimental Results of Passive SAR Imaging Using DVB-T Illuminators of Opportunity," in IEEE Geoscience and Remote Sensing Letters, vol. 13, no. 8, pp. 1124-1128, Aug. 2016.

[8]   K. Kulpa, M. Malanowski and P. Samczyński, "Passive radar: From target detection to imaging," 2019 IEEE Radar Conference (RadarConf), Boston, MA, USA, 2019, pp. 1-286.

[9]   Y. Fang, G. Atkinson, A. Sayin, J. Chen, P. Wang, M. Antoniou and M. Cherniakov, "Improved Passive SAR Imaging With DVB-T Transmissions," in IEEE Transactions on Geoscience and Remote Sensing, vol. 58, no. 7, pp. 5066-5076, July 2020.

[10]   J. Brown, K. Woodbridge, H. Griffiths, A. Stove and S. Watts, "Passive bistatic radar experiments from an airborne platform," IEEE Aerospace and Electronic Systems Magazine, pp. 50-55, November 2012.

[11]   J. Palmer, M. Ummenhofer, A. Summers, G. Bournaka, S. Palumbo and D. Cristallini, "Receiver platform motion compensation in passive radar," IET Radar, Sonar and Navigation, pp. 922-931, 2017.

[12] B. Dawidowicz, P. Samczynski, M. Malanowski, J. Misiurewicz and K. S. Kulpa, "Detection of moving targets with multichannel airborne passive radar," IEEE Aerospace and Electronic Systems Magazine, pp. 42-49, 2012.

[13] B. Dawidowicz, K. Kulpa, M. Malanowski, J. Misiurewicz, P. Samczynski and M. Smolarczyk, "DPCA detection of moving targets in airborne passive radar," IEEE Transactions on Aerospace and Electronic Systems, pp. 1347-1357, April 2012.

[14] P. Wojaczek, F. Colone, D. Cristallini, P. Lombardo and H. Kuschel, "The application of the Reciprocal Filter and DPCA for GMTI in DVB-T PCL," in International Conference on Radar Systems, Belfast, 2017.

[15] P. Wojaczek, F. Colone, D. Cristallini and P. Lombardo, "Reciprocal-Filter-based STAP for passive radar on moving platforms," IEEE Transactions on Aerospace and Electronic Systems, vol. 55, no. 2, pp. 967-988, April 2019.

[16] P. Wojaczek and D. Cristallini, "The Influence of Channel Errors in Mobile Passive Radar using DVB-T Illuminators of Opportunity," 19th International Radar Symposium (IRS), Bonn, 2018, pp. 1-10.

[17] G. P. Blasone, F. Colone, P. Lombardo, P. Wojaczek and D. Cristallini, "A two-stage approach for direct signal and clutter cancellation in passive radar on moving platforms," 2019 IEEE Radar Conference (RadarConf), Boston, MA, USA, 2019, pp. 1-6.

[18] P. Wojaczek, D. Cristallini and F. Colone, "Minimum variance power spectrum based calibration for improved clutter suppression in PCL on moving platforms," 2019 IEEE Radar Conference (RadarConf), Boston, MA, USA, 2019, pp. 1-6.

[19] P. Wojaczek, D. Cristallini, D. W. O'Hagan, F. Colone, G. P. Blasone and P. Lombardo, "A three-stage inter-channel calibration approach for Passive Radar on moving platforms exploiting the minimum variance power spectrum," in Sensors 2021, 21(1), 69.

[20] G. P. Blasone, F. Colone, P. Lombardo, P. Wojaczek and D. Cristallini, "Passive Radar DPCA Schemes with Adaptive Channel Calibration," in IEEE Transactions on Aerospace and Electronic Systems, vol. 56, no. 5, pp. 4014-4034, Oct. 2020.

[21] G. P. Blasone, F. Colone and P. Lombardo, "Facing channel calibration issues affecting passive radar DPCA and STAP for GMTI," 2020 IEEE International Radar Conference (RADAR), Washington, DC, USA, 2020, pp. 31-36.

[22] G. P. Blasone, F. Colone, P. Lombardo, P. Wojaczek and D. Cristallini, "Passive Radar STAP detection and DOA estimation under antenna calibration errors," in IEEE Transactions on Aerospace and Electronic Systems, doi: 10.1109/TAES.2021.3061803.

[23] G. P. Blasone, F. Colone, P. Lombardo, P. Wojaczek and D. Cristallini, "Dual cancelled channel STAP for target detection and DOA estimation in Passive Radar," submitted for publication in Sensors.

[24] X. Neyt et al., "Feasibility of STAP for passive GSM-based radar," 2006 IEEE Conference on Radar, Verona, NY, USA, 2006, pp. 1-6.

[25] J. Raout, X. Neyt and P. Rischette, "Bistatic STAP using DVB-T illuminators of opportunity," 2007 IET International Conference on Radar Systems, Edinburgh, UK, 2007, pp. 1-5.

[26] P. Wojaczek, A. Summers and D. Cristallini, "Preliminary experimental results of STAP for passive radar on a moving platform," 22nd International Microwave and Radar Conference (MIKON), Poznan, 2018, pp. 589-592.

[27] Q. Wu, Y. D. Zhang, M. G. Amin and B. Himed, "Space–Time Adaptive Processing and Motion Parameter Estimation in Multistatic Passive Radar Using Sparse Bayesian Learning," in IEEE Transactions on Geoscience and Remote Sensing, vol. 54, no. 2, pp. 944-957, February 2016.

[28] J. R. Lievsay and N. A. Goodman, "Modeling Three-Dimensional Passive STAP With Heterogeneous Clutter and Pulse Diversity Waveform Effects," in IEEE Transactions on Aerospace and Electronic Systems, vol. 54, no. 2, pp. 861-872, April 2018.

[29] K. Kulpa, M. Baczyk, J. Misiurewicz, M. Malanowski and D. Gromek, "Limits of Ground Clutter CLEAN Based Cancelation in Mobile PCL Radar," 2018 19th International Radar Symposium (IRS), Bonn, 2018, pp. 1-7.

[30] C. Berthillot, A. Santori, O. Rabaste, D. Poullin and M. Lesturgie, "DVB-T Airborne Passive Radar: clutter block rejection," 2019 International Radar Conference (RADAR), TOULON, France, 2019, pp. 1-5.

[31] C. Berthillot, A. Santori, O. Rabaste, D. Poullin, and M. Lesturgie, "BEM reference signal estimation for an airborne passive radar antenna array," IEEE Transactions on Aerospace and Electronic Systems, vol. 53, no. 6, pp. 2833– 2845, December 2017.

[32] F. Wojaczek, D. Cristallini, J. Schell and D. O'Hagan, "Polarimetric antenna diversity for improved reference signal estimation for airborne passive radar," 2020 IEEE Radar Conference (RadarConf), Florence, Italy, September 2020.

[33] G. Chabriel and J. Barrère, "Adaptive Target Detection Techniques for OFDM-Based Passive Radar Exploiting Spatial Diversity," in IEEE Transactions on Signal Processing, vol. 65, no. 22, pp. 5873-5884, November 2017.

[34] V. Navrátil, A. O'Brien, J. L. Garry and G. E. Smith, "Demonstration of space-time adaptive processing for DSI suppression in a passive radar," 2017 International Radar Symposium (IRS), Prague, 2017, pp. 1-10.

[35] S. Gelli, A. Bacci, M. Martorella and F. Berizzi, "Clutter Suppression and High-Resolution Imaging of Noncooperative Ground Targets for Bistatic Airborne Radar," in IEEE Transactions on Aerospace and Electronic Systems, vol. 54, no. 2, pp. 932-949, April 2018.

[36] Digital Video Broadcasting (DVB): Framing structure, channel coding and modulation for digital terrestrial television, European Telecommunications Standards Institute (ETSI), 650 Route des Lucioles, F-06921 Sophia Antipolis Cedex - France, October 2015.

[37] Digital Video Broadcasting (DVB): Transmission to Handheld Terminals (DVB-H), ETSI TR 102 401 V1.1.1, Validation Task Force Report, ETSI, 650 Route des Lucioles F-06921 Sophia Antipolis Cedex - France, May 2015.

[38]   D. Poullin, "Passive detection using digital broadcasters (DAB, DVB) with COFDM modulation," IEE Proceedings - Radar, Sonar and Navigation, vol. 152, no. 3, pp. 143–152, June 2005.

[39]   M. Cherniakov, Ambiguity Function Correction in Passive Radar: DTV-T Signal, M. Cherniakov, Ed. John Wiley & Sons, Ltd, 2008.

[40]   J. Palmer, H. Harms, S. Searle and L. Davis, "DVB-T Passive Radar Signal Processing," IEEE Transactions on Signal Processing, 61 (8), pp. 2116-2126, 15 April 2013.

[41]   F. Colone, D. Langellotti and P. Lombardo, "DVB-T signal ambiguity function control for passive radar," IEEE Transactions on Aerospace and Electronic Systems, vol. 50, no. 1, pp. 329–347, January 2014.

[42]   M. Glende, "PCL-signal-processing for sidelobe reduction in case of periodical illuminator signals," in 2006 International Radar Symposium, May 2006, pp. 1–4.

[43]   S. Searle, J. Palmer, L. Davis, D. W. O'Hagan and M. Ummenhofer, "Evaluation of the ambiguity function for passive radar with OFDM transmissions," in IEEE Radar Conference, Cincinnati, 2014.

[44]   G. Gassier, G. Chabriel, J. Barrère, F. Briolle, and C. Jauffret "A Unifying Approach for Disturbance Cancellation and Target Detection in Passive Radar Using OFDM," in IEEE Transactions on Signal Processing, Vol. 64, Issue 22, pp. 5959-5971, 2016.

[45]   P. Wojaczek, D. Cristallini, I. Walterscheid and D. O'Hagan, "Range compression strategies for passive radar on airborne platforms," 2020 IEEE International Radar Conference (RADAR), Washington, DC, USA, 2020, pp. 25-30.

[46]   R. Klemm, "Principles of Space-Time Adaptive Processing," 3rd edn., IET, 2002.

[47]   J. R. Guerci, "Space-Time Adaptive Processing for Radar," Artech House radar library, 2003.

[48]   W. L. Melvin, "A STAP overview," IEEE Aerospace and Electronics Systems Magazine, vol. 19, no. 1, pp. 19–35, Jan 2004.

[49]   W. L. Melvin, "Clutter Suppression Using STAP," SciTech Publishing, Inc., 2012.

[50]   J. Ward, "Space-Time Adaptive Processing for Airborne Radar", Technical Report 1015, Lincoln Laboratory, Massachusetts Institute of Technology, Lexington, MA, 1994.

[51]   H. Wang and L. Cai, "On adaptive spatial-temporal processing for airborne surveillance radar systems," in IEEE Transactions on Aerospace and Electronic Systems, vol. 30, no. 3, pp. 660-670, July 1994.

[52]   F. Le Chevalier, L. Savy and F. Durniez, "Clutter calibration for space-time airborne MTI radars," Proceedings of International Radar Conference, Beijing, China, 1996, pp. 82-85.

[53]   M. A. Koerber and D. R. Fuhrmann, "Radar Antenna Calibration Using Range-Doppler Data," IEEE Seventh SP Workshop on Statistical Signal and Array Processing, Quebec, City, QC, Canada, 1994, pp. 441-444.

[54] F. C. Robey, D. R. Fuhrmann and M. A. Koerber, "Array calibration and modelling of steering vectors," Conference Record of Thirty-Fifth Asilomar Conference on Signals, Systems and Computers (Cat. No.01CH37256), Pacific Grove, CA, USA, 2001, pp. 1121-1126 vol.2.

[55] E. H. Attia and B. D. Steinberg, "Self-cohering large antenna arrays using the spatial correlation properties of radar clutter," in IEEE Transactions on Antennas and Propagation, vol. 37, no. 1, pp. 30-38, Jan. 1989.

[56] C. N. Franz and R. A. Scholtz, "Multipath interferometry technique for airborne array calibration," in IEEE Transactions on Aerospace and Electronic Systems, vol. 35, no. 4, pp. 1369-1382, Oct. 1999.

[57] C. D. Richmond, "The theoretical performance of a class of space-time adaptive detection and training strategies for airborne radar," Conference Record of Thirty-Second Asilomar Conference on Signals, Systems and Computers (Cat. No.98CH36284), Pacific Grove, CA, 1998, pp. 1327-1331 vol.2.

[58] R. S. Blum and K. F. McDonald, "Analysis of STAP algorithms for cases with mismatched steering and clutter statistics," in IEEE Transactions on Signal Processing, vol. 48, no. 2, pp. 301-310, Feb. 2000.

[59] A. Liu, H. Sun, K. C. Teh, C. J. Baker and C. Gao, "Robust space-time adaptive processing for nonhomogeneous clutter in the presence of model errors," in IEEE Transactions on Aerospace and Electronic Systems, vol. 52, no. 1, pp. 155-168, February 2016.

[60] J. Ender, "The airborne experimental multi-channel SAR system AERII," in Proc. Eur. Conf. Synth. Aperture Radar (EUSAR), March 1996, pp. 49–52.

[61] C. H. Gierull, "Digital channel balancing of along-track interferometric SAR data," Defence Research and Development Canada (DRDC), Tech. Rep. TM-2003-024, 2003.

[62] S. Baumgartner, M. Gabele, N. Gebert, R. Scheiber, G. Krieger, K. H. Bethke, A. Moreira, "Digital Beamforming and Traffic Monitoring Using the new FSAR System of DLR," in International Radar Symposium (IRS), Cologne, 2007.

[63] E. Makhoul, S. Baumgartner, M. Jäger, A. Broquetas, "Multichannel SAR-GMTI in Maritime Scenarios With F-SAR and TerraSAR-X Sensors," IEEE Journal of Selected Topics in Applied Earth Observations and Remote Sensing, vol. 8, no. 11, pp. 5052-5067, Nov. 2015.

[64] J. Heckenbach, H. Kuschel, J. Schell and M. Ummenhofer, "Passive radar based control of wind turbine collision warning for air traffic PARASOL," 2015 16th International Radar Symposium (IRS), Dresden, 2015, pp. 36-41. doi: 10.1109/IRS.2015.7226394

[65] W. Shrader and V. G. Hansen, "MTI Radar," in Radar Handbook, M. I. Skolnik, Third Edition, McGraw-Hill, 2008.

[66] M. A. Richards, "Fundamentals of Radar Signal Processing," McGraw-Hill, 2005, pp. 244-250.

[67] J. L. Garry, C. J. Baker and G. E. Smith, "Evaluation of Direct Signal Suppression for Passive Radar," in IEEE Transactions on Geoscience and Remote Sensing, vol. 55, no. 7, pp. 3786-3799, July 2017.

[68] F. Colone, D. W. O'Hagan, P. Lombardo and C. J. Baker, "A Multistage Processing Algorithm for Disturbance Removal and Target Detection in Passive Bistatic Radar," IEEE Transactions on Aerospace and Electronic Systems, pp. 698-722, April 2009.

[69] F. Colone, C. Palmarini, T. Martelli, and E. Tilli, "Sliding extensive cancellation algorithm for disturbance removal in passive radar," IEEE Transactions on Aerospace and Electronic Systems, vol. 52, no. 3, pp. 1309–1326, June 2016.

[70] C. Schwark and D. Cristallini, "Advanced multipath clutter cancellation in OFDM-based passive radar systems," in IEEE Radar Conference (RadarConf), Seattle, 2016.

[71] E. J. Kelly, "An Adaptive Detection Algorithm," in IEEE Transactions on Aerospace and Electronic Systems, vol. AES-22, no. 2, pp. 115-127, March 1986.

[72] D. Pastina, P. Lombardo and T. Bucciarelli, "Adaptive polarimetric target detection with coherent radar. Part I: Detection against Gaussian background," IEEE Transactions on Aerospace and Electronic Systems, vol. 37, no. 4, pp. 1194-1206, Oct. 2001.

[73] J. Ward, "Maximum likelihood angle and velocity estimation with space-time adaptive processing radar," Conference Record of The Thirtieth Asilomar Conference on Signals, Systems and Computers, Pacific Grove, CA, USA, 1996, pp. 1265-1267 vol.2.

[74] F.C. Robey, D.R. Fuhrmann, E.J. Kelly, and R. Nitzberg, "A CFAR Adaptive Matched Filter Detector," IEEE Transactions on Aerospace and Electronic Systems, Vol.AES-28, No.1, January 1992, pp.208-216.

[75] J. Ward, "Cramér-Rao bounds for target angle and Doppler estimation with space–time adaptive processing radar" Proc. 29th ASILOMAR Conf. on Signals Systems and Computers, Nov. 1995, pp.1198-1203.

[76] R. Klemm, "Cramér-Rao analysis of reduced order STAP processors," IEEE International Radar Conference, Alexandria, VA, USA, 2000, pp. 584-589.

[77] U. Nickel, "Monopulse estimation with adaptive arrays", IEE Proc. Radar Signal Process., 1993, 140, (5), pp. 303–308.

[78] U. Nickel, "An overview of generalized monopulse estimation", IEEE AES Mag., 2006, 21, (6), pp. 27–55, Part 2: Tutorials.

[79] P. Lombardo and F. Colone, "A dual adaptive channel STAP scheme for target detection and DOA estimation," Proceedings of the International Conference on Radar (IEEE Cat.No.03EX695), Adelaide, SA, Australia, 2003, pp. 115-120.

[80] F. Colone, D. Cristallini, D. Cerutti-Maori and P. Lombardo, "Direction of arrival estimation performance comparison of dual cancelled channels space-time adaptive processing techniques," in IET Radar, Sonar & Navigation, vol. 8, no. 1, pp. 17-26, January 2014.